PB80-190515

Investigation of CARS and Laser-induced Saturated Fluorescence for Practical Combustion Diagnosis

United Technologies Research Center
East Hartford, CT

Prepared for

Industrial Environmental Research Lab.
Research Triangle Park, NC

May 80

U.S. Department of Commerce
National Technical Information Service
NTIS.

PB80-190515

United States
Environmental Protection
Agency

Industrial Environmental Research
Laboratory
Research Triangle Park NC 27711

EPA-600/7-80-091
May 1980

EPA

Investigation of CARS and Laser-induced Saturated Fluorescence for Practical Combustion Diagnosis

Interagency Energy/Environment R&D Program Report

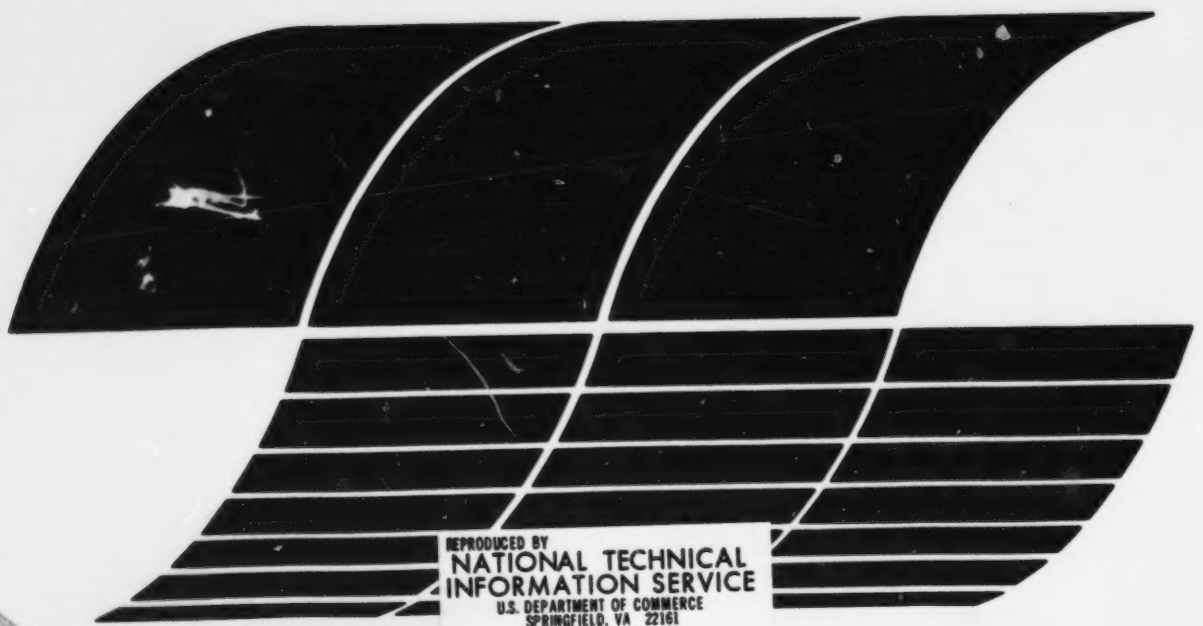

REPRODUCED BY
NATIONAL TECHNICAL
INFORMATION SERVICE
U.S. DEPARTMENT OF COMMERCE
SPRINGFIELD, VA 22161

RESEARCH REPORTING SERIES

Research reports of the Office of Research and Development, U.S. Environmental Protection Agency, have been grouped into nine series. These nine broad categories were established to facilitate further development and application of environmental technology. Elimination of traditional grouping was consciously planned to foster technology transfer and a maximum interface in related fields. The nine series are:

1. Environmental Health Effects Research
2. Environmental Protection Technology
3. Ecological Research
4. Environmental Monitoring
5. Socioeconomic Environmental Studies
6. Scientific and Technical Assessment Reports (STAR)
7. Interagency Energy-Environment Research and Development
8. "Special" Reports
9. Miscellaneous Reports

This report has been assigned to the INTERAGENCY ENERGY-ENVIRONMENT RESEARCH AND DEVELOPMENT series. Reports in this series result from the effort funded under the 17-agency Federal Energy/Environment Research and Development Program. These studies relate to EPA's mission to protect the public health and welfare from adverse effects of pollutants associated with energy systems. The goal of the Program is to assure the rapid development of domestic energy supplies in an environmentally-compatible manner by providing the necessary environmental data and control technology. Investigations include analyses of the transport of energy-related pollutants and their health and ecological effects; assessments of, and development of, control technologies for energy systems; and integrated assessments of a wide range of energy-related environmental issues.

EPA REVIEW NOTICE

This report has been reviewed by the participating Federal Agencies, and approved for publication. Approval does not signify that the contents necessarily reflect the views and policies of the Government, nor does mention of trade names or commercial products constitute endorsement or recommendation for use.

This document is available to the public through the National Technical Information Service, Springfield, Virginia 22161.

TECHNICAL REPORT DATA
(Please read Instructions on the reverse before completing)

1. REPORT NO.	2.	3. RECIPIENT'S ACCESSION NO.
EPA-600/7-80-091		PB80 190515

4. TITLE AND SUBTITLE	5. REPORT DATE
Investigation of CARS and Laser-induced Saturated Fluorescence for Practical Combustion Diagnosis	May 1980
	6. PERFORMING ORGANIZATION CODE
7. AUTHOR(S)	8. PERFORMING ORGANIZATION REPORT NO.
A. C. Eckbreth, P. A. Bonczyk, and J. F. Verdieck	
9. PERFORMING ORGANIZATION NAME AND ADDRESS	10. PROGRAM ELEMENT NO.
United Technologies Research Center East Hartford, Connecticut 06108	INE623
	11. CONTRACT/GRANT NO.
	68-02-3105
12. SPONSORING AGENCY NAME AND ADDRESS	13. TYPE OF REPORT AND PERIOD COVERED
EPA, Office of Research and Development Industrial Environmental Research Laboratory Research Triangle Park, NC 27711	Final; 8/78-8/79
	14. SPONSORING AGENCY CODE
	EPA/600/13

15. SUPPLEMENTARY NOTES IERL-RTP project officer is William B. Kuykendal, Mail Drop 62, 919/541-2557. EPA-600/7-77-066 and EPA-600/7-78-104 are related reports.

16. ABSTRACT The report gives results of experimental investigations aimed at developing nonperturbing, spatially precise, in-situ diagnostic techniques to measure species composition and temperature in flames. The investigations continued earlier development of coherent anti-Stokes Raman spectroscopy (CARS) and laser-induced saturated fluorescence. The program included two main, concurrent tasks. In Task 1, optical thermometry, the practical feasibility of CARS was demonstrated in a program of research-scale combustor testing (results agreed to within 5% for combustion zone temperature measurements made with CARS and with shielded thermocouples). In Task 2, optical composition, laser-induced saturated fluorescence was examined in regard to its capability for measuring CH, CN, and NO concentrations in flames. Saturation of the fluorescence in CH and CN was achieved and considerable insight into the physics of saturated fluorescence was obtained. Promising initial results of NO fluorescence in flames are described, but saturation was not observed for laser spectral intensities up to 6 million W/sq cm/cm.

17. KEY WORDS AND DOCUMENT ANALYSIS

a. DESCRIPTORS		b. IDENTIFIERS/OPEN ENDED TERMS	c. COSATI Field/Group	
Pollution	Spectroscopy	Pollution Control	13B	
Combustion	Fluorescence	Stationary Sources	21B	20F
Flames	Lasers	Optical Composition		20E
Measurement		Optical Thermometry	14B	
Optical Tests		CARS		
Temperature				

18. DISTRIBUTION STATEMENT	19. SECURITY CLASS (This Report)	21. NO. OF PAGES
Release to Public	Unclassified	
	20. SECURITY CLASS (This page)	22. PRICE
	Unclassified	

EPA Form 2220-1 (9-73)

EPA-600/7-80-091

May 1980

Investigation of CARS and Laser-induced Saturated Fluorescence for Practical Combustion Diagnosis

by

A.C. Eckbreth, P.A. Bonczyk, and J.F. Verdieck

United Technologies Research Center
East Hartford, Connecticut 06108

Contract No. 68-02-3105
Program Element No. INE623

EPA Project Officer: William B. Kuykendal

Industrial Environmental Research Laboratory
Office of Environmental Engineering and Technology
Research Triangle Park, NC 27711

Prepared for

U.S. ENVIRONMENTAL PROTECTION AGENCY
Office of Research and Development
Washington, DC 20460

DISCLAIMER

This report has been reviewed by the Industrial Environmental Research Laboratory, U.S. Environmental Protection Agency, and approved for publication. Approval does not signify that the contents necessarily reflect the views and policies of the U.S. Environmental Protection Agency, nor does mention of trade names or commercial products constitute endorsement or recommendation for use.

FOREWORD

A broad based continuing research program is being sponsored by the Industrial Environmental Research Laboratory at Research Triangle Park to reduce emissions from stationary sources. A part of this research program is concerned with reducing air emissions via modification of the combustion process. In order to better achieve this goal, it is necessary to understand on a fundamental basis the combustion process. Combustion diagnostic measurements play a key role in developing this understanding.

The work reported herein covers research on two key measurements of significant interest in combustion research: combustion temperature measurements and specie concentration of CH, CN, and NO.

William B. Kuykendal
Process Measurements Branch
Industrial Environmental Research
Laboratory
Research Triangle Park

ABSTRACT

Under Contract 68-02-3105 sponsored by the Environmental Protection Agency, the United Technologies Research Center (UTRC) has conducted experimental investigations aimed at developing nonperturbing, spatially precise, in-situ diagnostic techniques to measure species composition and temperature in flames. The contract continued the development initiated under Contract 68-02-2176 of coherent anti-Stokes Raman spectroscopy (CARS) and laser-induced saturated fluorescence. The program was divided into two main, concurrent tasks. In Task I, Optical Thermometry, the practical feasibility of CARS has been demonstrated in a program of research scale combustor testing. In Task II, Optical Composition, laser-induced saturated fluorescence has been examined in regard to its capability for measuring CH, CN, and NO concentrations in flames. Saturation of the fluorescence in CH and CN was achieved and considerable insight into the physics of saturated fluorescence has been obtained. Promising, initial results of NO fluorescence in flames are described but saturation was not observed for laser spectral intensities up to $6(10^6)$ W/cm^2 cm^{-1}.

Investigations of CARS and Laser-Induced
Saturated Fluorescence for Practical Combustion Diagnosis

TABLE OF CONTENTS

	Page
DISCLAIMER	ii
FOREWORD	iii
ABSTRACT	iv
TABLE OF CONTENTS	v
LIST OF FIGURES	vii
SUMMARY	1
INTRODUCTION	4
CONCLUSIONS AND RECOMMENDATIONS	6
TASK I OPTICAL THERMOMETRY CARS INVESTIGATIONS IN PRACTICAL COMBUSTORS	8
Introduction	8
Combustion Facility	10
Portable CARS Instrument	10
Experimental Program	21
TASK II OPTICAL COMPOSITION INVESTIGATIONS OF LASER-INDUCED SATURATED FLUORESCENCE FOR TRACE SPECIES DETERMINATIONS	37
Introduction	37
Laser-Induced Saturated Fluorescence Theory	40

TABLE OF CONTENTS (Cont'd)

	Page
Experimental Investigations	47
General Discussion	86
REFERENCES.	88

LIST OF FIGURES

Figure No.	Title	Pages
1	Low Pressure Fundamental Combustion Facility	11
2	Combustors Used in CARS Demonstrations	12
3	Postrun Condition of Combustion Tunnel Windows	14
4	Schematic Layout of Portable CARS Apparatus	16
5	BOXCARS Setup in Jet Burner Stand	17
6	Portable CARS Instrument in Jet Burner Stand	18
7	Horizontal Dispersion Output Optical Arrangement	19
8	Temperature Variation of N_2 CARS Spectrum	22
9	Thermometry Algorithm for N_2 CARS Spectra	24
10	CARS Transmission Through a 60μ Dia , 20m Long, Optical Fiber	25
11	Temperature Variation with Stoichiometry in Model Combustor	26
12	Spatial Variation of Temperature in Model Combustor with Jet A Fuel	28
13	Stoichiometric CARS Temperature Variation in Swirl Burner with Refractory Back Wall	30
14	Single Pulse CARS Thermometry in Swirl Burner with Refractory Back Wall	32
15	Operational Temperature Variation in JT-12 Exhaust	33
16	BOXCARS Temperature Profile of JT-12 Exhaust	35
17	Single Pulse BOXCARS Thermometry in JT-12 Exhaust	36
18	Modified Two-Level Model for Saturated Fluorescence with Rotational Redistribution	44

LIST OF FIGURES (Cont'd)

Figure No.	Title	Pages
19	CH and CN Energy Level Diagrams	49
20	NO Energy Level Diagram	50
21	Laser Induced Fluorescence Apparatus	52
22	Laser Induced Fluorescence Apparatus Photograph	53
23	Stilbene Dye Laser Pulse	55
24	Rayleigh Pulse	57
25	CH Spectra	58
26	Principal Laser-Excited CH Lines	59
27	Laser Excited CH Flame Fluorescence	61
28	CH Concentration Data Reduction	62
29	Energy Level Diagram for CN	64
30	CN Saturated Fluorescence Experimental Arrangement	66
31	Experimental Arrangement for CN Saturated Fluorescence	67
32	Emission Spectrum of CN Violet System ($B^2\Sigma \longrightarrow X^2\Sigma$)	69
33	Laser-Induced Fluorescence of CN Radical	70
34	Laser-Induced Fluorescence of CN Radical	71
35	Laser-Induced Fluorescence of CN Radical	72
36	Laser-Induced Fluorescence of CN Radical	73
37	Laser-Induced CN Fluorescence:Saturation Behavior	75

LIST OF FIGURES (Cont'd)

Figure No.	Title	Pages
38	Saturated Fluorescence Power Versus Inverse Laser Spectral Irradiance	76
39	Horizontal Scan of Laser-Induced Fluorescence in CN Slot Burner	78
40	Laser Induced UV Fluorescence Apparatus	79
41	NO Spectra	82
42	NO Fluorescence Pulses	83
43	Laser Excited NO Flame Fluorescence	85

SUMMARY

Under Contract 68-02-3105, sponsored by the Environmental Protection Agency, the United Technologies Research Center (UTRC) has conducted experimental investigations aimed at developing non-perturbing, spatially precise, in-situ diagnostic techniques to measure species composition and temperature in flames. The contract continued the development initiated under Contract 68-02-2176 of coherent anti-Stokes Raman spectroscopy (CARS) and laser-induced saturated fluorescence. The program was divided into two main, concurrent tasks. In Task I, Optical Thermometry, the practical feasibility of CARS has been evaluated in a testing program in a research scale combustor. In Task II, Optical Composition, laser-induced saturated fluorescence has been examined in regard to its capability for measuring CH, CN, and NO concentrations in flames.

The feasibility of coherent anti-Stokes Raman spectroscopy for remote, spatially and temporally resolved, measurements in practical combustion systems has been demonstrated. Experiments were performed in a 50-cm dia. combustion tunnel with generous optical access, located in UTRC's Jet Burner Test Stand. The tunnel could be fitted with either a swirl burner or shrouded JT-12 can. The swirl burner could be fired with either gaseous or liquid fuels and permitted access to primary and secondary combustion zones. The JT-12 can was shrouded, restricting measurements to its exhaust region. The CARS instrument consisted essentially of transmitter and receiver optical assemblies and detection instrumentation. The CARS transmitter comprised the two laser sources required to generate CARS, and the requisite optics and transmitter lens to focus and cross the mixing optical beams in the combustor. The transmitter was arranged on a 3' x 6' optical pallet mounted on a portable cart. The pallet could be translated to allow measurements at various radial positions in the tunnel. The receiver optics were mounted on rails and linked to the transmitter permitting tandem translation of the optics. The CARS signal emerging from the combustor was processed by the receiver and piped out of the burner stand test cell employing 20 m long, 60μ dia. fiber optic guides. The fiber optic conduit delivered the CARS signal to the detection equipment, a 0.6 m spectrograph fitted with an optical multichannel analyzer, located in the control room, a more benign environment for delicate optical equipment. The optical multichannel analyzer permitted the capture of single 10^{-8} sec CARS spectra and time averaging of the spectra from regions of the combustion tunnel where the temporal fluctuations were modest. Thermometry is performed from the shape of the CARS signatures; in the tests reported herein CARS was generated always from N_2. Crossed-beam phase matching or BOXCARS was employed in all of the tests to remove any potential spatial resolution ambiguity. This also provided a more stringent test of the practical feasibility of CARS than the more conventional collinear phase matching.

Successful tests were conducted first in the swirl burner with gaseous propane as the fuel at several stoichiometries. Then Jet A fuel was run and, since no problems were encountered, all subsequent testing was with the liquid fuel. The Jet A fueled tests were quite impressive in that the combustion luminosity was extremely intense, difficult to view for any extended period. With the Jet A fueled swirl burner, high quality averaged and single pulse CARS spectra were obtained at several different spatial locations and stoichiometries, including the spray zone. In most cases, the spectra rival the quality of those obtained in laboratory studies. To simulate a furnace more closely, a refractory back wall was placed flush with the exit of the swirl burner. This caused no particular problem and good spectra were again obtained. Measurements were also made in the exhaust of the Jet A fueled JT-12 can. High quality averaged and single pulse CARS spectra were obtained at several sets of conditions. The temperature profile of the exhaust was obtained near the exit at the so-called cruise condition. CARS temperature measurements further downstream in the exhaust agreed quite well with those determined by an aspirating, thermocouple probe. All in all, these experiments constituted a fairly rigorous examination of the feasibility of CARS for practical combustion diagnosis.

Under Task II, Optical Composition, the technique of laser-induced saturated fluorescence was investigated for measurement of CH, CN, and NO radical concentrations in laboratory flames. These species were chosen because they are of extreme importance in combustion chemistry and pollutant formation. The laser-induced saturated fluorescence method is important for two reasons: the more important is the elimination of quenching corrections in determining concentrations; the second is that the maximum possible signal is obtained from a given set of experimental conditions. These two factors taken together contribute to a measurement technique of good precision and high sensitivity.

The CH, CN, and NO radicals absorb light in the blue (4300 Å), near UV (3880 Å), and far UV (2260 Å), respectively. Correspondingly, dye laser systems were constructed to provide short pulse length, $O(10^{-8}$ sec), narrow spectral width, $O(0.1\ cm^{-1})$, radiation at the appropriate wavelengths. Each of these systems was optically pumped with a 10 Hz repetition rate pulsed neodymium:YAG laser; either the second harmonic (2xNd:YAG = 5320 Å) or third harmonic (3xNd:YAG = 3533 Å) was employed. The resulting dye laser radiation was used directly to excite the radical fluorescence (in the case of CH), or mixed with the 1.06μ neodymium fundamental (1xNd:YAG) to generate UV radiation (for CN). For the excitation of NO fluorescence, both a frequency doubling of the dye laser radiation and subsequent sum-frequency mixing with 1.06μ was required. The resultant laser intensity was low, insufficient to saturate the NO fluorescence.

Laser-induced fluorescence of CH and CN was observed from the same premixed slot-burner using acetylene-oxygen, and acetylene-nitrous oxide, respectively. Prior to determining saturation curves for these two species, high resolution

fluorescence spectra were obtained by slowly scanning the appropriate regions. It is necessary to determine the laser-induced fluorescence spectrum of a particular species for several reasons. Probably, the most important reason is that examination of the spectrum provides some assessment of rotational relaxation, an assessment essential to proper data reduction. For experimental purposes, the spectrum also suggests the best combination of transition to excite and fluorescing transitions from which to collect signal (to minimize interference and maximize signal). Moreover, the actual fraction of fluorescence collected to total fluorescence must be determined from the laser-induced spectrum.

Saturation curves, plots of laser-induced fluorescence signal against laser intensity, were obtained by attenuating the laser beam with neutral density filters. The CN radical fluorescence was more easily saturated than that of the CH fluorescence, as expected. Concentrations of these species were determined from the fluorescence power data according to a modified two-level saturated fluorescence model. The model, developed in the report, presents the effects of rotational relaxation in a simple, direct manner. Using a frozen rotation data reduction scheme, concentration measurements found in these investigations agreed to within a factor of 2 to 3 with previous absorption measurements. Quenching rates were also obtained from the fluorescence power data.

Laser-induced NO fluorescence spectra were obtained from NO-doped methane-air flames. However, saturated fluorescence was not observed because the incident spectral irradiance fell short of the saturation values predicted by calculation. It is estimated that with the use of commercially available dye lasers, the saturated regime for the NO fluorescence can be attained.

INTRODUCTION

With the increasing availability of laser sources, light scattering and wave mixing spectroscopic techniques are assuming an ever-increasing role in a broad spectrum of physical investigations. Of particular importance is the application of laser spectroscopy to the hostile, yet easily perturbed, environments in which combustion occurs. Nonintrusive laser diagnostics should facilitate greatly improved understanding of a variety of combustion processes which, in turn, should lead to enhanced efficiencies and cleanliness in energy, propulsion, and waste disposal systems.

Under the sponsorship of the Environmental Protection Agency, the United Technologies Research Center (UTRC) has been conducting analytical and experimental investigations aimed at developing nonperturbing, spatially precise, in situ diagnostic techniques to measure species concentrations and temperature in flames. The present contract (68-02-3105) continued the development initiated under Contract 68-02-2176 of coherent anti-Stokes Raman spectroscopy (CARS) and laser-induced saturated fluorescence. The program was divided into two main, concurrent investigations, the results of which are reported herein. Under Task I, Optical Thermometry, the practical feasibility of CARS has been assessed in a program of research scale combustor testing. In Task II, Optical Composition, laser-induced saturated fluorescence has been examined in regard to its capability for measuring CH, CN, and NO concentrations in flames.

By way of perspective, it is instructive to review the results of the first contract (68-02-2176) which was divided into two serial tasks. In Task I, a comprehensive review (Refs. 1-3) was conducted of potential, unobtrusive, in situ techniques for chemical composition and temperature measurements in flames with particular emphasis on hostile environments such as research scale furnaces. The review focussed upon four laser techniques which appeared most promising, namely, spontaneous and near-resonant Raman scattering, laser-induced fluorescence, and CARS. Although they have received considerable attention for combustion diagnostics (Refs. 4, 5), spontaneous and near-resonant Raman scattering appeared to possess a low probability of successful application to highly luminous, particle-laden flames even with advanced state-of-the-art laser sources. Laser fluorescence appeared capable of measuring species concentrations to tens of ppm in practical flames and tenths of ppm in clean flames for selected molecules whose absorptions could be saturated. In this saturation approach, fluorescence magnitudes do not depend upon or can be experimentally corrected for quenching effects. The technique is applicable to several molecules of combustion interest, primarily radicals such as NO, OH, CH, CN, C_2, and NH. CARS was perceived capable of successful thermometry and major species measurements in practical environments, although potential jeopardies such as laser-soot interaction effects had then to be addressed. It should be noted that the two techniques, for the most part, are complementary in regard to their capabilities.

In Task II, experimental investigations of saturated laser-excited molecular fluorescence and CARS were conducted and are reported in Ref. 6. Saturated laser-induced fluorescence measurements using a tunable, flashlamp-pumped dye laser, were performed on the radicals CH and CN in atmospheric pressure flames (Ref. 7). Partial saturation of the fluorescence was achieved for both molecules with readily achieved laser spectral intensities in the 10^5 to 10^6 Watts/cm^2 cm^{-1} range. In order to test the validity of the fluorescence results, absorption measurements were made to independently determine the concentrations. The concentrations measured by absorption were found to be larger by about a factor of two for CH and five for CN than the saturated fluorescence values. It was believed that the fluorescence results were low, due to an overestimate of the fluorescence (i.e., species) sample volume arising from strong spatial gradients of concentration in the small, high pressure flames studied. Nevertheless, the experiments demonstrated the viability of saturated, laser-induced fluorescence for trace species detection of molecular radicals. Based upon these studies, it was proposed to refine the experimental approach, reexamine CH and CN and then proceed to attempt saturated fluorescence detection of NO. The experimental refinement consisted primarily of replacing the flashlamp-pumped dye laser with a dye laser pumped by an appropriate harmonic of a Q-switched neodymium:YAG laser. Such dye lasers typically possess far superior beam quality (i.e., focusability), narrower linewidths, higher intensities, and higher pulse repetition rates than flashlamp-pumped lasers.

The CARS investigations conducted demonstrated its promising potential for temperature and species probing of practical combustion environments. CARS spectra from N_2 over premixed flames displayed excellent agreement with computer generated model predictions. Single pulse (10^{-8} seconds) CARS spectra were obtained in flames and displayed the capability of CARS for "instantaneous" temperature measurements. Quite importantly, CARS was successfully performed from N_2 in highly sooting flames indicating that CARS should be applicable to practical systems. Although thermometry received the major emphasis in the CARS investigations, CO species sensitivity was also examined. From these investigations, a logical next step in the development of CARS was to examine its practical utility in tests in actual research scale combustors.

Based upon this foundation, the present contract was structured into the two parallel investigations mentioned earlier. The next section summarizes the conclusions reached during these investigations and contains recommendations for the future development of these techniques which are a logical extension to the investigations described herein. Then, the Task I Optical Thermometry investigations are described. Therein, the successful application of CARS thermometry, both averaged and single pulse, in liquid-fueled practical combustors, is reported. The last section contains the results generated under the Task II, Optical Composition investigations. With the improved experimental setups, the measurements of CH and CN are now closer to the previous values determined by absorption and considerable insight into saturated fluorescence physics has been obtained. Promising, initial results of NO fluorescence studies are also described.

CONCLUSIONS AND RECOMMENDATIONS

Coherent Anti-Stokes Raman Spectroscopy

The feasibility of coherent anti-Stokes Raman spectroscopy (CARS) for remote, spatially and temporally resolved, measurements in practical combustion systems has been demonstrated. N_2 CARS temperature measurements are reported at atmospheric pressure for two different liquid-fueled combustors, a swirl burner, and a JT-12 combustor can, situated in a 50-cm dia. tunnel. Crossed-beam CARS, i.e., BOXCARS, was employed to ensure good spatial precision. Delicate instrumentation was housed in a control room adjacent to the burner test cell, and the CARS signals were piped out employing 60 μ dia. fiber optic guides. Average temperature measurements and single pulse thermometry were performed. Based upon these and other investigations, CARS may be anticipated to see widespread applicability to a variety of practical combustion devices and problems.

In attempting to assess the potential for the routine application of CARS thermometry to combustion research, several points are worth bearing in mind. Expense: The capital equipment required for a complete CARS system including computer controlled data acquisition and reduction would be on the order of $150K to $200K. For an automated system, considerable software development would be required, perhaps two man-years worth. CARS computer codes would need to be developed, two man-years, or purchased. To operate the system, an engineer and technician would be required. Operating expenses, other than wages, would not be large, perhaps $10K/year. The major hurdle, financially, would be the initial outlay for equipment. Personnel: Initially, a fairly experienced scientist would be required to bring into operation and maintain the system. After a period of time, the technology could be transferred to lesser experienced (in CARS) personnel with periodic supervision or consulting with someone knowledgable in the technique and, preferably, near-by or in house. Presently, scientists/engineers experienced in CARS with application to combustion research are scarce. Applications: No use of CARS at the present time can be called routine in the sense that a low temperature ($\lesssim$ 1200 °K) thermocouple measurement might be called routine. For fundamental flame studies in the laboratory, it can become "routine" to an experienced scientist in a relatively short time. Practical applications, certainly initially, tend to be distinctly unique, requiring new approaches and twists. For example, the step from measurements in a one atmosphere, 50 cm dia. tunnel well equipped with optical access, to a 25-40 atm, annular, combustor can perhaps twice as large, or a 3m dia. furnace is neither easy or straightforward. On the other hand, it is not impossible,

and one should not view such applications as improbable. To date, CARS has been successfully demonstrated in an internal combustion engine and simulations of furnaces, gas turbine combustors and other turbomachines. Based on these recent advances, one may anticipate that CARS will provide for considerable advances in combustion science in the coming years.

Laser-Induced Saturated Fluorescence

The application of the laser-induced saturated fluorescence technique for spatially-resolved, remote measurement of radical concentrations in a flame was confirmed by this investigation, although data reduction questions still need to be resolved. Resolution of these issues would greatly enhance measurement accuracy. In particular, CN and CH radical concentrations were measured; both species were readily saturated with laser-pumped dye-lasers of 10 nanosecond pulse duration, narrowband (~ 0.1 cm^{-1}) spectral width, and reasonable beam divergence (2-3 milliradians). The extrapolated detectivity limits for concentration measurements based upon the dye lasers used in this study for a clean flame environment are: CN ~ 2 ppm; CH ~ 14 ppm. These estimates are based upon a minimum detectable number of photons equal to 100 and a quantum efficiency of 0.25.

Laser-induced fluorescence spectra of NO were obtained from an NO-doped flame in this investigation, but the saturated fluorescence regime could not be attained because of insufficient laser power at 2260 Å. Because of the extreme importance of nitric oxide as a pollutant, further investigation of the saturated fluorescence measurement of NO, using a more powerful dye laser, is certainly warranted.

Finally, it is recommended, that, in order to truly understand how rotational relaxation affects the interpretation of saturated fluorescence data, computer-generated, time-dependent solutions to the rate equations be generated and studied. Time-dependent solutions for some general cases have already been obtained by R. J. Hall of this laboratory. Such computer solutions, with time-dependent variation of the pertinent rates, could help greatly in understanding the data reduction problem, particularly if compared with well-designed experiments. Rates for rotational energy transfer can be measured experimentally by observing the time dependence of the rotational structure of the laser-induced fluorescence spectra.

TASK I - OPTICAL THERMOMETRY

CARS INVESTIGATIONS IN PRACTICAL COMBUSTORS

Introduction

Coherent anti-Stokes Raman spectroscopy, CARS, (Refs. 2, 8-10 and the references therein) has received considerable attention in the last several years for remote combustion diagnosis because of its potential applicability to practical systems, e.g.,furnaces, gas turbine combustors, etc.. Spontaneous Raman scattering has also been widely investigated in this regard (Refs.4, 5) but, due to its weak signal strength and incoherent character, is generally limited to use in relatively clean flames. In practical combustion environments, laser induced incandescences from soot (Refs. 2, 11, 12) or fluorescences from fuel fragments (Ref. 13) can mask detection of the Raman signals, often by several orders of magnitude.

CARS is a nonlinear, light wave mixing process capable of both high spatial and temporal resolution and is described in detail in the aforementioned references and the reports (Refs. 1, 6) prepared under the preceeding EPA Contract 68-02-2176. Very briefly, laser beams at frequencies ω_1 and ω_2, termed the pump and Stokes frequencies respectively, with a frequency difference appropriate to the molecular species being probed, are focussed and "mixed" by overlapping to generate a laser-like CARS signal beam. Temperature measurements derive from the spectral distribution of the CARS radiation (Ref. 14), concentration measurements from the signal intensity (Ref. 15) or, in certain ranges, also from spectral shapes (Ref. 14). The practical potential of CARS has been exhibited in several investigations and recently was displayed when CARS was employed to map the temperature field throughout a highly sooting, laminar propane diffusion flame (Ref. 16), and for single pulse measurements, in a small highly turbulent flame (Ref. 17). Despite these advances, concern over practical feasibility has been exhibited in regards to the possibly deleterious effects of large scale turbulence, turbulence over a large physical dimension and the presence of liquid fuel droplets. Large scale turbulence, i.e., scales on the order of the laser beam diameter, and strong spatial gradients can cause steering of the laser beams and deterioration of their focussing properties (Ref. 18). Small scale turbulence also degrades phasefront coherence and, when integrated over a substantial path, results in reduced focal volume intensities. Fuel droplets can attenuate, scatter and refract the incident laser beams. These effects can seriously degrade CARS signal generation efficiency. There may exist situations where these distortions are so severe that CARS or optical probing of any sort will be precluded. To address these points, CARS investigations in practical combustion environments were performed under Task I of the contract. Specifically, this section of the report describes

successful CARS measurement demonstrations, both averaged and single pulse, in the primary zone of a highly swirled burner fueled with either propane (g) or Jet A, and in the exhaust of a JT-12 can burning Jet A. These combustors were selected to evaluate CARS in several different types of combustion regions.

CARS has been recently demonstrated in an internal combustion engine (Ref. 19), a bluff-body stabilized, gaseous propane diffusion flame in a combustion tunnel (Ref. 20), and in the exit plane of a kerosene-fueled burner (Ref. 21). Subsequent to the investigations described herein, the combustion tunnel CARS experiments reported in Ref. 20 were extended to liquid fuels as well (Ref. 22). Due to the scale of a typical internal combustion engine and its repetitive behavior, a CARS approach different than that required for probing large volume, nonstationary sources can be employed. In nonstationary systems, spectrally broadband Stokes lasers must be used to generate and capture the entire CARS spectrum with each pulse. In a cyclical process, a narrowband Stokes laser can be scanned synchronously with the engine cycle to generate the CARS spectrum piecewise but, nevertheless, temporally resolved vis-a-vis the engine cycle. The magnitude of turbulent fluctuations at a given point in the cycle cannot be obtained, however, unless the broadband approach is used. For small-scale devices with modest radial gradients, collinear mixing of the input beams can probably be employed without loss of spatial resolution, although the validity of this approach should be verified.

The experiments reported here differ from the tunnel work in Refs. 20, 22 in several respects. Here crossed-beam phase matching or BOXCARS (Ref. 23) was adopted over collinear mixing. By crossing the incident laser beams, in a manner similar to laser velocimetry, CARS is generated only at the beam intersection. This manner of phase matching yields fine and, perhaps more importantly, unambiguous spatial resolution. In turbulent combustion environments, this approach provides a stringent test for CARS since the crossing beams traverse different optical paths. Further, longer optical paths were examined in this work since the tunnel used was, by chance, 50 cm in diameter in contrast to the 25 cm tunnel employed in the (Refs. 20, 22) studies. Lastly, delicate instruments, such as the spectrometer and optical multichannel analyzer, were not located in the burner stand test cell, but rather in the adjacent control room. The CARS signals upon exiting from the combustor were focused into a 20-meter long, 60-μ dia., optical fiber and transmitted to the remotely located instrumentation. Remote detection of CARS signals using fiber optics can be highly useful, particularly for diagnostic application in intense vibratory environments (Ref. 24).

In the next section, the combustors and combustion tunnel employed in these experiments will be described. The CARS instrument assembled for these tests will then be discussed followed by a presentation of the experimental results.

Combustion Facility

The CARS experiments were performed in the combustion tunnel schematically illustrated in Fig. 1. The tunnel was fitted with either a swirl burner or shrouded JT-12 combustor can shown in Figs. 2a and 2b, respectively. Characteristics of the swirl burner and combustion tunnel are summarized in Table 1. The tunnel is of double-wall, stainless steel construction and water-cooled. It is 50-cm in internal diameter and 150-cm long and contains four rows of rectangular quartz windows, 6.4 cm x 12.8 cm, every 90° about the tunnel axis. When the windows are not in use, steel insert plates are used to blank off the tunnel. Each row contains eight window locations, numbered sequentially beginning upstream. Due to the expense of large quartz windows, 5 cm dia. windows in a specially constructed blank were used instead for the CARS apertures. The windows were offset from the combustor outer wall by a cylindrical standoff purged with dry nitrogen. The unobstructed window aperture was approximately 3.8 cm. In Jet A fueled tests, the windows would coat with soot on the time scale of an hour. Lesser deposition occurred where the high laser intensities passed, as seen in Fig. 3; in effect the laser beams were self cleaning. A similar observation was made in Ref. 19. Although the tunnel can be operated at pressures up to four atmospheres, all of the tests reported here were at a constant pressure of one atmosphere.

The swirl burner, Fig. 2a, is modeled after those developed at the International Flame Research Foundation (Ref. 25) and is of stainless steel construction. It contains a movable block swirl generator with an adjustable swirl number range of 0 to 2.5. The fuel nozzle tube is 1.5 cm dia. inside a 6.6 cm dia. air duct which diverges to 12.7 cm dia. at its exit plane, as shown. The quarl exit plane is approximately 21 cm from back wall of the tunnel and 8 cm upstream of the center of window #1. The JT-12 combustor can, shown unshrouded, is pictured in Fig. 2b. Its exit diameter is comparable to that of the swirl burner, and it protrudes into the tunnel 30 cm from the back wall. The can is welded into a cylindrical shroud to duct the air into and around the combustor. In the experiments to be described, the air mass flow was held approximately constant at 0.15 lb/sec for the swirl burner and about 1 lb/sec for the JT-12 can. The swirl burner swirl number was held constant at approximately 1.2. Air preheat was used for the JT-12, but not for the swirl burner.

Portable CARS Instrument

Figures 4 and 5 illustrate the optical layout of the portable CARS instrument and its arrangement about the combustion tunnel. Two different output orientations, nearly optically identical, were used, a horizontal arrangement shown in Fig. 4 and the vertical setup depicted in Fig. 5. A photograph of the CARS instrument in the burner stand test cell is shown in

FIGURE 1. ATMOSPHERIC PRESSURE COMBUSTION FACILITY

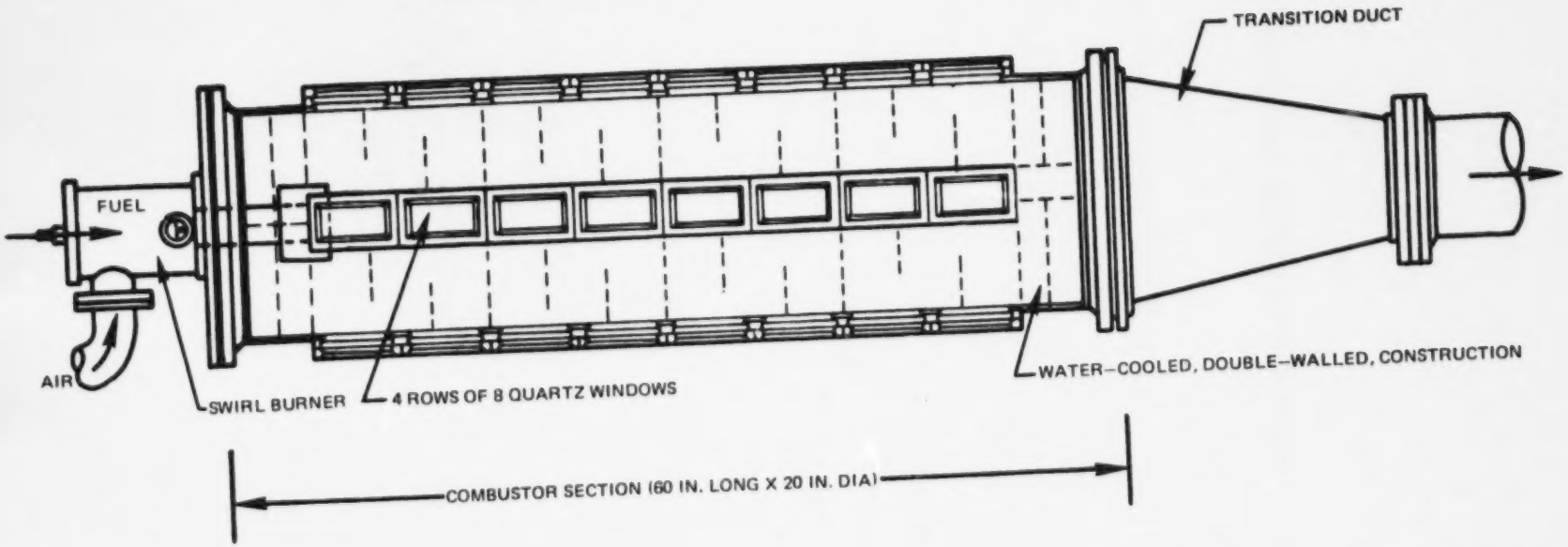

79-06-11-5

FIGURE 2. COMBUSTORS USED IN CARS DEMONSTRATIONS

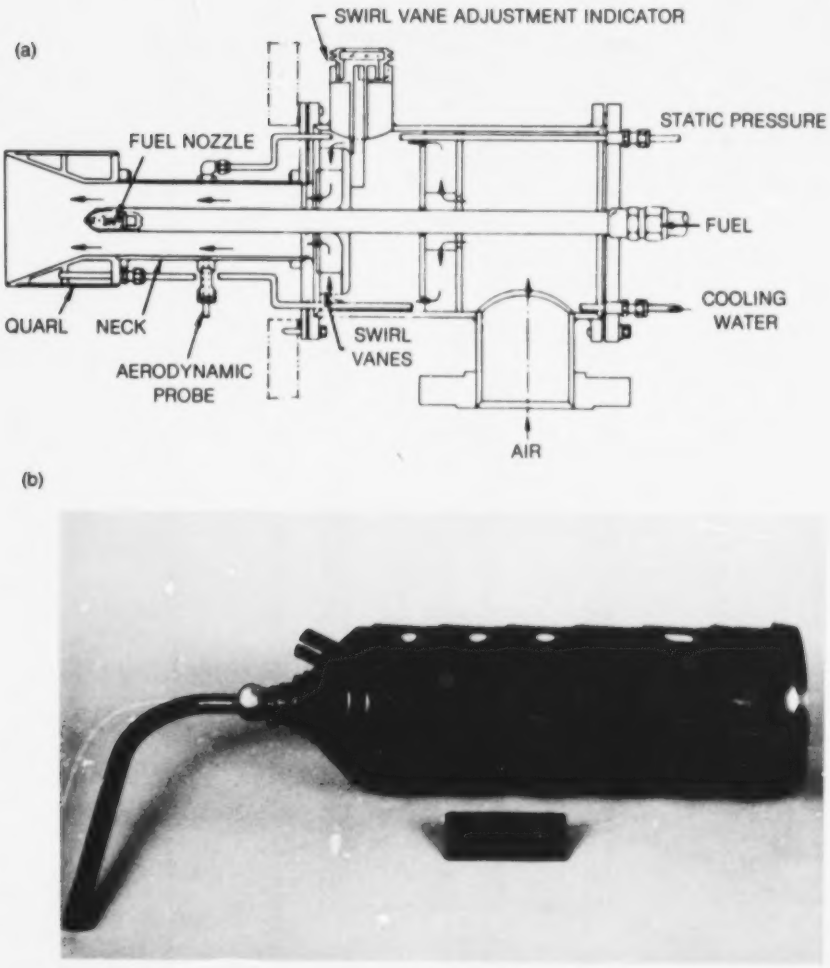

79-09-1-18

TABLE 1

UTRC ALTERNATIVE FUELS COMBUSTION FACILITY

General Characteristics and Specifications

Burner:	
Type	Swirl stabilized, air/fuel annular burner
Construction	Stainless steel
Swirl generator	Movable block
Swirl number range	Adjustable from 0 to 2.5
Fuel nozzle diameter	1.5 cm (0.60 inch) max.
Air annulus inside diameter	1.9 cm (0.75 inch)
Air annulus outside diameters	6.6 cm (2.6 inch), 5.1 cm (2.0 inch), 4.1 cm (1.6 inch)
Exit quarl diameter	12.7 cm (5.0 inch)
Fuel types	Gaseous, liquid, or pulverized solids
Air preheat temperature	400 °C (750 °F) max.
Operating pressure range	1 to 4 atm.
Nominal air flowrate	240 kg/hr (525 lb/hr)
Fuel flowrate range	8 kg/hr (17.6 lb/hr) to 14.3 kg/hr (31.5 lb/hr)
Firing rate range	3000,000 Btu/hr to 600,000 Btu/hr
Combustor	
Type	Double walled, water cooled can combustor
Construction	Stainless Steel
Inside diameter	50 cm (20 inch)
Length	150 cm (60 inch)
Optical windows	4 rows of 8 quartz windows each located at 0°, 90°, 180°, 270° around combustor
Window size	6.4 cm x 12.8 cm (2.5 inch x 5.0 inch) rectangle
Wall cooling features	20 uniformly distributed wall segments, each individually controllable
Operating pressure range	1 to 4 atm.

79-224-A

FIGURE 3. POSTRUN CONDITION OF COMBUSTION TUNNEL WINDOWS

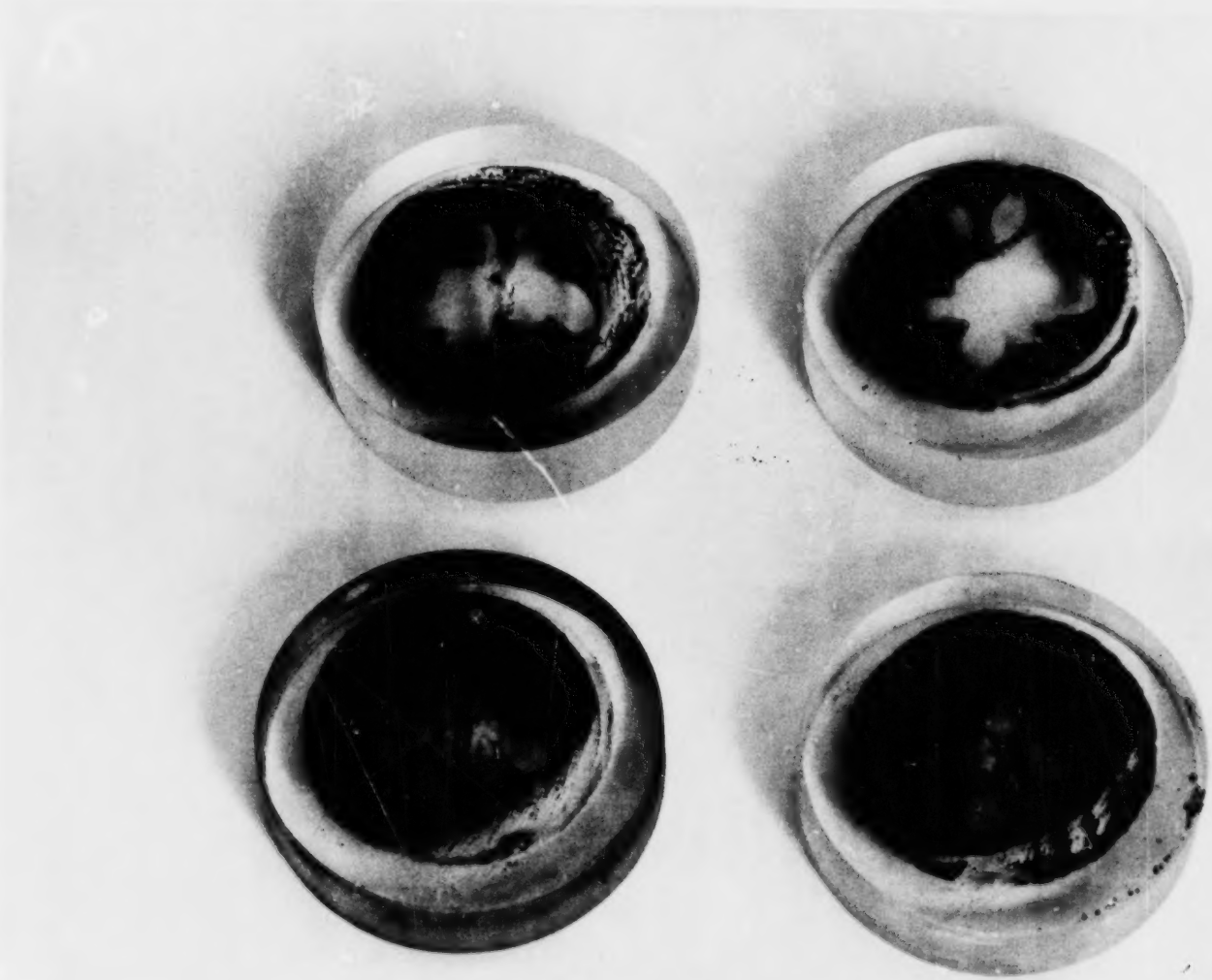

79-07-92-3

Fig. 6. The horizontal output arrangement is shown in the Fig. 7 photograph. All of the CARS components were mounted on a portable 3' x 6' Newport Research Corporation optical pallet which rode on pillow blocks and rails permitting the radial measurement location to be varied. The rails were attached to an angle iron frame fitted with heavy duty pneumatic tire casters and four permanently attached scissors jacks to raise the instrument to the proper height. The size of the pallet was dictated primarily by the size of the Quanta-Ray frequency-doubled neodymium:YAG laser. For simplicity, and since size was not a major problem, more sophisticated packaging arrangements were not investigated.

The laser emits two beams at 5320 Å by sequentially doubling the fundamental 1.06μ and residual 1.06μ from the first doubler. The primary beam energy is about 200 mJ/pulse, 10^{-8} sec pulse duration at 10 Hz. The secondary is about an order of magnitude lower. Referring to Fig. 4, the secondary green is dispersed from the remaining 1.06μ by a series of prisms and is used to optically pump the Stokes dye oscillator. The Stokes oscillator output is amplified in a dye cell in flow series with the oscillator dye cell. The amplifier is pumped by a fraction of the primary split off at a 33 percent beam splitter. The Stokes laser dye spectrum was centered at 6067 Å, midway between the ground and first vibrational state Raman shifts of N_2, the molecular species used for all of the thermometry experiments reported herein. N_2 is ideal for CARS thermometry investigations in airfed combustion processes, because it is the dominant molecular constituent and is present everywhere in high concentration independent of the extent of the chemical reaction. The dye spectrum was centered in comparison with a neon lamp spectrum by adjusting the concentration of the rhodamine 640 dye (Exciton Chemical Co.) dissolved in ethanol. The dye spectrum was approximately 170 cm^{-1} (63 Å) wide FWHH.

The Stokes laser output is magnified by a factor of two or three, passes through an optical flat which can be rotated to vary the BOXCARS phase-matching angle (Ref. 23) and reflects off the dichroic D to the beam crossing and focussing lens. The remaining primary beam is split into two components in the manner shown; these components are aligned parallel and sent to the crossing/focussing lens after transmission through the dichroic. Based upon the size of the combustor and the desire to be able to radially vary the measurement location, long focal length crossing/focussing lenses, i.e., 480 mm, were employed. This diminishes the CARS generation efficiency, e.g., relative to a laboratory situation, due to the strong dependence of the signal on laser intensity. The pump beams were crossed at a half angle of 1.1° or 0.77° depending on when the tests were performed. With the latter configuration, the spatial resolution was experimentally measured by generating CARS from within a translatable 1 mm thick microscope slide. Ninety-percent of the spatially integrated CARS was generated over a 1.2 cm axial extent. The measurement volume is a cylinder approximately 0.5 mm in diameter by 1.2 cm long oriented

FIGURE 4. SCHEMATIC LAYOUT OF PORTABLE CARS APPARATUS

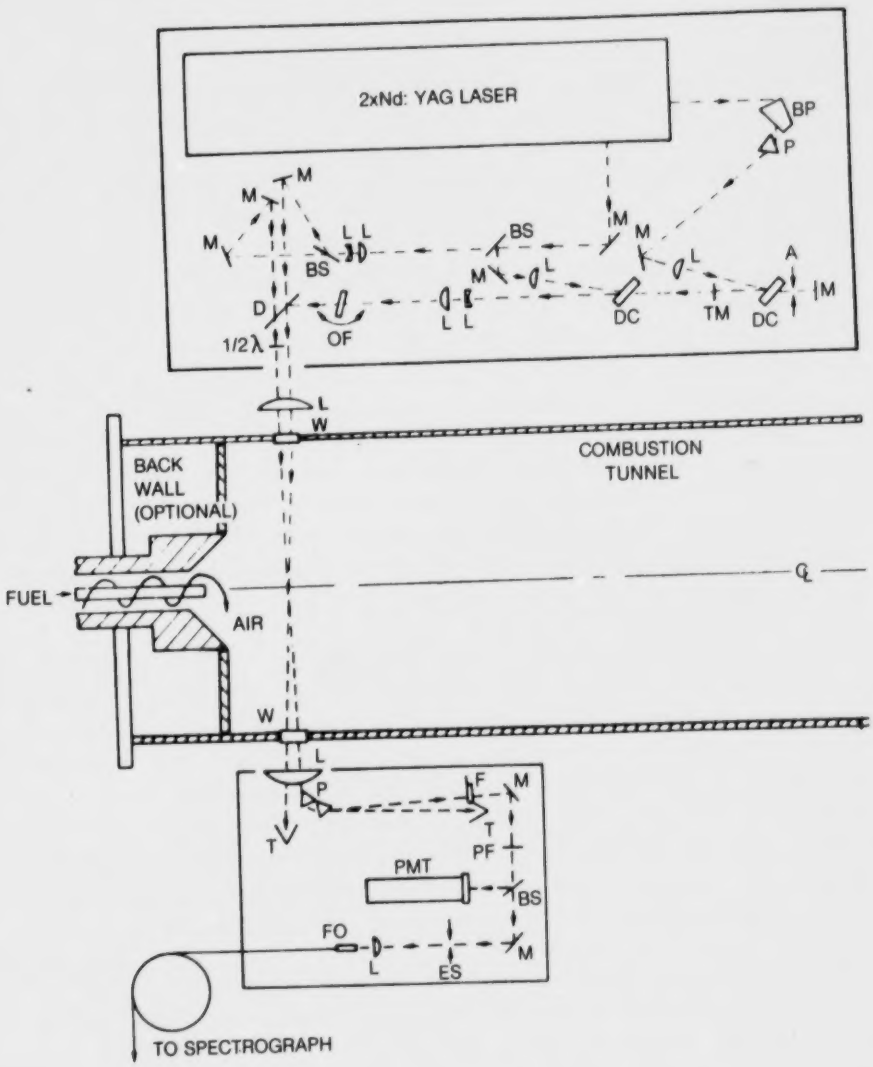

79-09-1-17

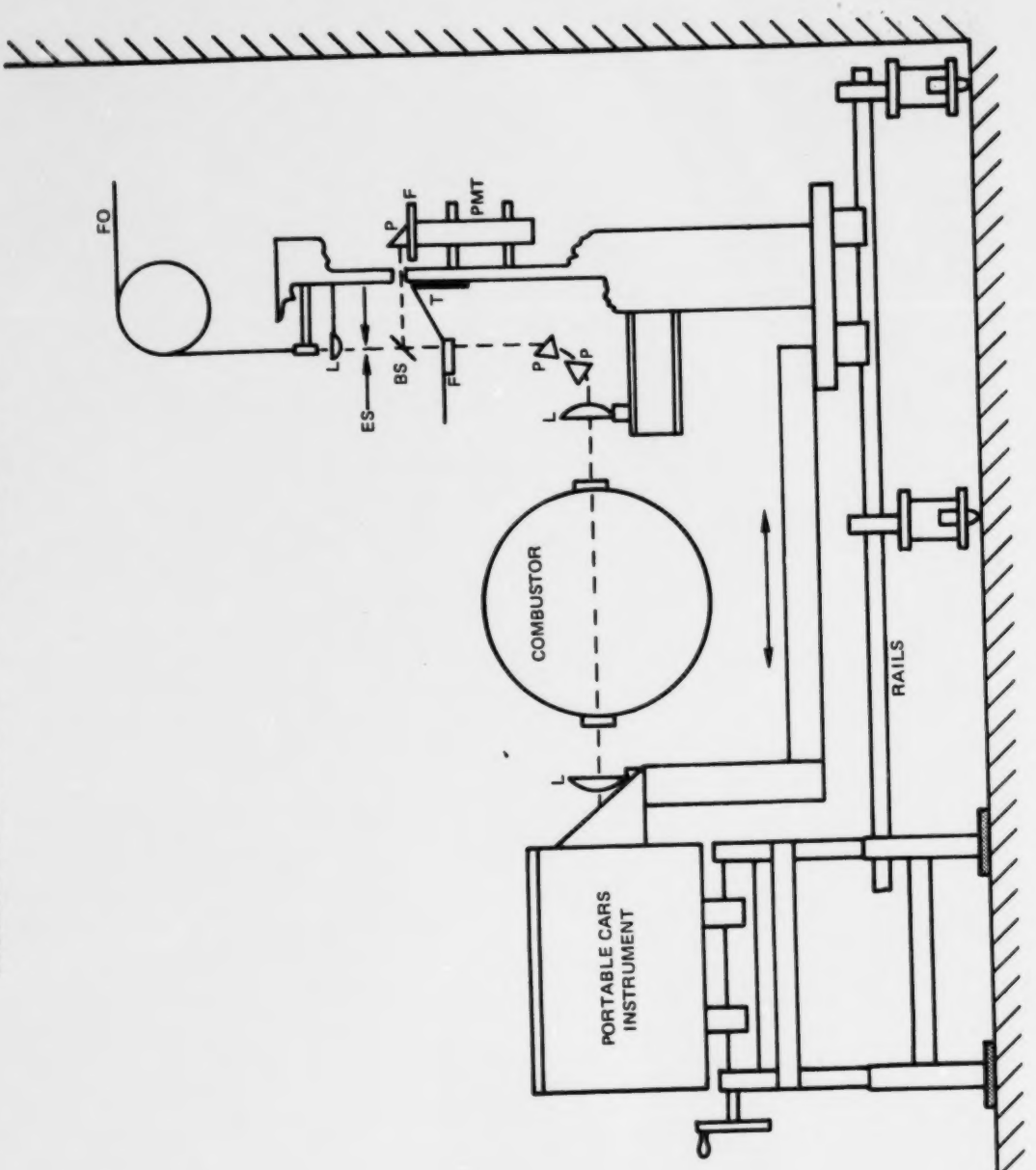

FIGURE 5. BOXCARS SETUP IN JET BURNER STAND

79-06-11-2

FIGURE 6. PORTABLE CARS INSTRUMENT IN JET BURNER STAND

79-172-C

79-07-92-1

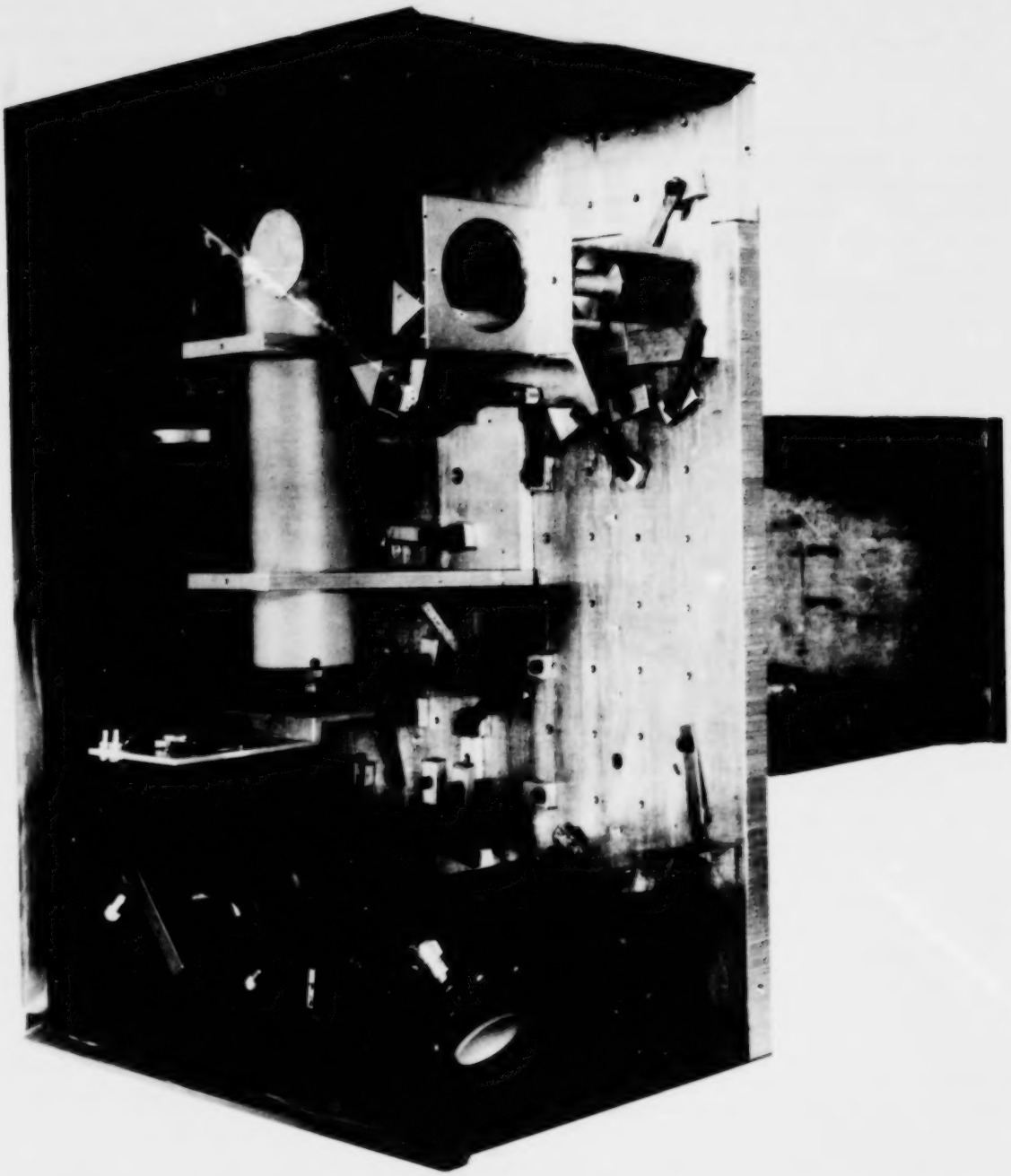

FIGURE 7. HORIZONTAL DISPERSION OUTPUT OPTICAL ARRANGEMENT

79-224-8

79-07-92-2

transverse to the flow axis. The axial resolution would be slightly better at the larger crossing angle, ~ 0.9 cm. A telescope (M = 0.83 or 1.2) is inserted in the primary leg to vary the wavefront curvature so that the beam waists coincide at the crossing point.

Upon emerging from the combustor, all beams are recollimated by a lens, and the one pump component and adjacent Stokes beam are trapped. The CARS is dispersed from the remaining, overlapping pump component by the prisms shown. This pump component is trapped and the CARS passes through cutoff and polarization filters. A microscope slide intercepts a fraction of the CARS signal which is sent to a photomultiplier tube fitted with a narrowband (10 Å) interference filter, which spectrally integrates the CARS signature. The output of the photomultiplier is sent to a boxcar averager, which is used for peaking up the optical alignment of the setup. In principle, this integrated signal, if appropriately normalized, could be employed for density determination (Ref. 15). The CARS radiation after the splitter slide passes through an electronic shutter to a lens which focusses the CARS into a 60 μ dia. optical fiber (Siecor 133) which is 20-m long. The fiber transmits the CARS to the spectrometer/optical multichannel analyzer located in the benign environment of the nearby control room. The electronic shutter is used to sample individual CARS pulses from the 10 pps train of signal pulses if desired.

The signal dispersion and collection were performed either horizontally (Fig. 4) or vertically (Fig. 5). In either case, the assembly was attached to a base fitted with pillow blocks riding on 2.5 cm dia. rails. The assembly is mechanically linked to the input side of the CARS instrument permitting tandem translation of the optics. The laser beams employed were horizontally polarized. With the vertical dispersion setup, a half-wave plate was added to one of the pump components to rotate its polarization to the vertical. This rotates the CARS polarization into the vertical plane (Ref. 26) and provides better CARS transmission through the dispersing prisms. In such a case, the CARS is generated from the combined third order susceptibility components, $\chi_{1122} + \chi_{1212}$, where the subscripts refer to the polarization orientation of ω_3, ω_1, ω_1, and ω_2, respectively. The CARS spectrum in this case is identical to that generated with aligned polarizations, i.e., through χ_{1111}, for a major molecular species such as N_2 possessing a small depolarization ratio. In the results to be shown, the output orientation employed is identified by the susceptibility component(s) used. The horizontal arrangement was ultimately employed to permit greater radial traversing than that permitted by the vertical scheme which was limited by overhead obstructions.

The CARS radiation emerging from the 60-μ dia. optical fiber was inserted directly into the spectrometer, an Instruments SA 0.6 m HRP, fitted with an optical multichannel analyzer (PARC 1205A and 1205D SIT). A small diameter fiber was purposely chosen to achieve good spectral resolution and to eliminate

the requirement for transfer optics (Ref. 24). The CARS transmission efficiency through the spectrometer was approximately 30 percent, the loss occurring since the f number of the spectrometer ($\sim$ 6.5) exceeded that of the optical fiber, $\sim$ 3.6. Except for small input and output coupling losses, about 10 percent collectively, all of the CARS was transmitted through the low loss optical fiber (< 10 dB/km). The spectral resolution with this arrangement at the N_2 CARS frequencies was checked using a xenon lamp and found to be slightly better than 2 cm^{-1}.

Experimental Program

Calibration

Prior to transport to the jet burner test stand, the CARS system was calibrated by performing temperature measurements in a premixed CH_4/air flame. Previous studies at UTRC (Refs. 14, 27) indicated that CARS temperature measurements from N_2 were accurate to within 40K at flame temperatures, using constant Raman linewidth computer codes. With improved codes, which calculate the Raman linewidth as a function of temperature and rotational quantum number, similar accuracies are also attained (Ref. 28). These refinements occurred subsequent to the conduct of the investigations described. Temperature is deduced from the shape of the CARS signature which is very temperature sensitive as shown in Fig. 8. There, as an example, is displayed the calculated temperature dependence of the N_2 CARS spectrum at a resolution of 1 cm^{-1}. At low temperatures, one sees the $v = 0 \rightarrow 1$ band containing low J value Q branch transitions, i.e. $\Delta J = 0$, where J is the rotational quantum number. As is apparent the low J Q branches are unresolved. As the temperature increases the band broadens as the rotational population distribution spreads out due to the vibration-rotation interaction, $\alpha_e J(J + 1)$. At high temperatures, the spreading of the band is sufficiently large to permit the resolution of the individual even J Q transitions, ranging from Q(20) to Q(40). The odd Q transitions, which have a nuclear spin weighting equal to half of the even numbered transitions are reduced in intensity by a factor of four and do not stand out. At intermediate temperatures, few Q branch lines are resolvable. For Q branch transitions beyond Q(40), overlap with the $v = 1 \rightarrow 2$ band transitions occurs giving rise to two prominent peaks in the "hot" band, so termed because it appears only at higher temperatures. At the lower spectral resolution, $\sim$ 2 cm^{-1}, employed in the experiments here, the fine structure shown in Fig. 8 is not as pronounced. This is actually advantageous since the full width of the ground state band at half peak height (FWHH) exhibits a smoother temperature variation than at high resolution. Temperatures are deduced from the N_2 CARS spectra from the full width at half maximum of the ground state band (FWHH) and the ratio of the hot band to ground state band peak heights (phr) at elevated temperatures where a hot band is exhibited.

FIGURE 8. TEMPERATURE VARIATION OF N_2 CARS SPECTRUM

$\Delta\omega_1 = 0.8\ CM^{-1}$

$\Delta\omega_2 = 130\ CM^{-1}$

$SLIT = 0.75\ CM^{-1}$

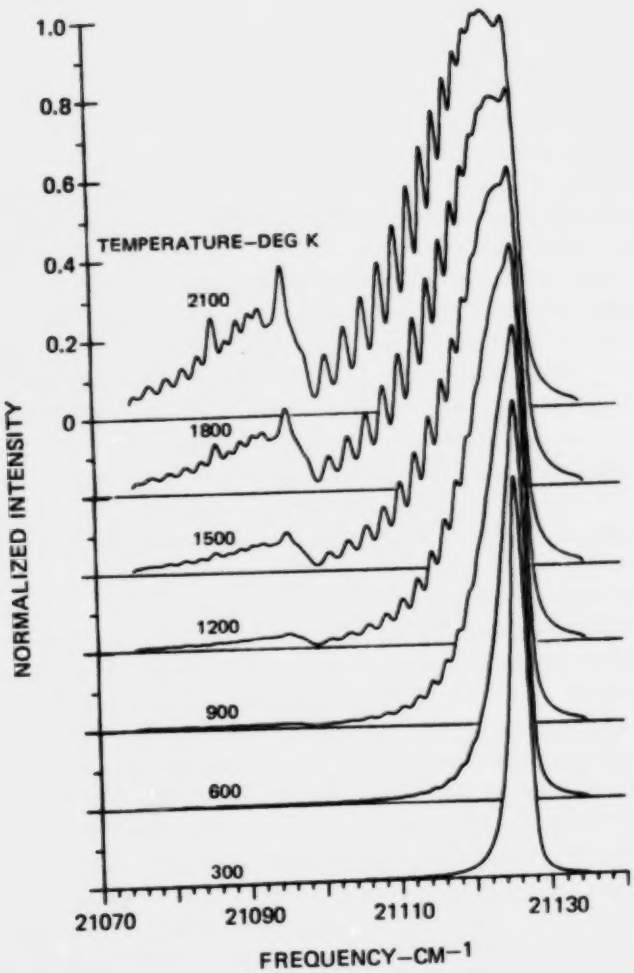

79-02-180-7

Computer code calculations of N_2 CARS spectra were performed in 100 K increments from 300°K to 2400°K for parameters corresponding to the portable CARS instrument, i.e., $\Delta\omega_1 = 0.8\ cm^{-1}$, $\Delta\omega_2 = 170\ cm^{-1}$, slit = $2cm^{-1}$. From these spectra, the FWHH and phr were obtained and are shown plotted as a function of temperature in Fig. 9. These curves serve as a simple algorithm to extract gas temperature from the N_2 CARS spectra. At this resolution, the FWHH variation is relatively smooth. The slight undulation at high temperatures is caused by some Q transition fine structure. In all of the data to be subsequently displayed, temperatures were deduced from the Fig. 9 curves.

Figure 10 displays a calibration point in a methane-air flame at 2110°K sustained on a 2.5 cm dia. array of hexagonally arranged, stainless steel hypo tubes. At the flow rates employed, the temperature was measured using a radiation-corrected, coated fine wire, thermocouple. The radiation correction was experimentally determined from sodium line reversal temperature measurements. The spectrum exhibits the features displayed in Fig. 8 but at slightly lower resolution. The dispersion on the optical multichannel analyzer was determined using a xenon lamp which has a multiplicity of transitions in the N_2 CARS wavelength region. The phr of 0.33 yields a temperature of 2140°K and the FWHH of 14.1 cm^{-1} indicates 2125°K in good agreement with the classically measured temperature of 2110°K. Later in the report, comparisons are presented of CARS temperatures and specially designed thermocouple probe measurements in the JT-12 can exhaust.

Swirl Burner Measurement Results

The initial measurements on the feasibility of CARS in practical environments were conducted in the swirl burner operating on gaseous propane. The propane was injected radially outward from the central fuel tube into the swirling, coannular air stream to promote rapid fuel/air mixing. In these tests, attention was focussed primarily on the feasibility and quality of CARS generation rather than on measurement acuracy per se.

In Fig. 11 are displayed CARS signatures of N_2 for various stoichiometries as indicated by the overall equivalence ratio at the window #1 axial location (x = 6 cm downstream of the quarl exit plane) and slightly off-axis. The CARS spectra were averaged on the optical multichannel analyzer (OMA) for 10-15 seconds corresponding to 100-150 laser pulses. In situations where turbulent temperature fluctuations are large, it is not valid to average the CARS spectra to extract average medium properties due to the nonlinear behavior of the CARS signal level with temperature and density. In examining the real time display on the OMA, the spectra exhibited minor fluctuations and the averaged spectra are probably representative of the mean temperature. Single pulse spectra

FIGURE 9. THERMOMETRY ALGORITHM FOR N_2 CARS SPECTRA

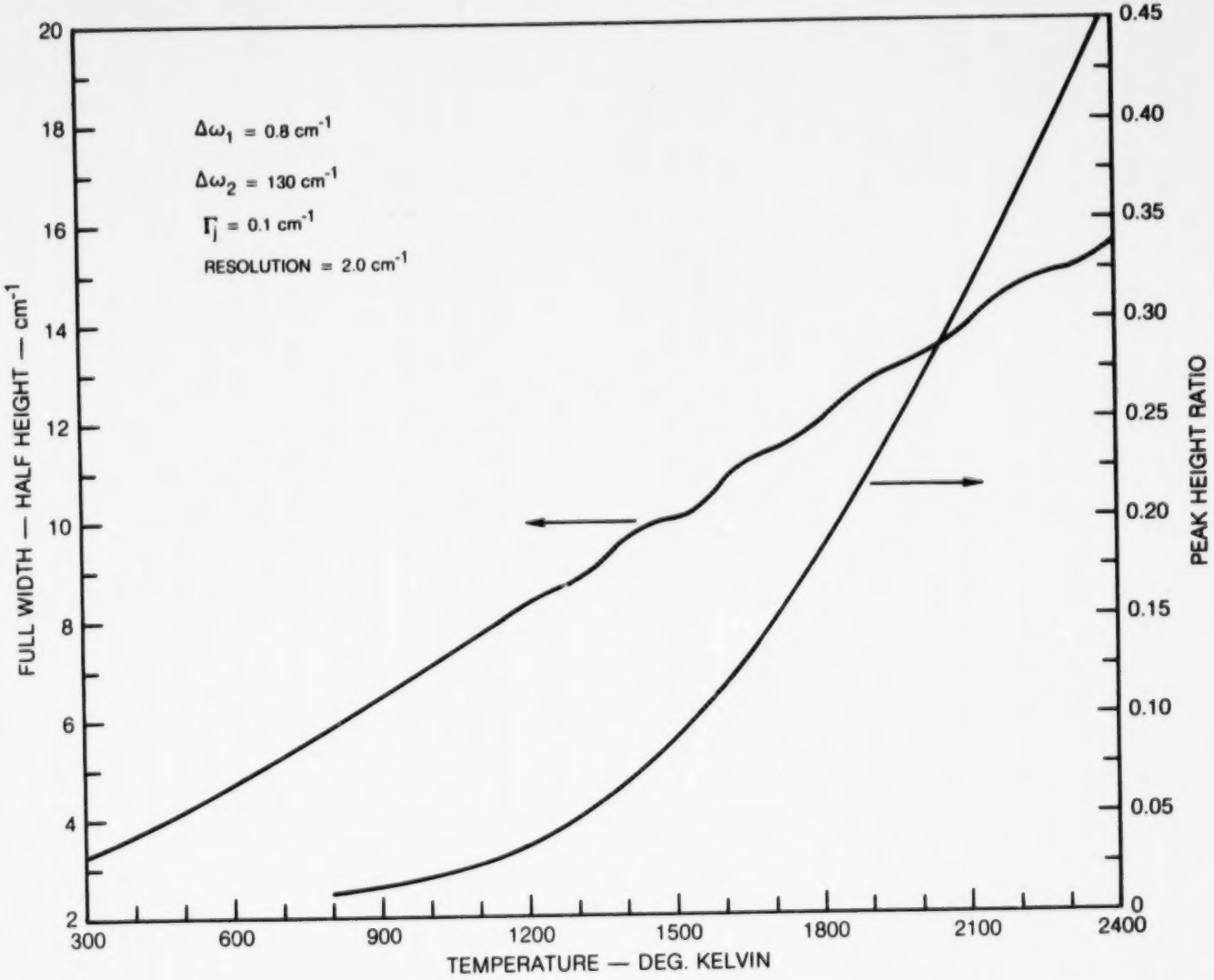

79-09-1-19

FIGURE 10. CARS TRANSMISSION THROUGH A 60μ DIA., 20m LONG, OPTICAL FIBER

SPECTRUM FROM FLAME N_2 AT ~2110°K

4/12/79–5a

79-04-96-1

FIGURE 11. TEMPERATURE VARIATION WITH STOICHIOMETRY IN MODEL COMBUSTOR

AIR 0.15 lb/sec, FUEL C_3H_8(g); $\bar{r}$ = 5cm, x = 6cm; $\chi_{1212} + \chi_{1122}$

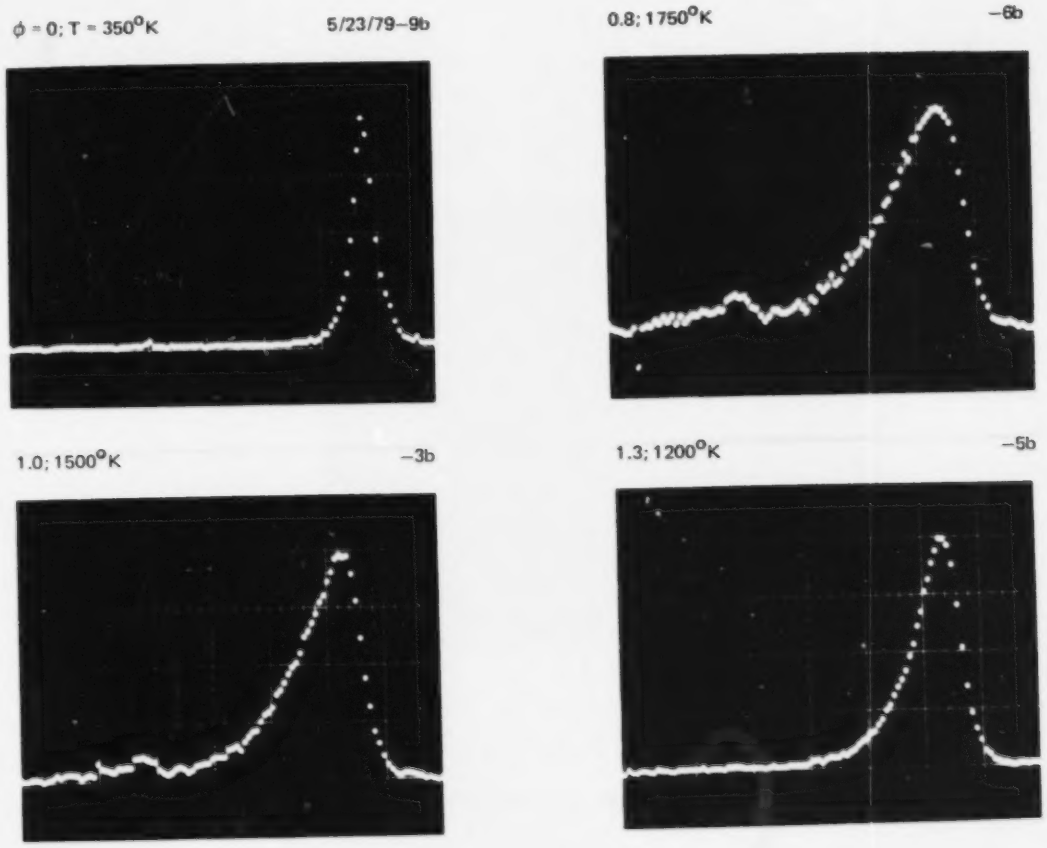

will be displayed later. The Fig. 11 spectra are quite typical of N_2 spectra as described earlier and seen in a variety of other flames (Refs. 14, 16, 26, 27). For the high temperature data, the temperatures deduced from both the FWHH and phr were in very good agreement, i.e. within 50K. Shown for reference purposes in Fig. 11 is the CARS spectrum from flowing air just after combustor shutdown. The rounded and sloping nature of the lower right hand side of the Q-branch ground state bandhead is due to coma in the 0.6 m Czerny Turner monochromator and does not greatly affect data reduction. Because of the combustion tunnel volume and water-cooled walls, the peak temperatures produced are well below the nominal adiabatic flame temperature. The highest temperature recorded at the specific measurement location was at an overall equivalence ratio, ϕ of 0.8 and was 1750°K. With increases in fuel flow, the temperature decreased to 1500°K at ϕ = 1.0 and to 1200° at ϕ = 1.3 due probably to a shift in the peak heat release location farther downstream in the tunnel.

The propane flame exhibited only a slight degree of sooting in the measurement location at which the Fig. 11 data were taken. Thus potential soot attenuation effects are likely to be negligible. This permits an assessment of the effects of turbulence on CARS generation, at least in this instance. Factoring out signal variations due to the density changes at the various temperatures, the Fig. 11 spectra were of comparable magnitude over the range of stoichiometries examined. Furthermore, the magnitude of the ground state band peak scaled in accordance with computer code predictions (Ref. 14) when the flame was extinguished, i.e., when comparing the flame and cold gas signal levels. In addition, the cold gas signal showed little effect of turning the air flow on and off. Thus the presence of combustion and flow had little influence on the efficiency of CARS generation other than that anticipated. The signal levels of the Fig. 11 data are low due to optical fiber damage, which resulted in over an order of magnitude attenuation in signal transmission through the fiber. The fiber was replaced prior to the Jet A fuel tests which are described below and to which a discussion of absolute signal levels is deferred.

In Fig. 12 are shown data taken with Jet A fuel at two different axial locations in the model combustor at an overall equivalence ratio of 0.8. With Jet A fuel, the combustion process was extremely luminous and highly sooting. Visually it was difficult to view for any extended period. With the degree of swirl employed, the flame, as perceived from the soot luminosity, expanded rapidly and appeared to fill most of the tunnel. At the window #1 location, CARS measurements were made through the spray 11 cm downstream of the fuel nozzle and the temperature was found to be about 900°K. Moving downstream to window #3, where the flame was very luminous and turbulent, the temperature increased to 1500°K. The hot spectrum displayed in Fig. 12 is of very high quality and as fine as those typically produced in laboratory experiments, e.g. Fig. 10. It was obtained after averaging for 10 sec (100 pulses) and the per

FIGURE 12. SPATIAL VARIATION OF TEMPERATURE IN MODEL COMBUSTOR WITH JET A FUEL

AIR 0.15 lb/sec , $\phi = 0.8$ r = 5mm

x = 6cm T = 900°K

5/25/79–2b

x = 38cm T = 1500°K

–10b

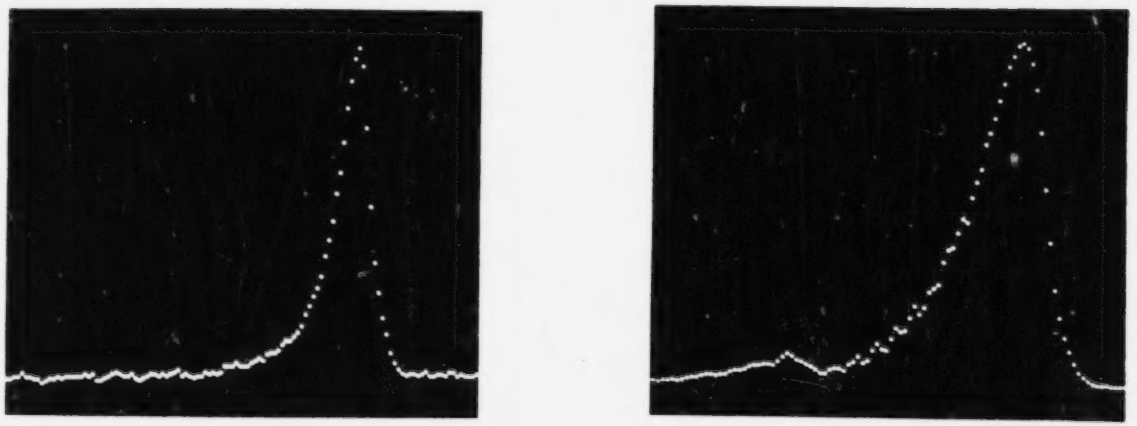

FREQUENCY ⟶ 0.586 cm^{-1}/DOT

pulse peak height count is about 350 on the optical multichannel analyzer, which corresponds to about 4400 photons in a thin spectral slice about the peak. This is about a factor of eight below the intensity one would calculate for the experimental parameters employed (Ref. 2), but quite typical of the signal magnitude agreement between pulsed CARS calculations and experiments, even in well characterized situations (Refs. 9, 10). The strength of the 1500°K spectrum also scales appropriately, to within a factor of two, from the cold gas signal levels. Furthermore, the signals were comparable to those obtained in laboratory simulations in flat flames. All of this is indicative that at this equivalence ratio, 0.8, the combined effects of soot and turbulence in this case were not very severe. Single shot measurements in the spray, i.e., at x = 6 cm, indicated fairly large fluctuations in temperature, and, thus, averaging of the spectra to extract a mean temperature there is suspect. The temperature listed is a density weighted average, probably to the low side of the true mean temperature, and likely to be in error by 100K or more. There is also evidence that the efficiency of CARS generation was lower in the region of the spray, perhaps by an order of magnitude. A more thorough investigation would be required to quantize these effects rigorously. Nevertheless, these initial investigations of CARS generation through the spray are encouraging. With proper window purging, operation with Jet A fuel posed no particular problems relative to gaseous fuels except for the increased window sooting tendency. Due to this fact, all further testing was conducted using the liquid fuel.

In an attempt to simulate a furnace more closely, a refractory back wall was fabricated from asbestos millboard and placed flush with the burner exit plane as sketched in Fig. 4. This alteration posed no particular problems for the CARS measurements. CARS measurements were again made at window location #3 and are displayed in Fig. 13 for three different stoichiometries with Jet A fuel. The small temperature changes which occur with variation in the stoichiometry are indicative of the temperature sensitivity of the CARS spectra. As before the temperatures are believed accurate to about 50K. At the overall equivalence ratio of 0.8, the signal level as before, is consistent with expectations. With increases in fuel flow to overall equivalence ratios of 1.0 and 1.2, the CARS signals decreased by factors of about three and ten, respectively. At least half of these decreases are attributable to increased window fouling, i.e., when the fuel was quickly leaned out, the signal returned to only half of its former level. Despite the attenuation experienced at the higher soot loadings, laser-induced soot interferences, sometimes encountered in highly sooting flames (Ref. 17) were not seen. For thermometry, which derives from the shape of the spectrum, the attenuation by soot should cause no particular problem as long as the CARS signals remain acquirable and with good photon statistics. For density measurements, which depend upon the absolute signal level, this will be more problematical. The attenuation will have to be measured and then corrected for, a procedure likely to degrade measurement accuracy. One approach would be to place parallel CARS reference cells (Ref. 15) both before and after the test region; these would not only normalize pulse-to-pulse signal variations in the usual manner, but permit estimation of the soot extinction encountered.

FIGURE 13. STOICHIOMETRIC CARS TEMPERATURE VARIATION IN SWIRL BURNER WITH REFRACTORY BACK WALL

JET A FUEL, AIR FLOW 0.15 lb/sec; x = 38 cm; χ_{1111}

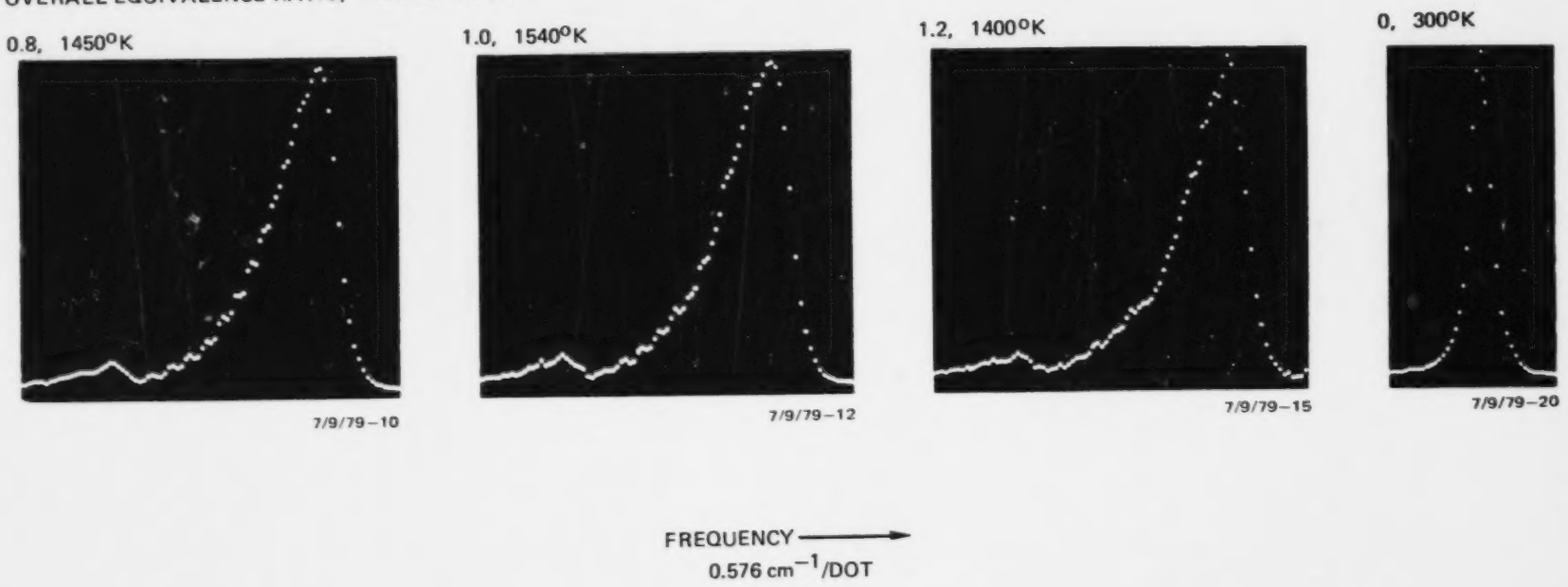

79-07-80-2

As alluded to earlier, in highly turbulent environments characterized by large fluctuations in density and temperature, the CARS spectrum must be captured and temperature information extracted with each pulse. By repeating these measurements a statistically significant number of times, one is able, barring sampling biasing errors, to obtain the temperature probability distribution function, pdf. From the pdf, the average temperature at any one location and the magnitude of the turbulent temperature fluctuations there can be ascertained. In Fig. 14 is shown a single 10 nanosecond CARS spectrum of N_2 at window #3 in the swirl burner fueled with Jet A. A single pulse was captured from the 10 Hz train using the electronic shutter with an aperture duration of $\sim$75 millisec. This permits capture, with high probability, of only a single pulse. Also shown for comparison purposes, is the CARS spectrum averaged for 13 seconds ($\sim$130 pulses). The single pulse spectrum is of slightly lower quality due to the weakness of the signal ($\sim$500 counts at peak) and the high dark current on the OMA vidicon. The latter leads to poor noise subtraction over the ten cycle scan used to "read" the tube. Some irregularity in the single pulse spectrum also occurs due to spectral structure on the Stokes dye laser, i.e., it is not perfectly smooth. These dye spectrum irregularities average out in time. The data displayed in Fig. 14 demonstrate the feasibility of single pulse CARS thermometry and, when coupled with computer controlled data acquisition, will permit pdfs to be acquired in a reasonable amount of time, e.g. 1-2 minutes. The single pulse spectral temperature at any instant should not necessarily agree with the average temperature and depends on the scale of the turbulent fluctuations. The single pulse temperature was 1485°K from phr and 1550°K from FWHH. The hot band contains about 50 counts at peak and thus is susceptible to a statistical variation of $\pm$ 14%, i.e., $N^{-1/2}$, or a phr temperature uncertainty of $\pm$ 60 K. The single pulse measurement error, conservatively, may be as high as $\pm$ 100 K. In assembling a probability distribution function, these statistical uncertainties would tend to average out and the pdf would be more accurate than the individual single shot measurement accuracy however.

JT-12 Combustor Exhaust Measurements

CARS measurements were also performed in the exhaust of a shrouded JT-12 combustor can burning Jet A fuel. The air flow rate of about 1 lb/sec is about seven times that employed for the previously described swirl burner. The can possesses an exit diameter of 12.5 cm and CARS measurements were made 13 and 82 cm downstream of the can exit. CARS signatures at the former location are displayed in Fig. 15. CARS measurements were made at the latter location since temperature probe data was available there for several operational conditions (Ref. 29). The probe used was a water-cooled, aspirating thermocouple (Aero Research Instruments, Model T-1006-6). In Table 2 is presented a comparison of the CARS and thermocouple measurements at several operational settings together with the air and fuel flowrates and air inlet temperature for

FIGURE 14. SINGLE PULSE CARS THERMOMETRY IN SWIRL BURNER WITH REFRACTORY BACK WALL

ϕ = 0.8, JET A FUEL, AIR FLOW 0.15 lb/sec; x = 38 cm; X_{1111}

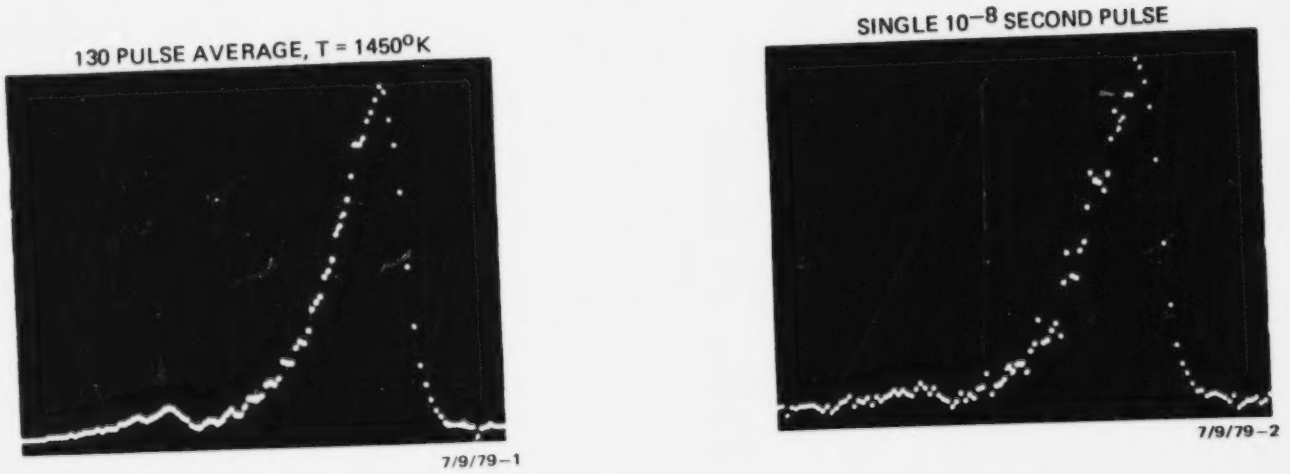

79-07-80-1

FIGURE 15. OPERATIONAL TEMPERATURE VARIATION IN JT–12 EXHAUST

CARS MEASUREMENT : 13.2 CM DOWNSTREAM OF CAN EXIT PLANE

FLOWRATES :	AIR	FUEL (JET A)	T_{IN}
IDLE	1.07 LB/SEC	40.9 LB/HR	333°K
CRUISE	1.02 LB/SEC	52.5 LB/HR	513°K

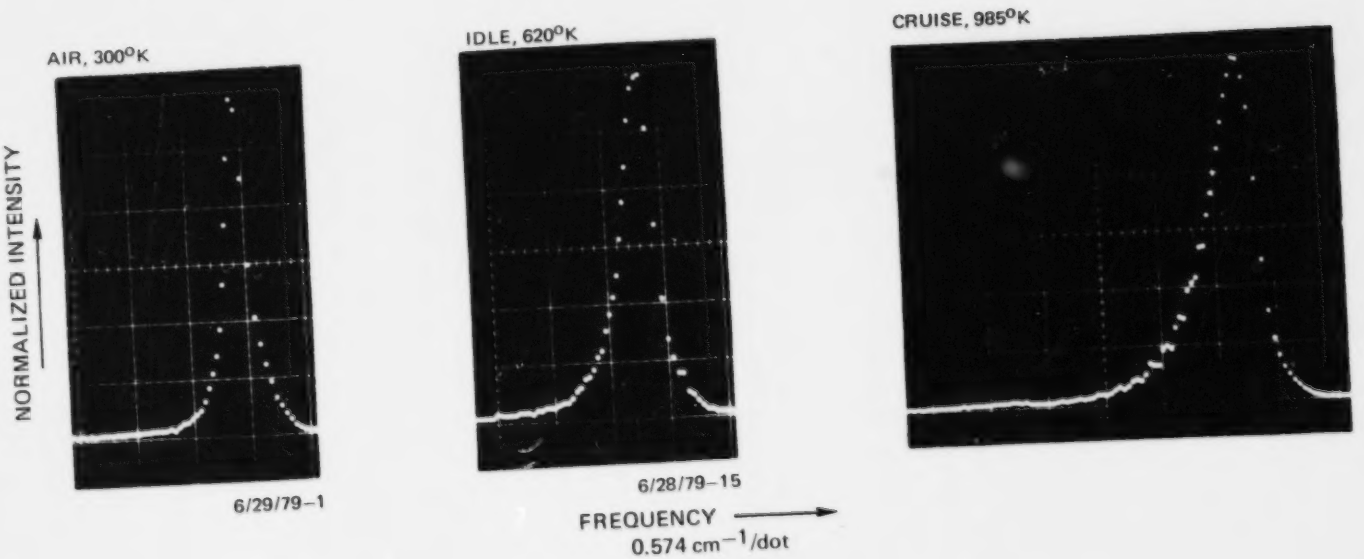

79–06–163–2

those conditions. The variation on the thermocouple measurements is believed to be representative of the resetability of combustion conditions in the JT-12 over a period of time. This is appropriate in the present context since the probe and CARS measurements were made several weeks apart. Similar variations in combustor operation were also found during a given run from the CARS measurements. As can be seen, considering the circumstances, the agreement between the two sets of data is fairly good and lends credibility to the CARS measurements.

With the horizontal dispersing arrangement (Fig. 4), the CARS measurement location could be radially translated by about $\pm$ 6 cm. In Fig. 16 is shown the radial temperature profile from the JT-12 can at cruise conditions 13 cm downstream from the can exit. As might well be expected, the temperature profile is relatively flat. The temperature variation at the centerline is due to variations in the fuel and air settings over a period of time. Similar temperature variations could also be expected at the other radial locations if more data had been taken. Also shown is a centerline measurement at the idle condition.

In Fig. 17 is shown a comparison of a single CARS pulse and an averaged CARS spectrum in the JT-12 exhaust at cruise. Due to the lower temperatures in the JT-12 exhaust relative to the swirl burner and, hence, higher gas densities, the single pulse spectra are of higher quality and nearly identical qualitatively to the average as can be seen. The single pulse and average temperatures deduced from FWHH are 980 and 1050°K, respectively. Here the discrepancy results probably from some single pulse fine structure on the Stokes laser which is evident in the single pulse CARS spectrum. Such effects could most likely be minimized by ascertaining the temperature from a spectral fitting routine, e.g., least mean squares. For all of the averaged JT-12 measurements displayed (Fig. 15), the CARS signal to the OMA was attenuated by an order of magnitude with a neutral density filter to prevent the vidicon from saturating.

TABLE 2

COMPARISON OF CARS AND THERMOCOUPLE MEASUREMENTS
IN JT-12 COMBUSTOR EXHAUST

Operating Condition	Idle	Cruise	Max. Continuous
Air Flow (lb/sec)	1.07	1.02	1.00
Jet A Flow (lb/hr)	40.9	52.5	54.9
T_{inlet} (^{o}K)	333	513	522
T_{CARS} (^{o}K)	580	875	875
T_{TC} (^{o}K)	590 $\pm$ 50	900 $\pm$ 50	920 $\pm$ 50

FIGURE 16. BOXCARS TEMPERATURE PROFILE OF JT–12 EXHAUST

13.2 CM DOWNSTREAM OF CAN EXIT PLANE

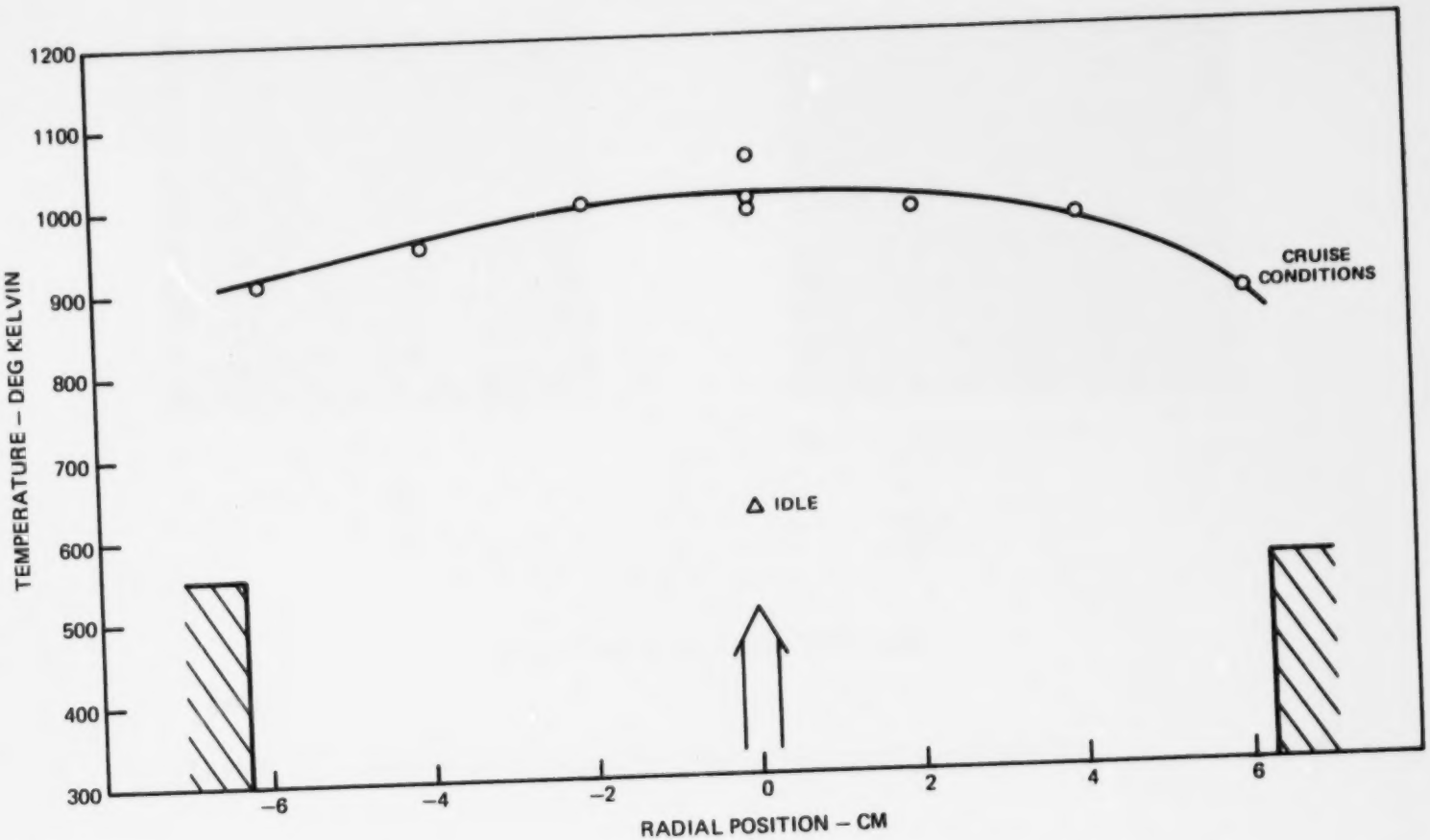

79–06–163–3

FIGURE 17. SINGLE PULSE BOXCARS THERMOMETRY IN JT–12 EXHAUST

CRUISE CONDITION, P = 1 ATM, $T_{CARS} \cong 1050^{o}K$

SINGLE PULSE (10^{-8}SEC)

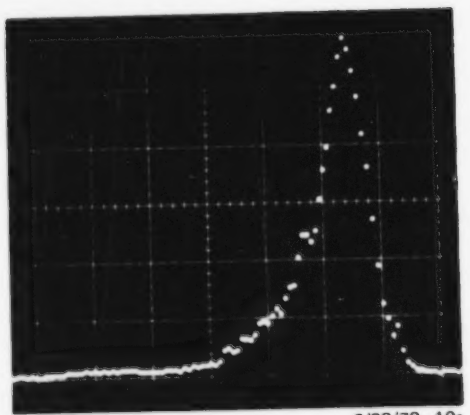

6/28/79–10a

100 PULSE AVERAGE (10 SEC)

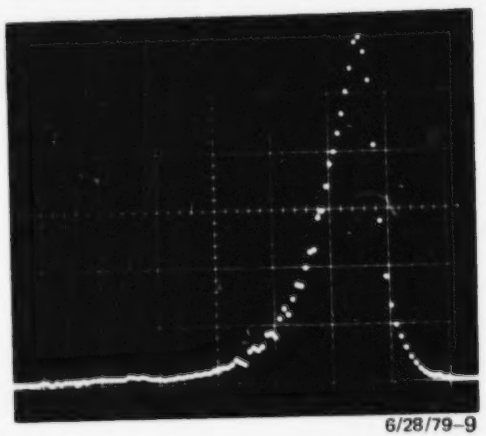

6/28/79–9

FREQUENCY ⟶

0.574 cm^{-1}/dot

79–06–163–4

TASK II-OPTICAL COMPOSITION

INVESTIGATIONS OF LASER INDUCED SATURATED FLUORESCENCE FOR TRACE SPECIES DETERMINATIONS

Introduction

There is an obvious need for diagnostic techniques which measure atomic and molecular species concentrations in combustion media. Such techniques will facilitate a better understanding of the kinetics of combustion processes which, in turn, could lead to a more optimum utilization of alternate fuels and perhaps, to a reduction in pollutant emission levels. Two different approaches to species measurement are probe and optical sampling. Probe sampling suffers the disadvantages of physical intrusion into the medium under study, and sample change by reaction in lines before analysis, for example, by a mass spectrometer. Optical techniques have the advantage that they are nonperturbing and capable of in-situ measurements. Of these, optical absorption, laser-induced fluorescence spectroscopy (LIFS), and coherent anti-Stokes Raman spectroscopy (CARS) are being used for species identification and for temperature measurement. Optical absorption is a well-established technique, but inherently yields poor spatial resolution. The measured species concentration is in fact averaged over the optical absorption path length. For an inhomogeneous medium, this average may differ significantly from the actual concentration at any one point. In contrast, LIFS is a spatially precise technique which is very sensitive and capable of trace species detection. Basically, the concentration is found from the intensity of the LIFS emission. Historically, a problem associated with fluorescence techniques has been the need to make quenching corrections to the measured fluorescence intensity. This is difficult to do accurately and, indeed, impossible unless constituent partial pressures and quenching rates are known a priori. Fortunately, the quenching problem can be avoided if one employs optical saturation of the electronic transition producing the LIFS emission. For this case quenching rate corrections are not needed, or can be extracted from the saturated fluorescence data along with the species concentration. Also, under saturation conditions the fluorescence signal is a maximum; hence, species detectivities are increased, particularly in instrumentally hostile environments such as flames or discharges. The CARS technique is capable of high spatial precision, and is regarded as complementary to LIFS in that is is applicable to temperature measurements and to major species determination (concentration of 0.1% or higher). This is a most fortunate coincidence because the species measurable with CARS, i.e., N_2, O_2, H_2O, CO, and CO_2, do not have strong electronic absorptions in the visible-near ultraviolet spectral region and are precluded from LIFS measurements.

LIFS is not applicable to all atomic and molecular species since there are specific criteria which must be met. First, the molecule, upon excitation to a higher energy state by absorption of laser radiation, must not dissociate prior to emission; obviously, in such a case, the molecule would

have no emission spectrum. Unfortunately, this is the case with many polyatomic species. Second, the molecular absorption wavelength must be accessible to a tunable laser source in the UV-visible region. Third, it is necessary to know the Einstein coefficient for spontaneous emission of the emitting level. Finally, the uncertainties introduced by quenching of the fluoresence must be dealt with. As indicated above, a way to avoid the quenching problem is to saturate the absorbing transition with a laser having high spectral intensity. The additional requirement for saturation of the laser-excited transition restricts the number of molecular species which are viable candidates for quantitative LIFS measurements. Section VII of Ref. 1 describes how the choice can be made; Section III of Ref. 1 provides the necessary spectroscopic data for making the choice.

To date, saturated LIFS concentration measurements have been made for a very limited number of molecular species. The earliest case is that of C_2 (Refs. 30, 31). CH and CN have been measured in flames in this laboratory as described below. Much work has been performed on the OH radical because of its easily resolved spectrum and ease of production (a moderately abundant hydrocarbon flame component), but only one case of saturation of OH radical fluorescence has been reported (Ref. 32). As regards other molecular species, Pasternack, Baronavski, and McDonald (Ref. 33) recently have demonstrated saturated LIFS for MgO. Recent lifetime measurements of the excited ($A^2\pi^+$) SH radical by Becker and Haaks (Ref. 34) indicate that this species may be a candidate as well. The SH radical is important in various fast reactions which couple sulfur compounds in flames. Recent work along these lines by Müller, Schofield, Steinberg, and Broida (Ref. 35) indicates that in addition to SH, the radicals S_2 and SO might be amenable to saturated LIFS detection. With regard to atomic species, saturated LIFS has been demonstrated for Na by Daily and Chan (Ref. 36), and by Smith, Winefordner and Omenetto (Ref. 37), for Mg by Kuhl and Spitschan (Ref. 38), and for Tl, Cr, Sr and Zr by Omenetto et. al., (Ref. 39). Atomic species serve as ideal cases for saturation because the number of quantum states is small and the electronic transitions are typically strong.

Under Contract 68-02-2176, sponsored by the Environmental Protection Agency and carried out at UTRC, the laser-induced saturated fluorescence technique has been applied successfully to the measurement of CH and CN radical species concentrations in laboratory-scale flames. The results of this work are contained in the Task II Technical Report under the above Contract (Ref. 6), and have been reported in the open literature (Ref. 7). The saturated LIFS measurements were performed on CH and CN in atmospheric pressure acetylene flames with a tunable, low pulse rate, flashlamp-pumped dye laser. Fluorescence was observed from the $A\ ^2\Delta$ state of CH at 4315 A and from the $B\ ^2\Sigma$ state of CN at 3880 A. For both radicals, the dependence of fluorescence intensity on laser spectral intensity exhibited a pronounced departure from linearity at high laser spectral intensity, indicating saturation. These were the first

observations of saturated fluorescence for these radicals, and the data permitted evaluation of the species concentration for both CH and CN. Since the saturated fluorescence technique was new and subject to some uncertainty, it was important to have an independent measurement of radical concentration in order to test the validity of the saturated fluorescence results. To this end, optical absorption measurements were performed in a single pass on a specially constructed slot burner operating at atmospheric pressure. The CH concentration was about 60 ppm in an oxy/acetylene flame, and the CN concentration approximately 150 ppm in a nitrous oxide/acetylene flame, both measured by absorption. The concentrations measured by absorption were larger by about a factor of two for CH and five for CN than the values determined by saturated fluorescence. A possible explanation for the discrepancy suggested an overestimate of the fluorescence sample volume size, which led to an underestimate of the species concentration. That this overestimate may occur is due to the size of the smallest possible focussed laser spot relative to the concentration gradients known to exist across the radial dimension in small, high pressure flames. For accurate saturated fluorescence results, the characteristic fluorescence sample volume dimension should be considerably smaller than that of the flame spatial gradient. Significantly, in the experiments reported in Refs. 6, 7, the laser focal diameter was limited by the poor beam quality of the flashlamp-pumped dye laser. With laser-pumped dye lasers, the beam quality is generally much better, permitting finer scale probing. Such a laser system contributed significantly to removing this ambiguity in the CH and CN saturated fluorescence results reported herein.

The principal objectives of the present program were to remeasure CH and CN by means of saturated fluorescence with improved precision and further, to attempt to apply the saturated fluorescence technique to NO. To improve the CH and CN measurements, a repetitively-pulsed, laser-pumped tunable dye laser was employed. Specifically, in the work reported below, harmonics of a Nd:YAG laser are used as dye laser pumping sources. Such a laser system offers a number of advantages. The beam quality of the dye laser is good, which implies a small beam divergence and a correspondingly small focussed laser spot. A beam divergence of a few milliradians is readily achievable, which for a 10 cm focal length lens yields a 100 to 200 micron diameter. Typically, this is an order of magnitude smaller than the spot size reported in Ref. 6 and, therefore, offers the possibility of eliminating the source of discrepancy mentioned above. The smaller spot size also produces higher spectral intensities. The laser-pumped dye laser may be made to operate in a narrow spectral bandwidth which allows for very precise excitation of molecular transitions and equally importantly, contributes to a high laser spectral intensity which is essential to saturation. Since the laser spectral intensity is inversely proportional to the duration of the dye laser pulse, the (5-10) nsec time of laser-pumped dye laser pulses is distinctly superior to the (200-300) nsec associated with flashlamp-pumped dye laser systems. The shorter pulse durations also minimize species loss due to laser-enhanced excited-state chemistry and quenching to

slowly-relaxing vibrational states. Finally, a repetitively pulsed laser permits signal averaging of fluorescence emission to improve the signal-to-noise ratio (S/N), and to scan the entire LIFS spectrum. Examples of the latter are given in the results below. The optical absorption results for CH and CN given in Refs. 6, 7 are again used for comparison. Based upon determinations of the radical spatial gradient scale and the size of the probe beam used to make the absorption measurements, the absorption measurements are suspected to be low. The CH and CN fluorescence data were taken with the same burner used for the earlier optical absorption measurements, and the exact operating conditions of the burner were precisely repeated. The motivation for selecting NO for LIFS study stems from its importance as a major pollutant and, experimentally, from its stability relative to most radical species. NO may be contained indefinitely in a cell provided that other reacting species, especially oxygen, are not present. Consequently, saturated LIFS measurements may be carried out where the NO pressure is accurately known. This permits a well-calibrated test of the saturated fluorescence results for NO concentration. Another practical advantage with NO is that it may be doped into a flame in known quantities which also calibrates saturated fluorescence results for NO at flame temperatures.

Following this introduction, the general theory of laser-induced saturated fluorescence is given, including a discussion of the characteristic time to saturate a transition, and a development of a model which treats the importance of rotational energy transfer in analyzing fluorescence data. This is followed by three sections devoted separately to results for CH, CN and NO. Finally a general discussion and evaluation of the saturated fluorescence results is given.

Laser-Induced Saturated Fluorescence Theory

The original saturated fluorescence measurements on CH and CN performed at UTRC (Ref. 6) used a flashlamp-pumped dye laser with a pulse duration of 150-300 nanoseconds. A laser-pumped dye laser was used for the measurements described in this report because, among other reasons, the shorter pulse duration, 10 nanoseconds, yields much higher peak laser power. However, a question which arises is whether steady state saturation of the fluorescence transition can be achieved within the duration of a pulse of $O(10^{-8}$ sec).

Characteristic Time to Saturate

A straightforward analysis of the rate equations, under conditions of saturation, provides the answer to this question of laser pulse length. The complete rate equations for the upper and lower level populations N_2 and N_1, respectively, are

$$\frac{dN_2}{dt} = \frac{N_1 B_{12} I}{c} - N_2\left(\frac{B_{21} I}{c} + Q_{21} + A_{21}\right) \tag{1}$$

$$\frac{dN_1}{dt} = -\frac{N_1 B_{12} I}{c} + N_2\left(\frac{B_{21} I}{c} + Q_{21} + A_{21}\right), \tag{2}$$

B_{12} and B_{21} are the Einstein coefficients for induced absorption and induced emission, respectively, A_{21} is the Einstein coefficient for spontaneous emission, and Q_{21} is the electronic quenching rate. I is the laser spectral irradiance and c the speed of light. If saturation occurs, then the condition

$$(B_{12} + B_{21})I/c \gg Q_{21} + A_{21} \tag{3}$$

holds. Transitions between N_1 and N_2 are determined solely by the laser. If the conservation equation $N_1 + N_2 = N_{total}$ = constant is applied, then Eq. 1 may be written as

$$\frac{dN_2}{dt} = \frac{N_{tot} B_{12} I}{c} - \frac{N_2 (B_{12} + B_{21}) I}{c} \tag{4}$$

which may be integrated readily to

$$N_2 = C_1 + C_2 \exp\left[-\frac{(B_{12} + B_{21})It}{c}\right]. \tag{5}$$

The constants C_1 and C_2 are determined from initial ($t \leq 0$) and steady state ($t \to \infty$) conditions:

$$\text{for } t \leq 0, \quad N_2 = 0, \quad \text{then } C_1 = -C_2$$

$$\text{for } t \to \infty, \quad N_2 = \frac{N_1 B_{12}}{B_{21}} = C_1$$

Recall also that $g_1 B_{12} = g_2 B_{21}$, where the g s are the degeneracies of the respective states; then the final solution is

$$N_2 = N_1 g_2/g_1 \left[1 - \exp\left\{ - (1 + g_2/g_1) B_{12} It/c \right\} \right] \qquad (6)$$

Clearly, steady state is reached in a time $\tau_{sat} \lesssim c/B_{12}I$

τ_{sat} can be evaluated for typical values of B_{12} and the laser spectral irradiance I in order to find the characteristic time to saturate the transition. If the inequality (3) is true, then saturation occurs. A typical value of the spontaneous emission rate, A_{21}, is $10^8 sec^{-1}$. If $Q_{21} = 10^2 A_{21} = 10^{10} sec^{-1}$, then for the inequality (3) to hold, $B_{12}I/c \sim 10^{12} sec^{-1}$. Thus, a time of a few picoseconds is sufficient to saturate transitions corresponding to $A_{21} = 10^8 sec^{-1}$. For weaker transitions, A_{21} is of $O(10^6 sec^{-1})$, the characteristic time to saturate would be of $O(10^{-10} sec)$. This latter figure is still much shorter than a typical Q-switched laser pulse, $O(10^{-8} sec)$. Hence the ten nanosecond pulse used for the studies reported here is many times the characteristic time to saturate. Times of the order of microseconds, often used for saturated fluorescence studies, are not required, nor necessarily desirable because laser-induced chemistry may occur on such a time scale. A theoretical and experimental study of the time dependence of saturated fluorescence in atoms has been given by Olivares and Hieftje (Ref. 40). Their conclusions regarding the time required to saturate are in general agreement with those given here.

Rotational Energy Transfer Effects

Another question concerns the validity of the simple two-level, steady state model employed by many authors. The two-level model is based upon an atomic or molecular system which is essentially electronic in nature and has no vibrational-rotational structure (nor spin). Daily (Ref. 41) has treated the two-level and three-level cases. As would be expected, the two-level model describes well the saturation behavior of atoms and some molecular cases. In general, a molecular system is not a simple two-level system because of the vibrational-rotational partitioning of the electronic levels. Vibrational-rotational energy transfer, during the period of laser irradiation, must be considered for the laser-induced saturated fluorescence of any molecular system. For most molecules, vibrational relaxation can be neglected as being slow compared to typical laser pulse lengths. This is not true for rotational relaxation, which may have rates of $O(10^{12} sec^{-1})$ or even higher.

One of the first treatments of laser-induced saturated fluorescence which includes rotational relaxation is that of Lucht and Laurendeau (Ref. 42). These authors treat two sets of rotational levels, of which selected levels are

connected by laser excitation. A steady-state is assumed, and the resultant algebraic equations are solved with a computer. The rotational relaxation rate was varied relative to the electronic quenching rate. The significant result of this study was that complete Boltzmann equilibrium of rotational levels is not achieved unless rotational relaxation exceeds electronic quenching by a factor of $O(10^2)$. A second important result is that a linear relationship between the fluorescence power and the inverse of the laser spectral intensity, similar to the two-level case, is found. An important modification is a population factor which accounts for rotational level population redistribution caused by collisional energy transfer. As defined in Ref. 42, the population factor is the ratio of molecules involved in the laser-induced transition to the total number of molecules in the electronic state of interest. In the limit of very rapid rotational relaxation, the population factor goes over to unity, that is, the entire electronic state participates in the transition. For the other extreme limit of no rotational energy transfer during the laser pulse, there is only one rotational state involved in the transition; and the population factor is the inverse of the Boltzmann occupation probability described in more detail below. In a simplification of the Lucht-Laurendeau model, a similar relationship was found by Berg and Shackleford (Ref. 43) who, in one limit, considered the case of very fast rotational relaxation. Again, a two-level model result is obtained with a population factor which is essentially the entire population of the ground electronic state.

In order to apply the results of these models to the interpretation of experimental data, it would be necessary to have data comparing rotational relaxation rates with electronic quenching rates. Unfortunately, these relationships are not known for most radical species, certainly not for CH, CN, and NO.

Modified Two-Level Model with Rotational Redistribution

The basic two-level model for saturated fluorescence can be extended in a tractable manner as follows. Consider two energy level groups, shown as boxes in Fig. 18, which represent the rotational levels of two vibrational-electronic states. The upper group is empty, prior to excitation. The lower group has a total population, N_1, of which some fraction f is excited by laser radiation, $I_{\nu L}$ at an excitation rate $B_{12}\ I_{\nu L}/c$. The laser radiation is assumed narrowband, and selectively pumps only a particular rotational state of the lower group. However, because of rotational energy exchange, nearby rotational levels will feed into this selected level and participate in the transition. The fraction of N_1 that participates is denoted by the factor f.

In the limit of no rotational relaxation, only one rotational level is excited; and the factor f is the Boltzmann factor,

$$P_J = \frac{(2J + 1)\ \exp\left(-\frac{Bhc\ J(J + 1)}{kT}\right)}{Q_{ROT}} \qquad (7)$$

FIGURE 18. MODIFIED TWO-LEVEL MODEL FOR SATURATED FLUORESCENCE WITH ROTATIONAL REDISTRIBUTION

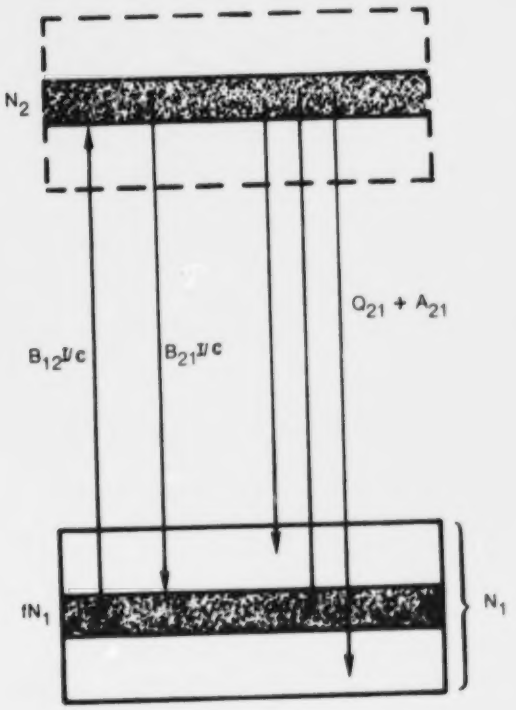

79-09-63-13

where J is rotational quantum number and Q_{ROT} the rotational partition function. For this limit, f is a small number, ~ 0.03, at flame temperatures for a molecule with a rotational constant, $B_{ROT} \sim 2\ cm^{-1}$ (e.g., N_2, CN, C_2). If some rotational relaxation occurs during the laser pulse, f is larger than the Boltzmann factor, P_J. f approaches unity for the other limiting case of very fast rotational relaxation. In this limit then, the entire lower group of rotational levels participate in the excitation process. N_2 is the total number of molecules in the upper group. With this preface, the rate equation for N_2 is stated and solved in terms of the total population.

$$\frac{dN_2}{dt} = fN_1 \frac{B_{12}I}{c} - N_2\left(\frac{B_{21}I}{c} + Q_{21} + A_{21}\right) \tag{8}$$

Assuming the steady-state approximation, the derivative is set equal to zero. Using the conservation relation, $N_{Total} = N_T = N_1 + N_2$, one can solve for N_T in terms of N_2

$$N_T = N_2\left[1 + \frac{B_{21}I/c + Q_{21} + A_{21}}{fB_{12}I/c}\right] \tag{9}$$

Recall $g_1B_{12} = g_2B_{21}$, then

$$N_T = N_2(1 + g_1/fg_2)\left[1 + \frac{Q_{21} + A_{21}}{f(1 + g_1/g_2f)\ \frac{B_{12}I}{c}}\right] \tag{10}$$

Inverting this equation for N_2

$$N_2 = \frac{fN_T}{(f + g_1/g_2)}\left[1 + \frac{(Q_{21} + A_{21})c}{(f + g_1/g_2)B_{12}I}\right]^{-1} \tag{11}$$

Fluorescence Power

Given N_2, Eq. (11), the experimentally observed quantity, S_F, the fluorescence power, can be written

$$S_F = N_2 \frac{hc}{\lambda_F} \frac{A_{21}}{4\pi} \Omega V \epsilon \tag{12}$$

where h is Planck's constant; c is the speed of light; λ_F, is the fluorescence wavelength; Ω is the light collection solid angle; and V is the volume of sample fluorescing. ϵ is an efficiency factor which accounts for spectrometer throughput, lens losses, etc. This expression is substituted in Eq. (11); at the same time the term in the brackets is expanded as unity plus a small term, because $B_{12}I/c >> (Q_{21} + A_{21})$. Hence, the fluorescence power is

$$S_F = \frac{N_{Tot} hc A_{21} \Omega V \epsilon f}{\lambda_f \, 4\pi \, (f + g_1/g_2)} \left[1 - \frac{Q_{21} + A_{21}}{(f + g_1/g_2) B_{12} I} \right] \qquad (13)$$

In the limit of very fast rotational relaxation, $f \rightarrow 1$, and this model coincides with the two-level model result of Baranovski and McDonald (Ref. 30). The limit f = 1 corresponds to complete rotational relaxation, that is, the entire lower group of levels participates in the laser-induced transition. Therefore, the entire lower group population can be measured. For $f < 1$, only a fraction of the total population is measured. In general, this fraction is unknown because the rotational relaxation rates are not available. For the extreme case of very slow relaxation, only a single rotational state is excited and f becomes the inverse of the Boltzmann factor, P_J, defined above. S_F plotted against the reciprocal laser spectral intensity will yield a straight line, a procedure first suggested by Baronavski and McDonald (Ref. 30). From the intercept S_F°, the total population N_{TOT} can be found, if f is known or can be reasonably estimated.

For the foregoing discussion, it is assumed that f is constant in time, which is true if the steady-state condition is true. But the steady-state approximation may not be valid for real laser pulse shapes, for rotational relaxation rates comparable to the induced absorption/emission rates, or for quenching to slowly relaxing vibrational states. Because steady-state models may fail to completely describe real molecular systems in saturated fluorescence, another approach is suggested. Time-dependent solutions to the population rate equations should be examined and compared with steady-state solutions. Since the rate equations are linear coupled differential equations, they are easily solved through use of a computer. The computer can generate sets of solutions incorporating a wide variation of parameters such as the rotational relaxation rates, electronic radiative and non-radiative rates, as well as laser pulse properties. In this manner, one can eventually determine the extent of rotational relaxation for a particular situation, in essence, determine the f-factor. One direct way to accomplish this is to compare computer generated fluorescence spectra with experimental spectra. Moreover, the availability of such synthetic

spectra could recommend the most efficient manner of performing experiments on a particular molecular species in a given environment.

It should be stressed that it is the total fluorescence, N_2A_{21}, which is considered in the modified two-level model presented above. Figure 18 attempts to indicate both radiative and nonradiative transitions, A_{21} and Q_{21}, from N_2 to states within and without the group fN_1. The experimentalist has the option, of course, of measuring all or some fraction of the total fluorescence, $A_{21}N_2$. If Rayleigh or Mie scattering is large, then the resonant fluorescence region would likely be excluded.

Focal Beam Profile

It is assumed that in the excitation of the fluorescence power, uniform illumination of the interaction volume is achieved. That is, the laser beam has a "top hat" or rectangular spatial distribution. This is not a realistic distribution for dye lasers, nor is the Gaussian distribution, often assumed. However, a distribution with low intensity wings, like a Gaussian, is probably not unreasonable. For such a case, if saturation occurs at a point in space which is coincident with the peak of the Gaussian distribution, it may or may not occur in the far wings of the distribution. If the laser spot size is significantly smaller than the characteristic flame dimensions, some molecules are saturated and others are not; this leads to errors in the measured species concentration. Detailed considerations along these lines have been given by Daily (Ref. 44). Pasternack, Baronavski, and McDonald (Ref. 33) have analyzed saturated fluorescence data for Na using three different beam profiles and observed the influence of this variation on calculated species concentration; these distributions were rectangular, Gaussian, and truncated Gaussian. The Gaussian profile was shown to be unsatisfactory for making concentration measurements, while the rectangular shape gave a result for Na concentration more nearly equivalent to that determined from optical absorption than did a truncated Gaussian. In light of this result and, in addition, the fact that beam profiles in the present work are not Gaussian, the rectangular beam approximation is used below. This simplified approach does not alter the fact that a satisfactory and consistent procedure is needed to account for intensity distribution, so as to make saturated fluorescence and optical absorption methods agree as regards species concentration.

Experimental Investigations

In this section, saturated laser fluorescence experiments are described for the radicals CH, CN and NO. As mentioned above, in order to apply the saturated LIFS technique to these species, a radiation source is required which may be tuned to an absorption band of these molecules. For CH and CN, strong

absorptions, which occur between the electronic ground state and an excited state pertinent to this work, are at 4315 Å and 3883 Å, respectively. Energy level diagrams for CH and CN are given in Fig. 19. CN differs from CH in that a third electronic level, $A\ ^2\pi$, is present. Each electronic level, in the case of both CH and CN, has a vibrational-rotational structure as indicated. For CH and CN excitation, a laser is needed which has 4315 and 3883 Å nominal operating wavelengths, respectively, and which may be tuned to individual vibrational-rotational levels. An energy level diagram for NO is given in Fig. 20, where, as indicated, a laser at 2260 Å is required. Unfortunately, it is not possible presently to configure a single tunable dye laser which, without modification, would be applicable to all three molecules. For CH at 4315 Å, a pulsed 3xNd:YAG laser at 3550 Å is used to pump a dye laser employing a stilbene/methanol solution. The laser wavelength is tuned by using a diffraction grating in the laser cavity. When pumped as indicated, the wavelength at which peak lasing energy occurs, coincides well with CH absorption lines. For CN, the stilbene is not useful since when pumped as indicated it does not emit at wavelengths suitable for CN excitation at 3883 Å. Although an alternate dye may be used, a significant reduction in laser pulse energy is likely to occur. Indeed, even for 3xNd:YAG pumping of stilbene, the pulse energies are not comparable to those obtained for 2xNd:YAG pumping of rhodamine 6G dye. Radiation at 3883 Å is obtained by using a 2xNd:YAG pump laser at 5320 Å to excite a rhodamine 640 dye which lases near 6100 Å. This output is then combined in a nonlinear type I KD*P mixing crystal with the fundamental 1.06 μ Nd:YAG output to yield frequency up-converted radiation at 3883 Å. This is an efficient process, despite its relative complexity, owing to the sizeable energies available at 6100 Å and 1.06 μ.

In the case of NO, an approach is required which is different than that for both CH and CN. Similar to the case for CN, a 2xNd:YAG pump laser is used to excite, in this case, a rhodamine 590 dye which lases near 5740 Å. This output is then frequency doubled in a KD*P crystal to yield radiation at 2870 Å, which in turn is combined with 1.06 μ radiation in a second nonlinear mixing crystal to obtain the required radiation at 2260 Å. This is a more complex process than those above and is capable of only moderate energy conversion efficiency. There is an alternative approach to obtaining 2260 Å radiation. One may elect to use the 3xNd:YAG pump to excite one of several coumarin dyes and thereby obtain lasing near 4520 Å. Then, the output would be frequency doubled in a KPB (potassium pentaborate) crystal to yield the desired wavelength. There were two reasons for not selecting this approach in this work, although it might be worth evaluating experimentally. First, blue dyes degrade rapidly when subject to laser pumping which results in a sharp reduction in laser energy. This was a significant but not a limiting difficulty for the present CH work with stilbene. Secondly, the frequency-doubling efficiencies in the 4520 Å region are known to be small, only a few percent or less as verified by Dewey (Ref. 45). More detailed descriptions of the laser sources for CH, CN and NO are given below.

FIGURE 19. CH AND CN ENERGY LEVEL DIAGRAMS

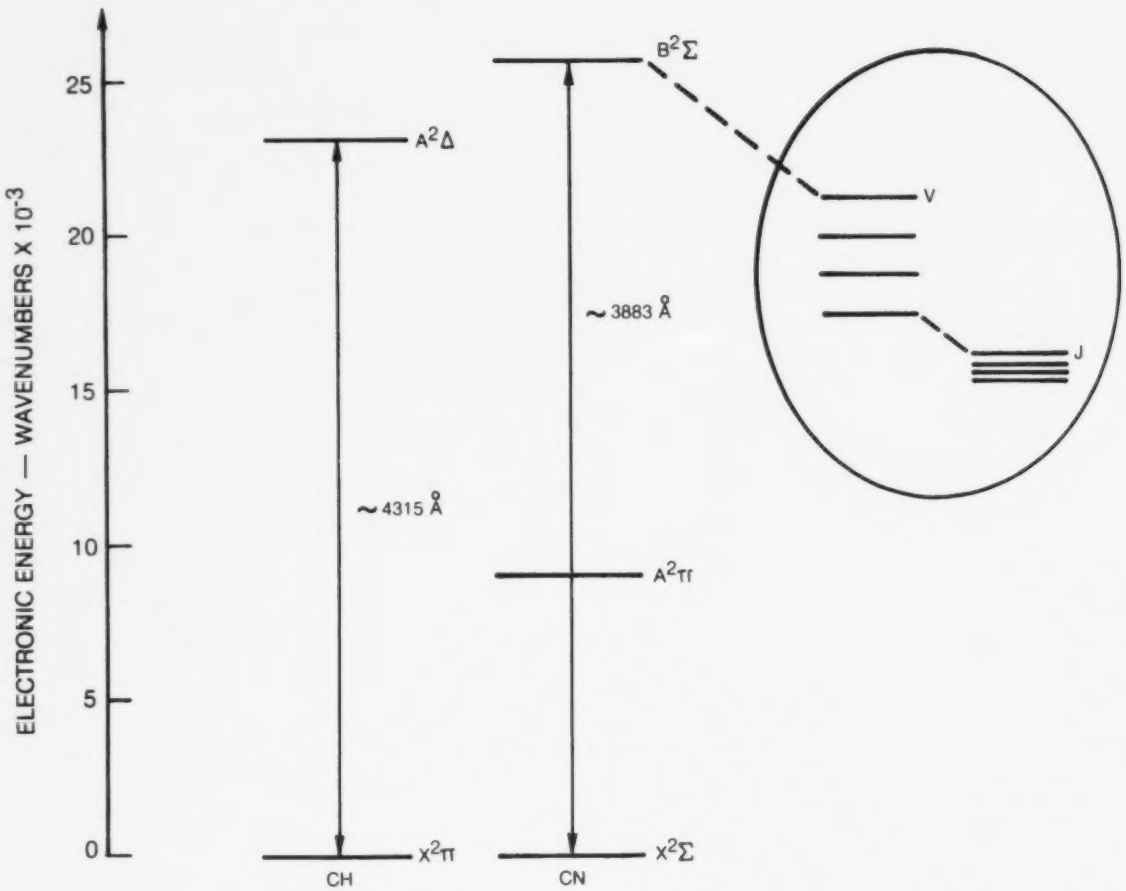

79-09-1-2

FIGURE 20. NO ENERGY LEVEL DIAGRAM

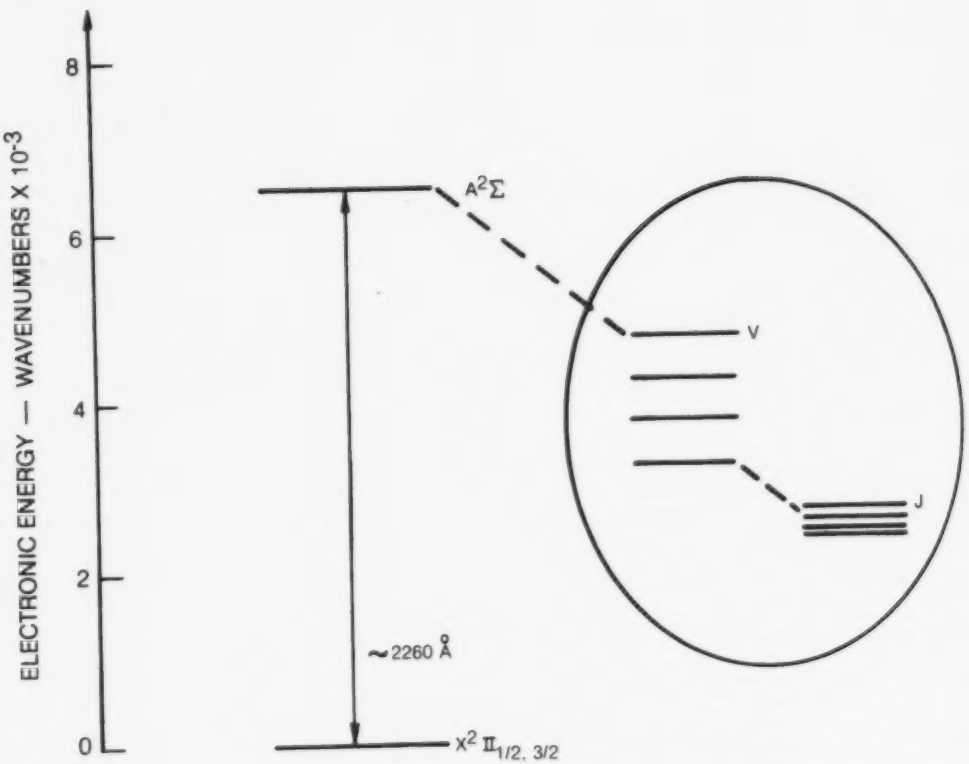

79-09-1-3

CH Investigations

The apparatus used for the CH measurements is shown schematically in Fig. 21. Figure 22 is a photograph of the apparatus used for the NO measurements; however, the layout of dye laser components in this case did not differ in any significant way than for CH. The CH apparatus may be regarded as consisting of a laser-pumped, pulsed tunable dye laser suitable for producing radiation at 4300 Å, a burner for CH production, laser focussing and light collection optics, and signal recording instrumentation.

The pump laser in Fig. 21 is a Quanta-Ray 1.06 μ Nd:YAG laser with a 10 nsec pulse width and a 10 Hz pulse repetition frequency. It has an oscillator and a single amplifier stage, and the combination yields upwards of 700 mJ of energy at 1.06-microns. As part of this system, frequency doubling and wave mixing crystals are incorporated so that 200 mJ and 100 mJ of energy are available at 5320 and 3550 Å, respectively. A Brewster prism, P, is used to turn the 3550 Å radiation by 90 degrees, and a half-wave plate, PL, rotates the linear, horizontally polarized pump radiation by 90 degrees to the vertical direction. For this polarization direction, about 10 percent of the pump radiation is reflected in turn by two quartz windows, W, while the remaining, transmitted pump light strikes two mirrors, M, at close to 45° angle of incidence resulting in near longitudinal excitation of a power amplifier dye cell, DC. Light reflected from the first window, W, is focussed by two cylindrical lenses, L, to form a thin line image close to the near inner surface of the first dye cell, DC. This excites a flowing stilbene/methanol dye solution and lasing occurs for the optical cavity defined by a grating and mirror, M. The four prisms, P, serve as a beam expander to spread light across the grating grooves. The increased dispersion narrows the spectral output from the oscillator section of the dye laser. The oscillator output is sent through a second dye cell which serves as a preamplifier excited in a manner identical to that in the oscillator section. The dye laser has a second or power amplifier stage pumped in a near longitudinal configuration. In order to match the size of the laser beam exiting the preamplifier with the pump beam, a beam expander is inserted between the amplifier dye cells, DC, which consists of two lenses, L, forming a Galilean-type telescope arrangement. The stilbene dye laser output energy was 10 mJ for 100 mJ of pump energy at 3550 Å, which represents an overall 10 percent energy conversion efficiency. The optical gain for the first amplifier was 4-5x and 3x for the second amplifier. Accordingly, the energy of the oscillator alone was in the range of 0.6 to 0.8 mJ. The laser energy peaked near 4270 Å for roughly 200 mg of stilbene in 1ℓ of methanol, while the spectral bandwidth was about 0.3 Å as measured with a 1/2-meter Jarrell-Ash spectrometer having a reciprocal linear dispersion of 16 Å/mm. The optimum resolution of the spectrometer at 4358 Å (Hg resonance line) was 0.2 Å, which, in this case, was adequate for a reasonably accurate determination of the laser spectral width. The 4270 Å laser wavelength was particularly suitable for CH excitation. A temporal display of the stilbene dye laser pulse

FIGURE 21. LASER INDUCED FLUORESCENCE APPARATUS

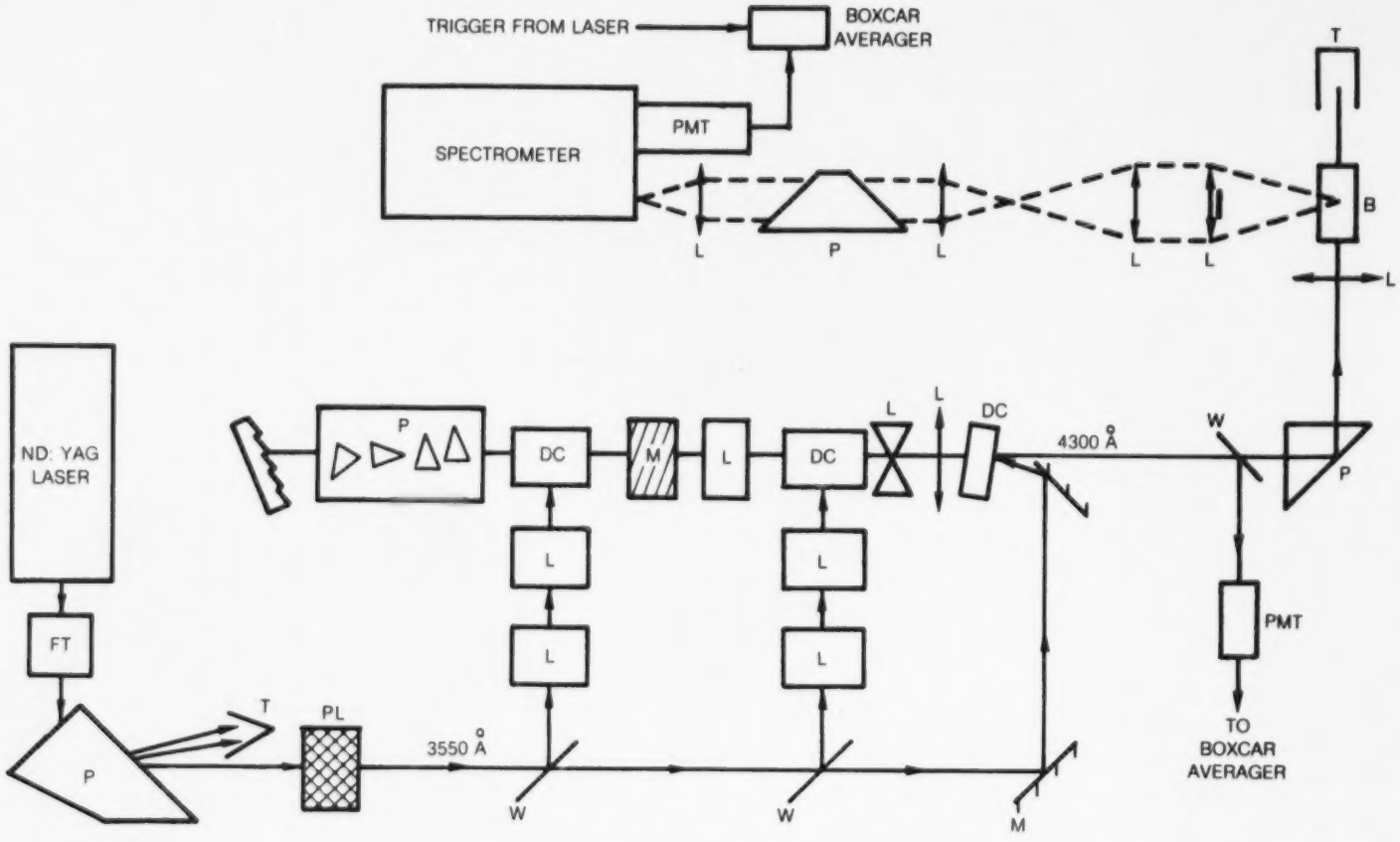

79-69-1-4

FIGURE 22. LASER INDUCED FLUORESCENCE APPARATUS

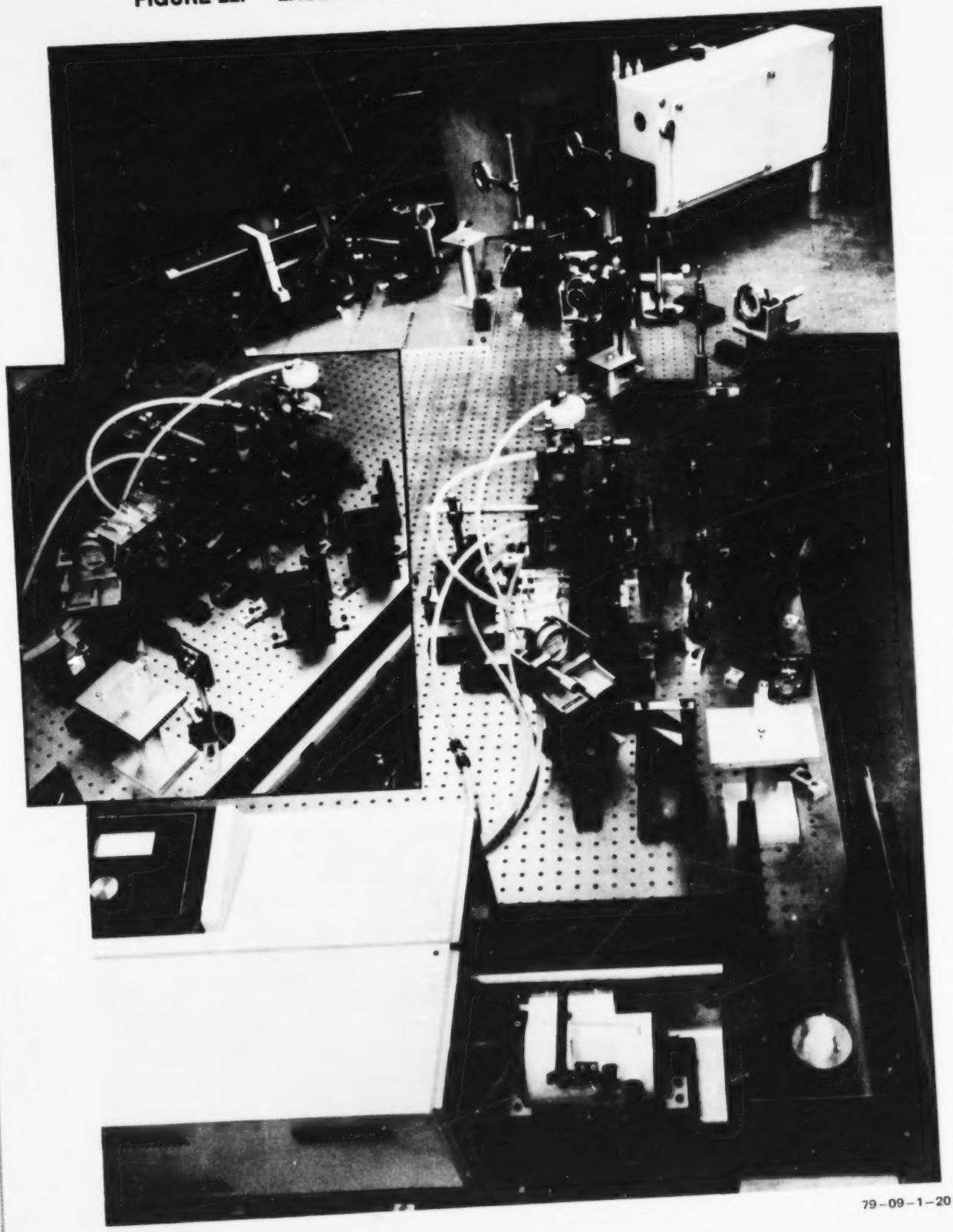

79-09-1-20

is given in Fig. 23. The photo exposure time was 10 sec so that a hundred or so pulses overlap, from which the pulse jitter may be estimated. This is a few nsec for a nominal pulse width of (5-10) nsec.

The burner in Fig. 21 is the same as used in previous CH measurements carried out at UTRC (Ref. 6). It is an oxy/acetylene welding torch modified to have a longer active path length for absorption measurements, which are described in Ref. 6. The flame emanates from a 0.2 mm x 2.4 cm slot, and an oxygen/acetylene mixture was burned for the CH measurements. Care was exercised to ensure that the flame operating conditions were the same as those for the previous optical absorption measurements in order that meaningful comparisons could be made as regards species concentration. As pointed out in Ref. 6, use of the slot burner has the disadvantage that sharp spatial gradients occur in the transverse flame direction which may lead to erroneous results for species concentration. However, it was not possible to find an adequate substitute for the slot burner which would yield both (10-100) ppm of CH and possess spatial homogeneity. In this regard, a Wolfhard-Parker type burner was constructed which is known to have a broader flame reaction zone (Ref. 46). It was not possible to achieve satisfactory stable operation of this burner with an oxygen/acetylene mixture. A methane/oxygen mixture burned well at atmospheric pressure, but CH flame emission intensities were several orders-of-magnitude smaller than those from the slot burner and laser induced fluorescence signals were not observed. That small quantities of CH were present was confirmed by computer-code evaluation of mole fractions of various species present in the flame for prescribed thermodynamic flame properties such as pressure, temperature, etc. In view of the foregoing difficulties, the slot burner was used for the present CH measurements.

A 14.5 cm focal length lens is used to focus the dye laser beam into the flame of the burner, B. A trap, T, helps prevent stray, background laser light from entering the spectrometer. The fluorescence is viewed at a right angle with respect to the direction of laser propagation. It is collected and focussed into the entrance slit of a 1/2-meter Jarrell-Ash spectrometer using four lenses, L, and a dove prism, P. The first two lenses in combination are such that the flame is imaged without magnification and the light collection corresponds to f/8 optics. A small opaque disk is placed directly in front of the first lens in order to limit the depth-of-field of the viewing optics. The dove prism, P, rotates the image formed by the first two lenses by 90-degrees. Consequently, a horizontal laser/flame interaction length is imaged vertically onto the spectrometer slit and limited to 1 cm by adjusting the slit height. The image rotation is used to increase the fluorescence intensity collected by the spectrometer while maintaining good spectral resolution and, thereby, improving the signal/noise ratio. The lenses, L, adjacent to the prism are there to ensure that collimated light enters the prism, since this is required for its proper operation, and, secondly, that f/8 optics are maintained to match that of the spectrometer.

FIGURE 23. STILBENE DYE LASER PULSE

$\lambda_{LASER} \simeq 4262$ A

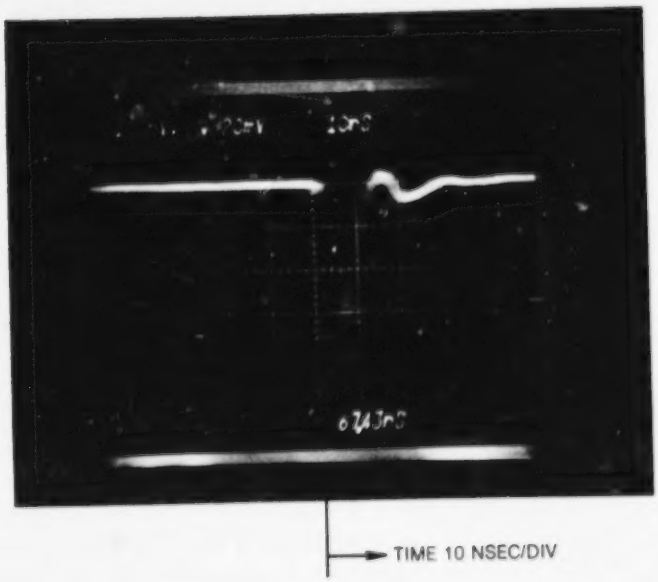

79-09-1-6

The signal recording electronics shown in Fig. 21 consists of two RCA Type 8575 photomultiplier tubes and a boxcar averager. These are supplemented by a fast oscilloscope, not shown in Fig. 21, in order to view laser and fluorescence pulses directly. One PMT records reference laser pulses, while the other, attached to the spectrometer, records fluorescence. The boxcar averager permits signal averaging which results in a considerable S/N enhancement.

Data

In order to evaluate species concentration from fluorescence intensity, it is necessary to know the optical collection efficiency of the apparatus, which from Eq. (12) is the parameter, ϵ . This factor may be determined by observing Rayleigh scattering of light since the Rayleigh signal intensity is directly proportional to ϵ. A typical Rayleigh signal used to evaluate ϵ for the present experiments is shown in Fig. 24. Details concerning the evaluation of ϵ from the signal intensity have been given previously in Ref. 6. It is evident from Eq. (12) above, that the sample volume size, V, must be known in order to compute species concentration from fluorescence power. V=Al, where A and l are sample cross-sectional area and length, respectively. l is the spectrometer slit height. A, which is the area of the focussed laser spot, must be evaluated. The Rayleigh scattering signal is also useful for this calibration. By measuring Rayleigh intensity as a function of spectrometer slit width, the focussed laser spot diameter may be measured. Following this procedure, the spot diameter was measured to be 270-microns; the diameter was taken as twice that distance from the center of the spot at which the peak intensity was reduced by a factor of e^{-2}. A 14.5 cm focal length lens was used to focus the laser radiation. The spot diameter, D, is the product, $f\theta$, where f is lens focal length and θ is laser beam divergence. A beam divergence of $\theta = 2 \times 10^{-3}$ radians is calculated which is fairly good.

Figure 25 displays CH spectra of ordinary flame emission and the laser-excited fluorescence. The pulsed dye laser and boxcar averager make it possible to scan the entire CH laser-induced fluorescence spectrum. It is worth stressing that this was not possible for the previous CH measurements reported in Ref. 6. The very large signal at the excitation wavelength near 4262 5 Å is due to Rayleigh scattering. The LIFS spectrum is significantly different from that observed in normal flame emission, indicating a non-Boltzmann distribution of population among rotational levels. The principal characteristics of Fig. 25b are readily understood. The three strong emissions near 4262, 4308, and 4359 Å are the R-,Q-, and P- branch lines, respectively, which originate from the rotational level in the upper, $^2\Delta$, electronic state excited by the laser. The R(8) resonance fluorescence line is heavily masked by the Rayleigh scattering signal at the laser wavelength. The preceding three lines are precisely identified in Fig. 26. The laser excites the transition K"=8 → K'=9, where K" and K' are rotational quantum numbers for the

FIGURE 24. RAYLEIGH PULSE

$$\lambda_{RAY} \equiv \lambda_{LASER} \simeq 4262\ \text{Å}$$

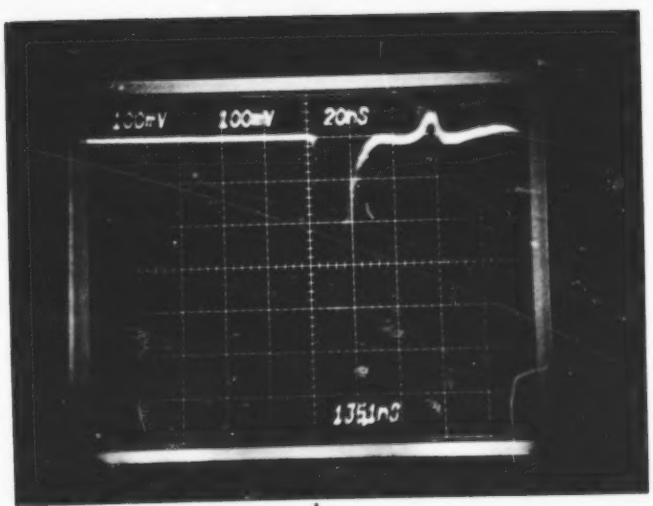

79-09-1-7

FIGURE 25. CH SPECTRA

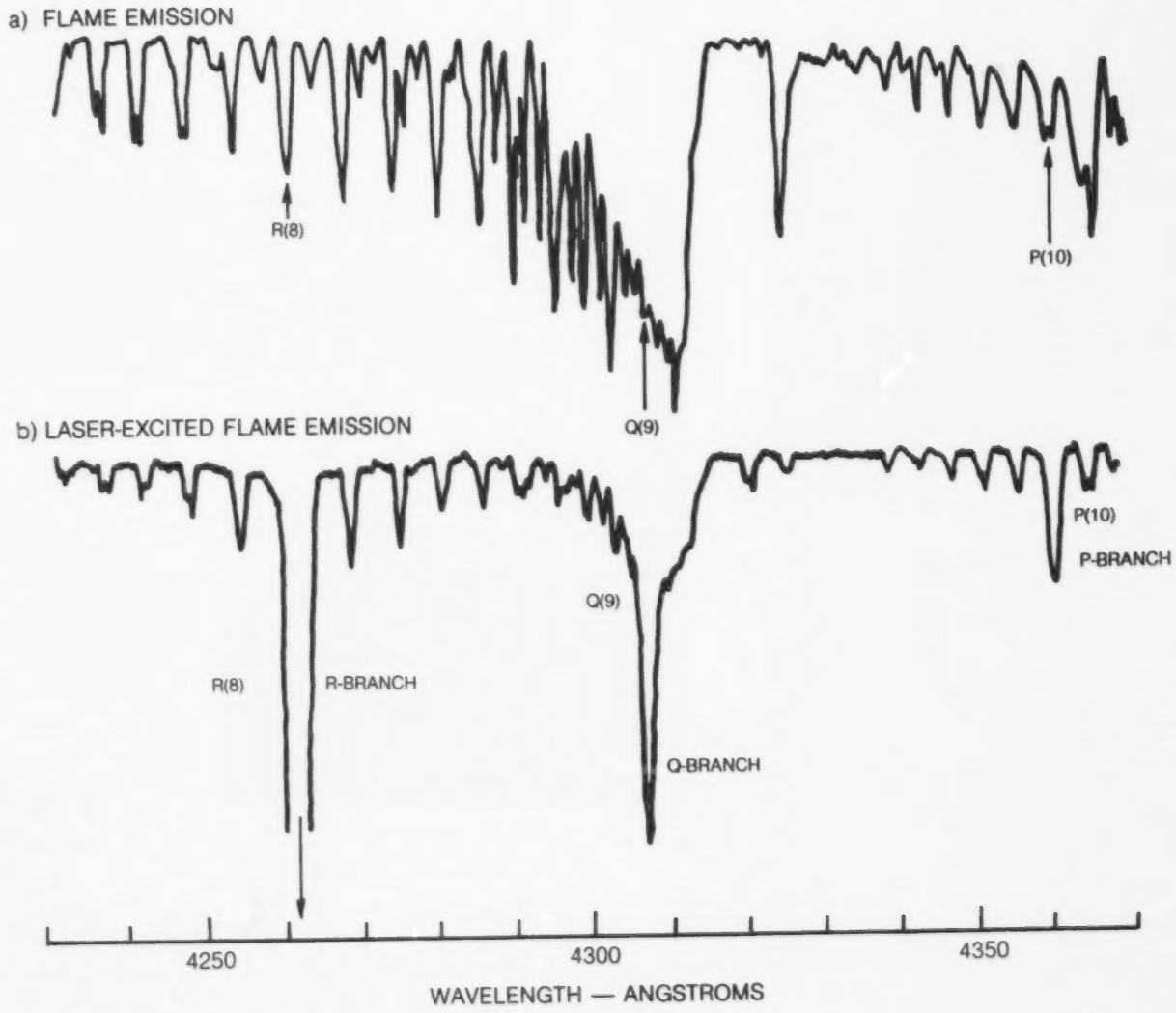

FIGURE 26. PRINCIPAL LASER-EXCITED CH LINES

$\lambda_{EXC} \simeq 4262$ Å $[^2\pi(V'' = 0),\ K'' = 8 \rightarrow {}^2\Delta\ (V' = 0),\ K' = 9]$

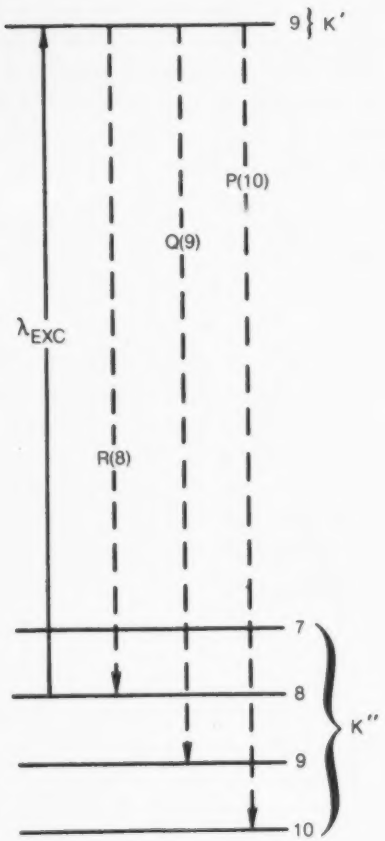

79-09-1-9

ground electronic $^2\pi$, v"=0 and excited $^2\Delta$, v'=0 levels, respectively. Since the selection rules for emission are $\Delta K=0, \pm 1$, the lines P(10), Q(9), and R(8) are observed in Fig. 25b. Other, weaker P-and R-branch lines clearly visible in Fig. 25b result as a consequence of rotational energy transfer out of K'=9 to other nearby rotational levels due to molecular collisions with subsequent emissions according to the preceding selection rules. From the rotationally nonequilibrated spectrum, one could conclude that the rate for rotational relaxation, R, does not greatly exceed the electronic quenching rate, Q, following the results of Lucht and Laurendeau (Ref. 42). However $R >> Q$ but $R < 1/\tau_L$ is also possible as described earlier. Smith, Crosley and Davis (Ref. 47) have made a detailed study of rotational nonequilibrium of laser-excited OH in an atmospheric presure flame. The ratio of rotational to electronic quenching was measured and found to vary with the rotational quantum number of the excited level, and the rates were not greatly different for large rotational quantum numbers. The rotational rate exceeded the quenching rate in all cases. A comparable, numerical analysis was not carried out in the present work owing to the small amount of available data and the relatively low spectral resolution present in Fig. 25b. On the other hand, since the rotational level spacings in OH and CH are approximately equal, the principal conclusions of Smith, Crosley, and Davis for OH relaxation may apply to CH as well.

Data for CH fluorescence as a function of laser energy are displayed in Fig. 27. Fluorescence was observed very near 4308 Å, which corresponds, principally, to laser-excited Q(9) emission at this wavelength. The departure from linearity between 0.01 and 0.1 millijoules, is indicative of saturation. Of particular significance is the very high S/N accompanying these measurements. It contrasts very favorably with earlier and similar data given in Fig. 14 of Ref. 6. The results of Fig. 27 are used below to compute species concentration and excited-state quenching.

CH Results

Following the procedure developed by Baronavski and McDonald (Refs. 30, 31) and the model developed in this report under Saturated Fluorescence Theory, the concentration and quenching for CH may be evaluated. Figure 28 is derived from Fig. 27; fluorescence intensity is plotted versus the inverse of the laser energy for data points corresponding to the highest laser energies in Fig. 27. The fluorescence power corresponding to the highest laser power used is equivalent to about 700 photons. As noted in Fig. 28, the intercept, S_F^o, of the straight line yields CH concentration, and the slope yields the excited state quenching rate, each modified by the f-factor which follows also from Eq. (13). A significant difference between the present approach and that used in Ref. 6 is the evaluation of the spectral fraction of fluorescence collected from the laser-excited CH fluorescence rather than from flame emission spectra. The latter procedure is based on the

FIGURE 27. LASER INDUCED CH FLAME FLUORESCENCE

λ_{EXC} = 4262 Å [$^2\Pi$(V'' = 0), K'' = 8 ⟶ $^2\Delta$(V' = 0), K' = 9]

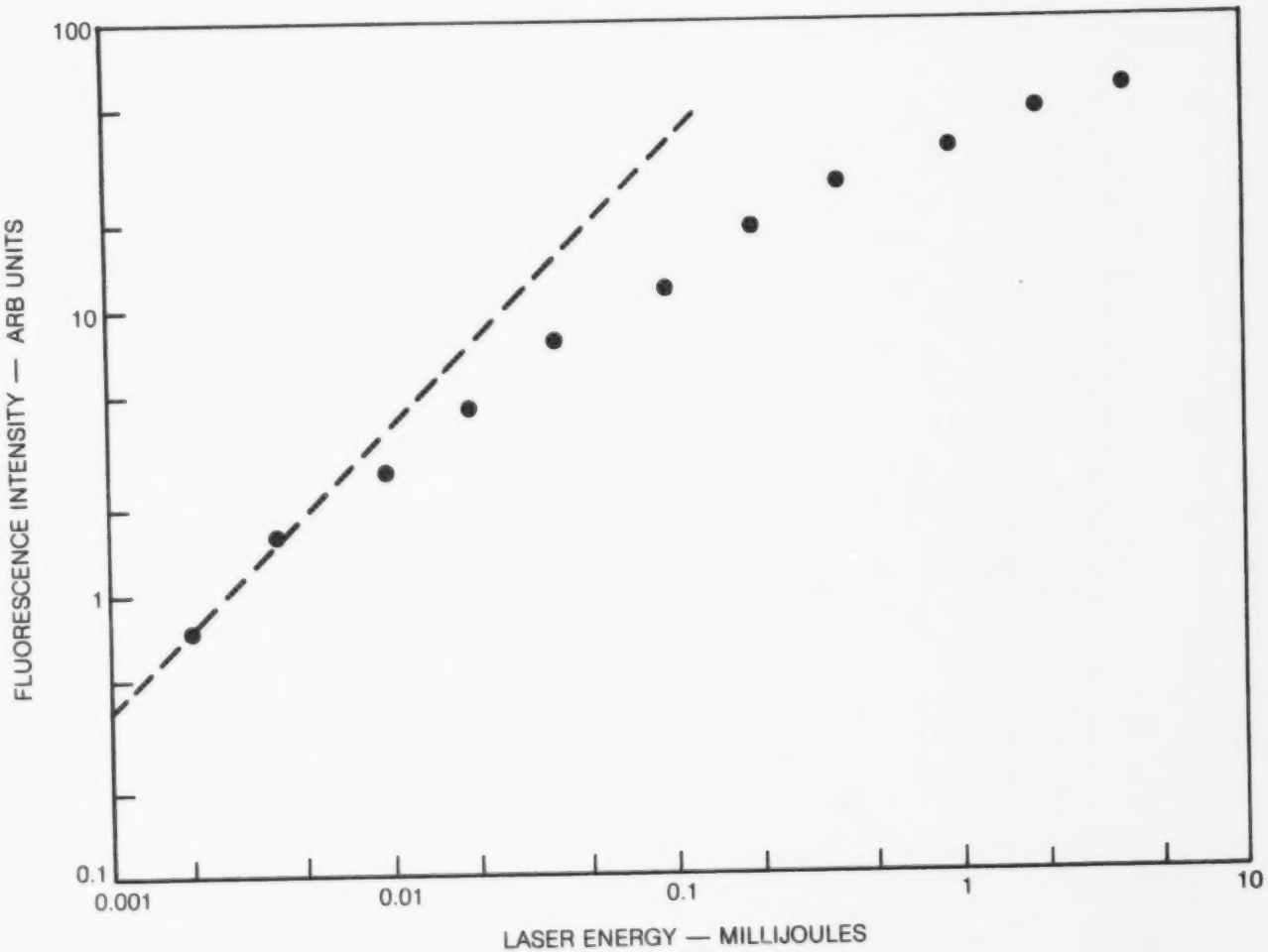

79-09-1-10

FIGURE 28. CH CONCENTRATION DATA REDUCTION

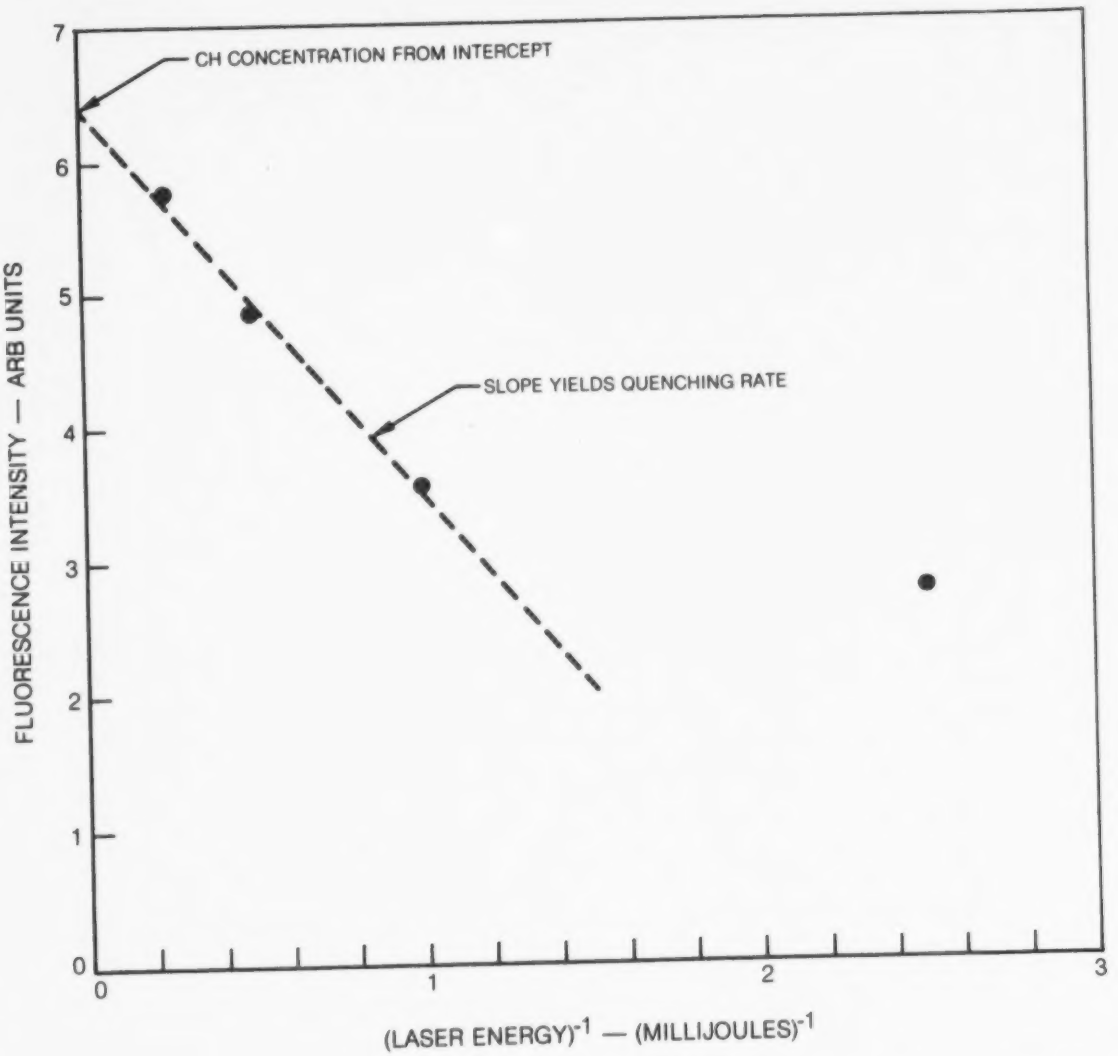

79-09-1-11

assumption of a Boltzmann equilibrium among rotational levels which was found to be approximately the case for the longer 300 nsec pulses previously used. With the shorter laser pulses employed here, rotational equilibration does not occur. Consequently, the fluorescence spectrum needs to be accurately and completely determined. The data point at 2.5 $(mJ)^{-1}$ in Fig. 28 corresponds to an energy for which the approximate expression for S_F in Eq. 13 is no longer valid. Table 3 gives the results for CH using the Boltzmann factor for f in Eq. 13; previous fluorescence as well as absorption results are included as well for comparison. The new fluorescence results may be high since some rotational redistribution occurs during the time of the pulse, thus the fraction of molecules actually pumped, f, exceeds the Boltzmann fraction, f_B, used in Eq. 13. However, the saturated fluorescence result from this investigation for the concentration agrees, within experimental error, with the previous absorption measurements, (Ref. 6). It should be noted that the improvements in the experimental apparatus have little effect on the experimental errors assigned which are fundamental to an absolute intensity measurement. The apparatus improvements affect the ability to saturate the transition, to excite a particular line, to minimize laser chemistry and to signal average.

TABLE 3

LASER-INDUCED SATURATED FLUORESCENCE
MEASUREMENTS SUMMARY

	PPM	$N(cm^{-3})$	$Q(Sec.^{-1})$
CH			
Absorption(1)	57 ± 20	$1.6 \pm 0.5 \times 10^{14}$	-
Sat. Fluor(1)	23 ± 10	$7.1 \pm 3.1 \times 10^{13}$	3×10^{9}
Sat. Fluor(2)	103 ± 50	$3.3 \pm 1.6 \times 10^{14}$	8×10^{11}
CN			
Absorption(1)	131 ± 34	$3.8 \pm 1 \times 10^{14}$	-
Sat. Fluor(1)	25 ± 11	$8 \pm 3 \times 10^{13}$	2×10^{9}
Sat. Fluor(2)	380 ± 150	$1.1 \pm .44 \times 10^{15}$	2×10^{13}

(1) Ref. 6
(2) This work

FIGURE 29. ENERGY LEVEL DIAGRAM FOR CN

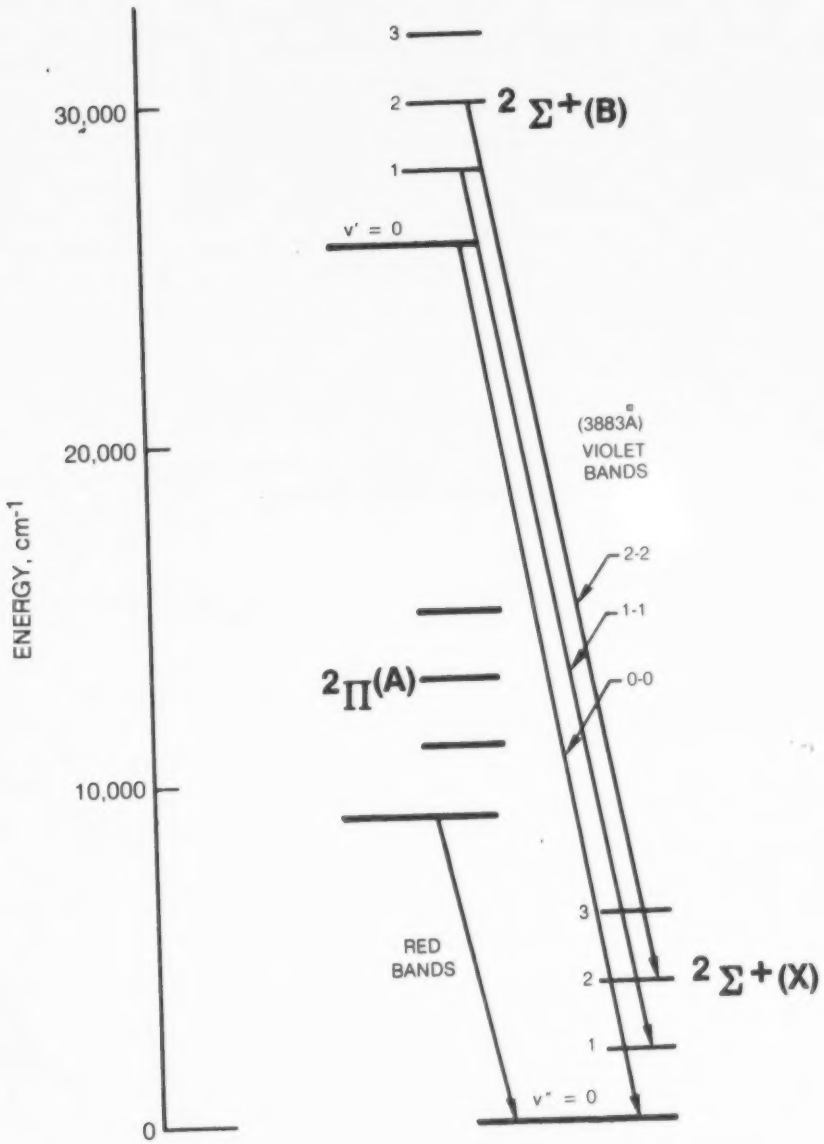

79-08-63-7

CN Investigations

Theoretical Considerations for the CN Radical

The cyano radical, CN, differs considerably from the methyne radical, CH, in two important ways. First, CN has a much smaller rotational constant, 1.9 cm^{-1}, compared to 14 cm^{-1} for CH. Apart from dipole moment considerations, this implies that the CN radical should have a much larger rotational relaxation rate than the CH radical. A second difference is that CN has three electronic states, X, A, and B, the ground, first, and second excited states respectively, any two of which are connected by radiative transitions. CH likewise has 3 important states to consider; however, the A and B states are not connected by a strong radiative transition. It is also noted that the CN B→X transition is approximately 10 times stronger than A→X in CH. Accordingly, CN should be easier to saturate than the CH radical.

A detailed energy level diagram for CN is shown in Fig. 29. The transition B→X, the "CN violet bands" chosen for this saturated fluorescence study are shown. The 0-0, 1-1, 2-2, etc. sequences are easily observed indicating a narrow Franck-Condon parabola, that is, the position of the potential minimum in the B state has shifted very little from that of the X state.

Experimental Considerations for CN

For the CN saturated fluorescence studies, it was decided to evaluate a different type of dye laser configuration than that used for the CH work. Rather than the prism beam expander-grating configuration, a grazing-incidence grating dye laser was employed. Both the double-grating configuration of Littmann (Ref. 48) and the grating-mirror arrangement (Refs. 49, 50) were tried. The former arrangement generated a time-averaged linewidth over several laser pulses no smaller than 0.1 cm^{-1} as measured with a Fabry-Perot interferometer. The grating-mirror combination yielded a similar linewidth at slightly higher power and appeared to be more stable. Hence, the grating-mirror configuration was employed for these studies.

The experimental layout is shown in the photograph (Fig. 30) and the schematic diagram (Fig. 31). In brief, a frequency-doubled neodymium:YAG (henceforth 2xNd:YAG) laser at 5320 Å pumps the grazing incidence rhodamine 640 dye laser oscillator operating near 6100 Å. The oscillator is followed by a preamplifier; both of these laser stages are transversely pumped. A third, power amplifier stage is longitudinally pumped. The orange dye-laser radiation is mixed with residual (from the frequency doubler) infrared radiation at 1.06μ in a potassium dideuterium phospate (KD*P) nonlinear optical crystal to generate the sum frequency in the ultraviolet in the range 3860 Å to 3880 Å. Emerging from the KD*P crystal are all three frequencies; the ultraviolet is separated with a Brewster angle 90° deviation

FIGURE 30. CN SATURATED FLUORESCENCE EXPERIMENTAL ARRANGEMENT

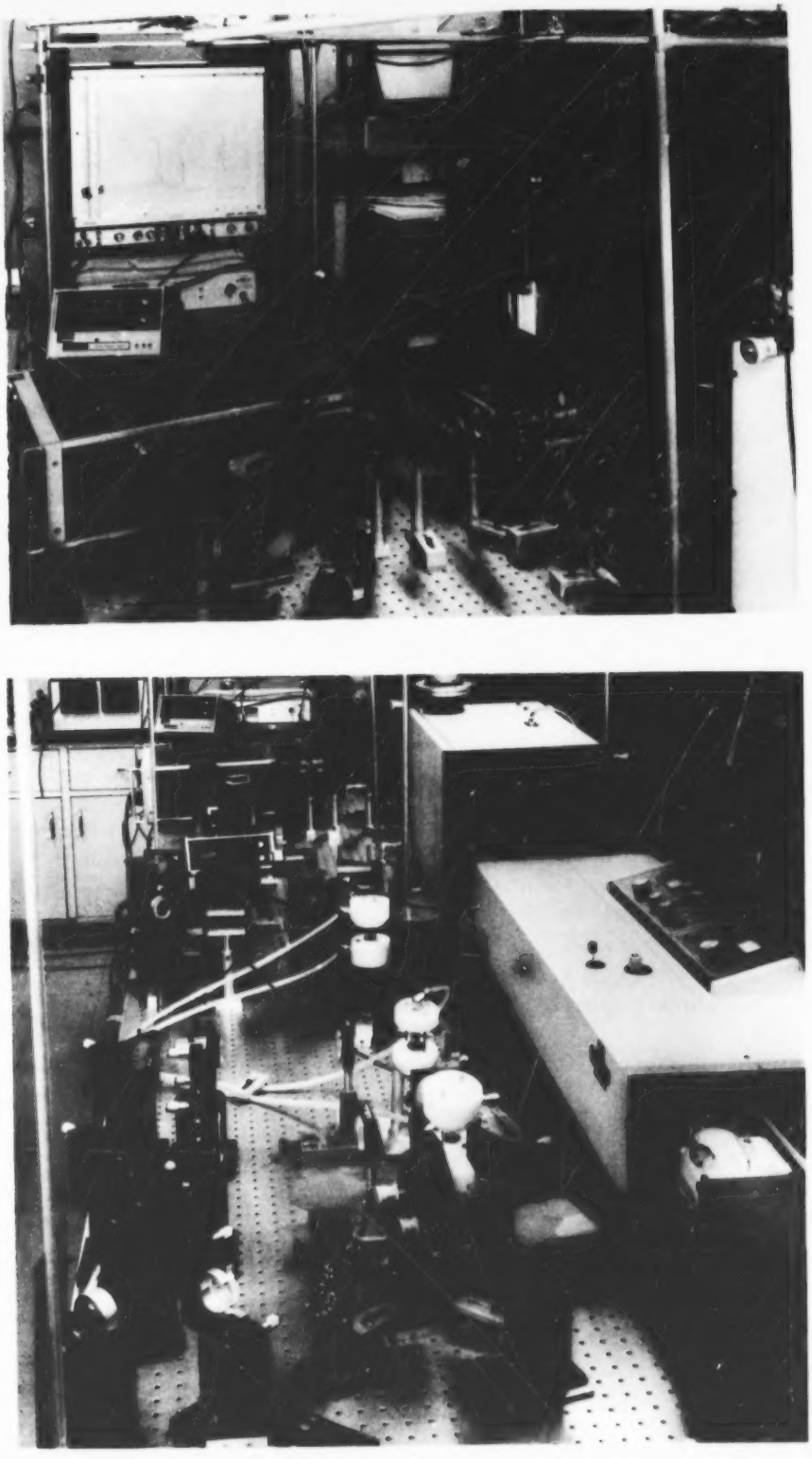

79-08-63-9

FIGURE 31. EXPERIMENTAL ARRANGEMENT FOR CN SATURATED FLUORESCENCE

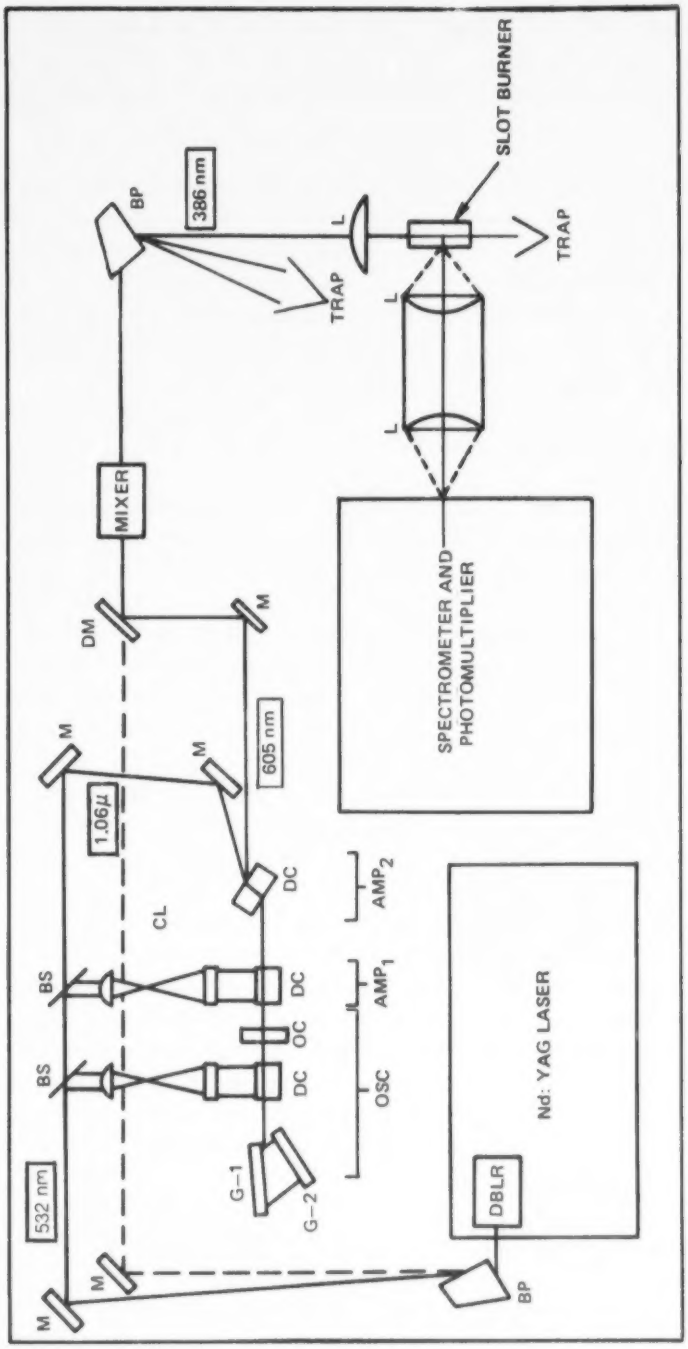

79-08-63-2

dispersing prism. The 6100 Å and 1.06μ beams are then trapped as shown in Fig. 31. The ultraviolet beam is focussed with a simple lens across the same slot burner as used for CH. In order to generate an easily observable amount of CN, the previously successful combination of acelytene and nitrous oxide was used.

The laser-induced fluorescence (and Rayleigh scattering) was collected with the two-lens system shown. The collection f no. was f/8 to match the spectrometer numerical aperture. Glass lenses, quite adequate for this range of the UV were employed throughout. The spectrometer was placed on its side so that the slit was horizontal in order to maximize the amount of fluorescence captured from the horizontal, focussed laser beam, while at the same time maintaining good spectral resolution.

Experimental Studies

Prior to performing laser-induced fluorescence measurements of the CN radical in the acetylene/nitrous oxide slot burner, a moderate resolution (0.16 Å) emission spectrum of CN was recorded. This is shown in Fig. 32. The 0-0, 1-1, and 2-2 band heads are indicated as is the origin of the 0-0 band. The origin is the place where the P-and R-branch meet (originate). It is the place where the Q-branch would be if it were present. Also indicated is J-20 of the R-branch of the 0-0 band which was chosen for the saturated fluorescence studies. The B → X transition in CN (the violet bands) is a $^2\Sigma \rightarrow ^2\Sigma$ transition with no Q-branch. Laser-induced fluorescence spectra shown in Fig. 33 through Fig. 36 demonstrate the effect of excitation into different rotational levels. It is evident that, in contrast to CH, that many rotational levels are populated because lines are observed up to J-30 and beyond. Presumably, the CN radical represents a case where the rotational relaxation rate is more pronounced, in contrast to the case of CH. This difference was mentioned earlier. These laser-induced fluorescence spectra were recorded at moderately high resolution using 10 μ slits equivalent to a spectral bandwidth of 0.16 Å, as was the flame emission spectrum, Fig. 32. Note that even though the narrowband laser excitation supposedly excites only a single rotational state of the ground vibrational level of the ground electronic state, the 1-1 bandhead appears in the fluorescence spectrum (and perhaps the 2-2 bandhead as well). This indicates either vibrational level communication or excitation overlap (in spite of the narrow laser linewidth).

The saturation behavior of the laser-induced fluorescence of CN was determined by reducing the laser input power by insertion of neutral density filters into the laser beam. As the laser input energy was so reduced, neutral density filters were removed from the collection optical train in order to keep the signal strength at the boxcar signal averager at a reasonable level. For these

FIGURE 32. EMISSION SPECTRUM OF CN VIOLET SYSTEM ($B\,^2\Sigma \longrightarrow X\,^2\Sigma$)

ACETYLENE–NITROUS OXIDE SLOT BURNER FLAME

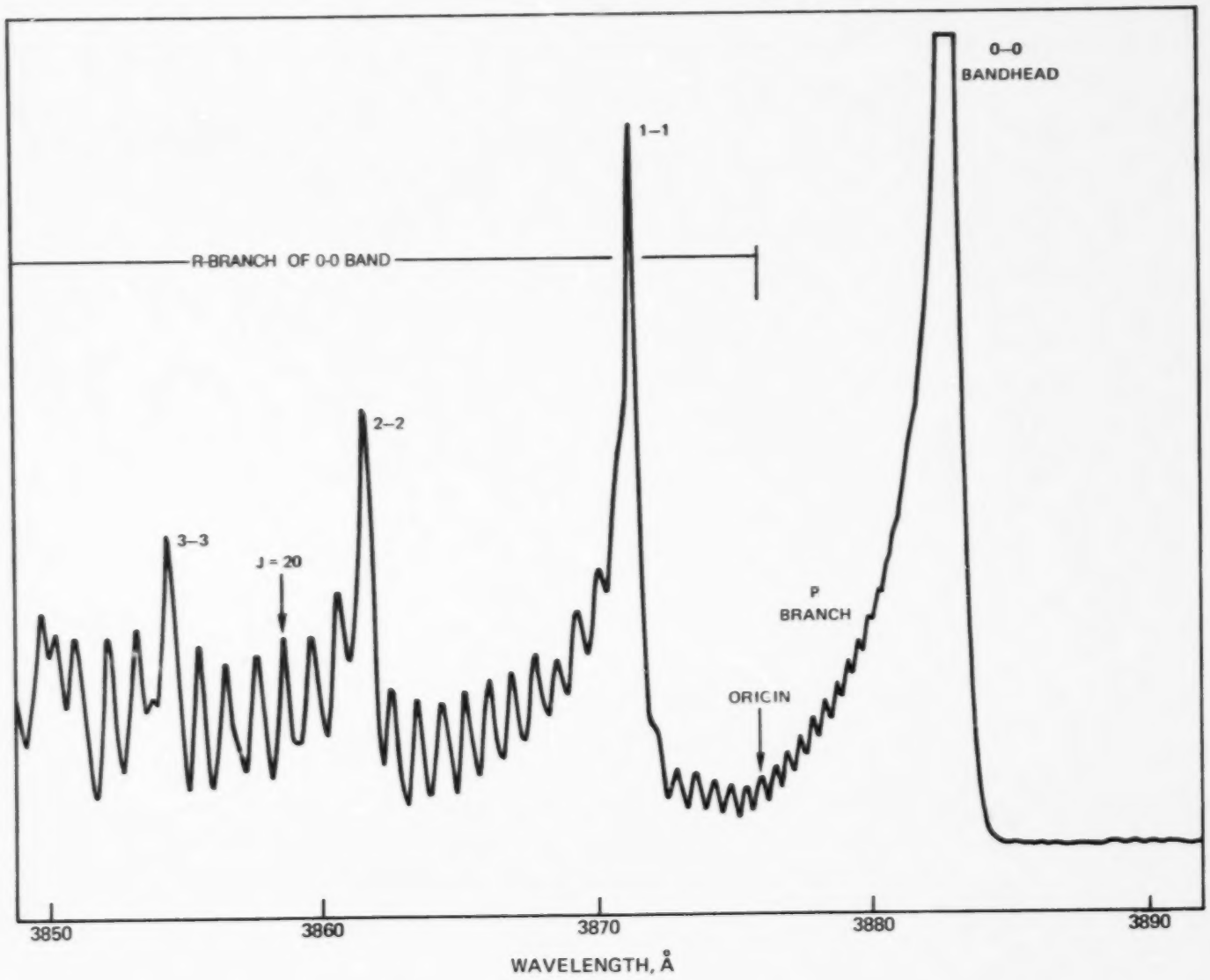

79–08–63–1

FIGURE 33. LASER-INDUCED FLUORESCENCE OF CN RADICAL
EXCITATION INTO $R_0(22)$

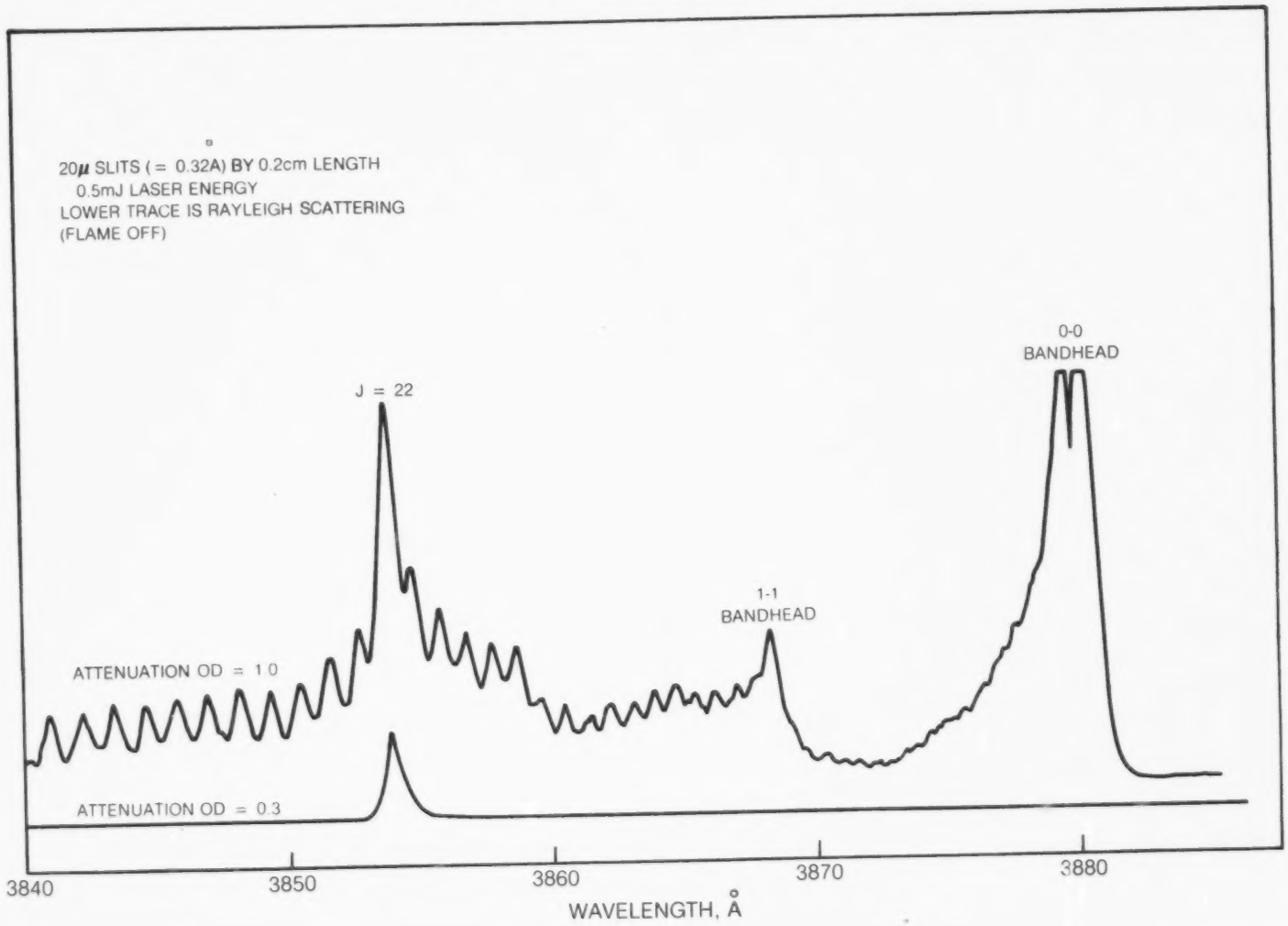

79-08-63-3

FIGURE 34. LASER INDUCED FLUORESCENCE OF CN RADICAL

EXCITATION INTO $R_0(14)$

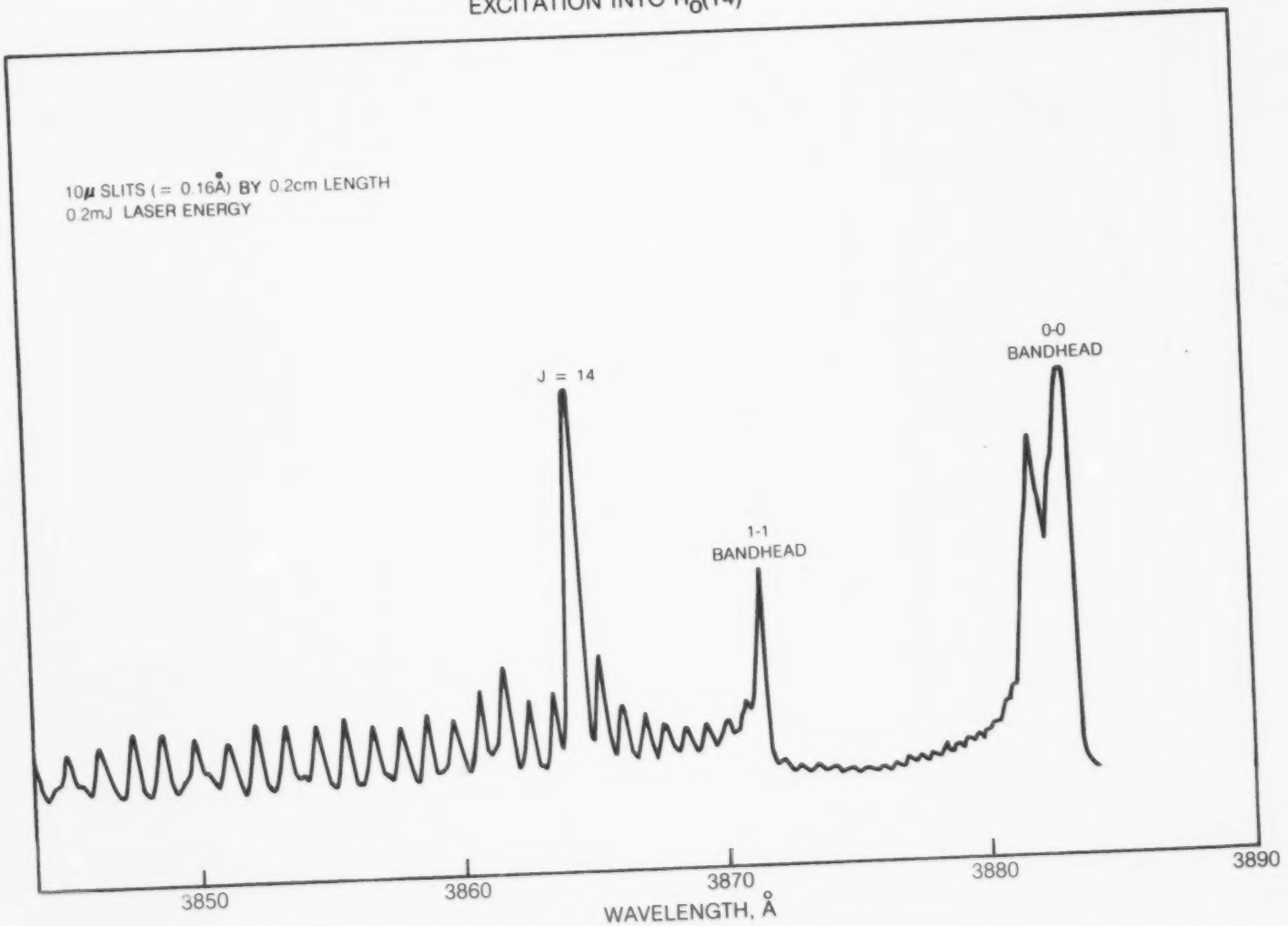

79-08-63-4

FIGURE 35. LASER-INDUCED FLUORESCENCE OF CN RADICAL
EXCITATION INTO $R_0(3)$

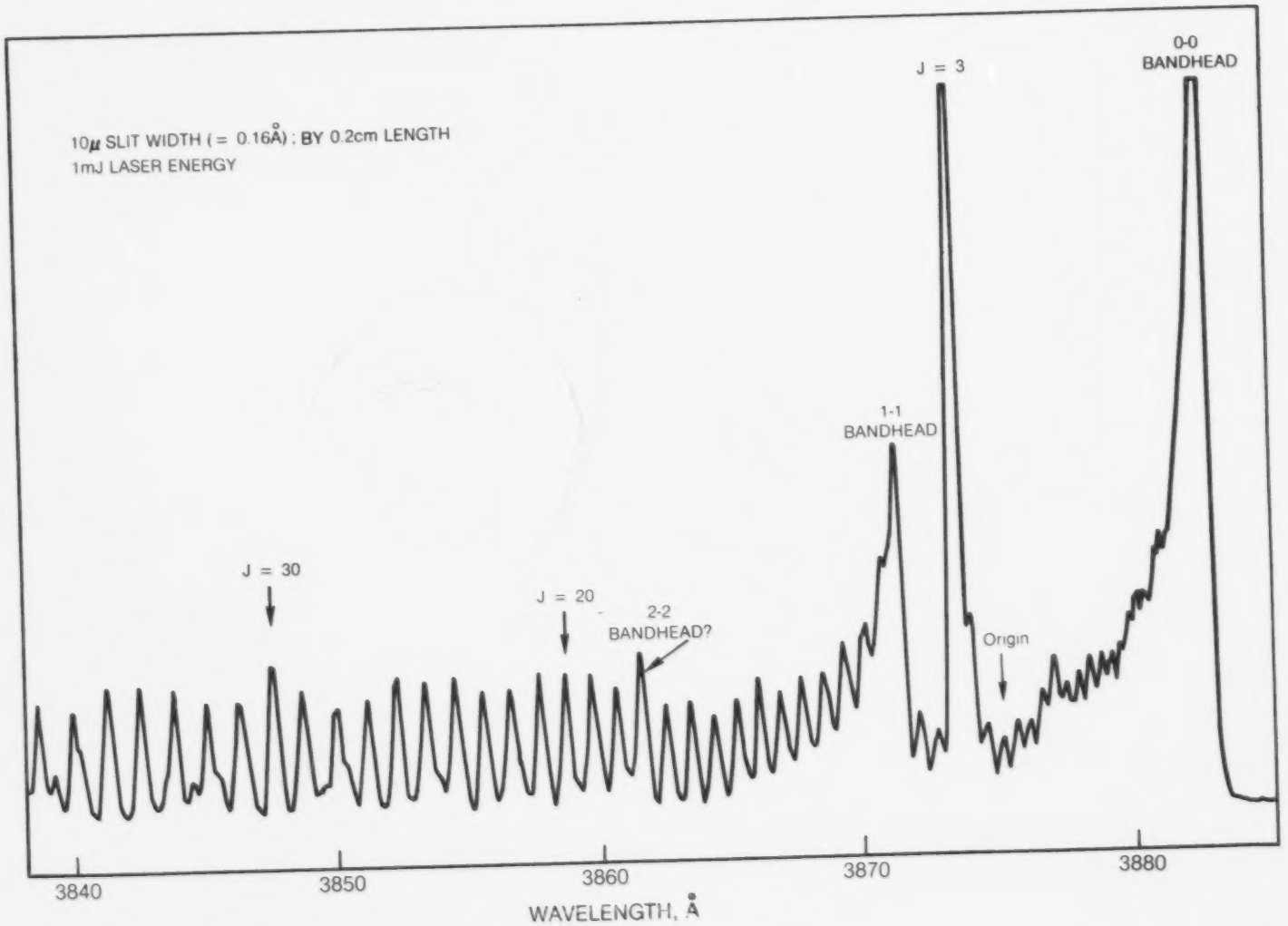

76-08-63-5

FIGURE 36. LASER-INDUCED FLUORESCENCE OF CN RADICAL

EXCITATION INTO $R_0(20)$

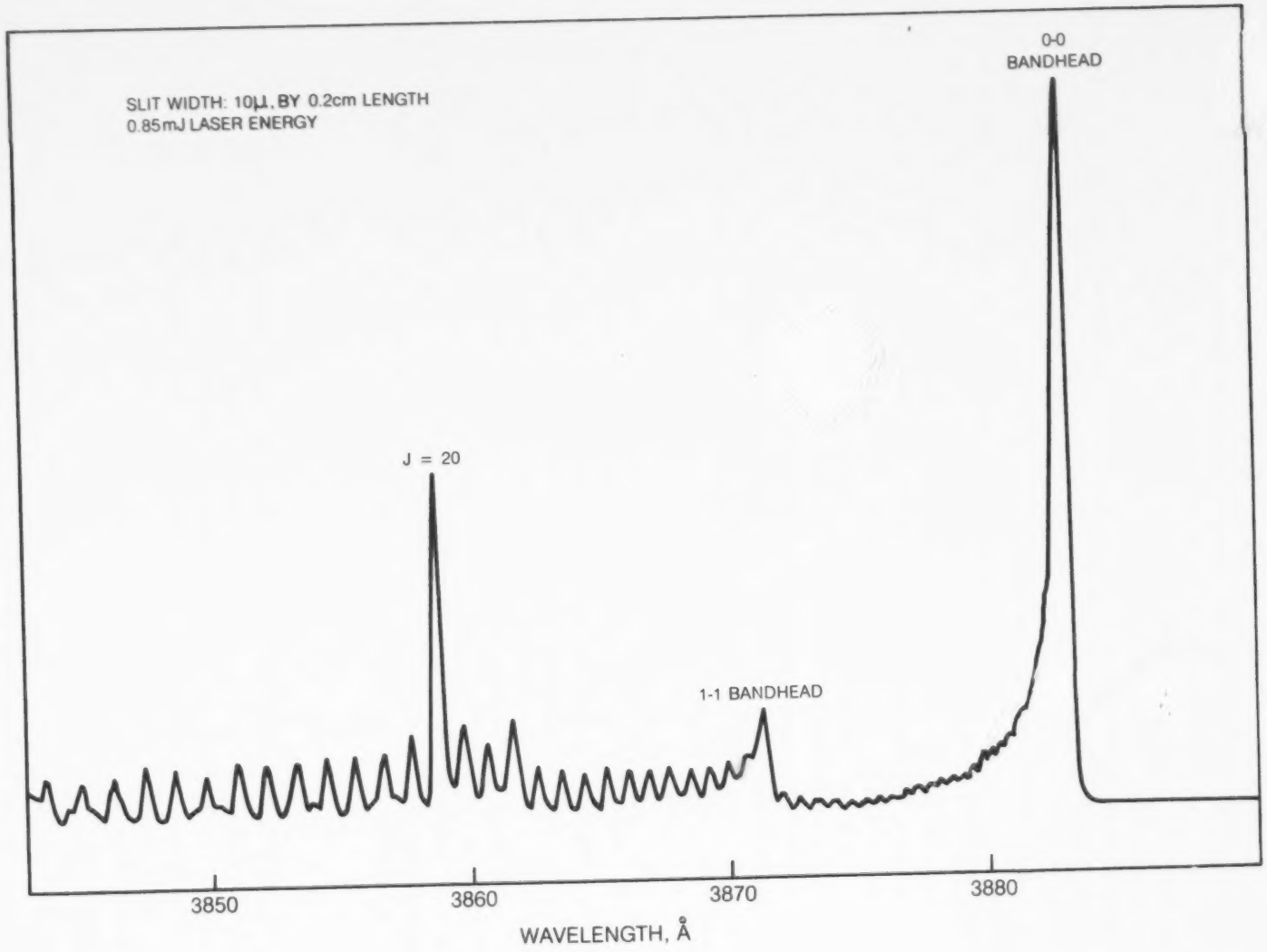

79-08-63-8

saturation measurements the spectrometer slits were opened to 300 μ and the spectrometer wavelength set to 3880 Å, the maximum of the 0-0 P-branch. For this case, the spectral slit width of the spectrometer is nearly 5Å. Because the P-branch forms a head, a large fraction of the total laser-induced fluorescence, ∿ 40%, is captured by means of this arrangement. Excitation occurred at R(20) which is the value of J for the maximum in the R-branch (very broad) at 2800°C.

The laser-induced fluorescence signal as a function of laser energy is shown in Fig. 37. At the lowest laser energies the curve is linear with unity slope but begins to roll over at about 10^{-4} millijoules. Thereafter a second linear region of slope 0.33 is attained. The second limiting linear region is in general agreement with the treatment of Daily (Ref. 44). For a Gaussian laser intensity distribution, he obtained a limiting slope of approximately 0.26. Another interpretation of this second linear region is due to Van Calcar and colleagues (Ref. 51) who note that for fluorescence signals integrated over the entire duration of the laser pulse, a limiting slope of 0.34 is reached. These results were obtained from experimental measurements on sodium. In summary then, the data indicate that the CN radical is easily partially saturated; however, full saturation is difficult to achieve.

The laser-induced fluorescence data can be treated according to the Baronavski-McDonald (Ref. 30) technique to extract the concentration and quenching rate. However, the fluorescence power intercept is now taken to be $S_F^o = fN_T$ consistent with the model developed in this report. A plot of the absolute laser-induced fluorescence signal strength (in Watts) as a function of the reciprocal laser spectral irradiance, Jcm^{-2} is shown in Fig. 38. This plot is linear at high laser energies but rapidly departs from linearity as the laser energy falls off. This behavior is consistent with the "partially-saturated" model of Ref. 30. The value for S_F^o is 7×10^{-7} W. This signal corresponds to approximately 14,000 photons.

Discussion

The number density which is obtained must be interpreted with reference to the modified two-level model developed earlier in this report. The number density, according to this model, can be found from the relation $N_T \curvearrowleft S_F^o/f$. f is the population factor defined previously. Recall that $f \to 1$ in the limit of very fast rotational relaxation, and $f \to f_{Boltzmann}$ for very slow rotational relaxation ($f_{Boltzmann} = P_J$, Eq. 7). The latter case was considered in analyzing the data.

FIGURE 37. LASER INDUCED CN FLUORESCENCE: SATURATION BEHAVIOR

λ_{EXC} = 3857Å $|^2\Sigma(V'' = 0)\, J = 21 \rightarrow {}^2\Sigma\,(V' = 0)\, J = 20]$

SLIT WIDTH 300μ BY 0.2 CM LENGTH, SPECTROMETER AT 3883 °A

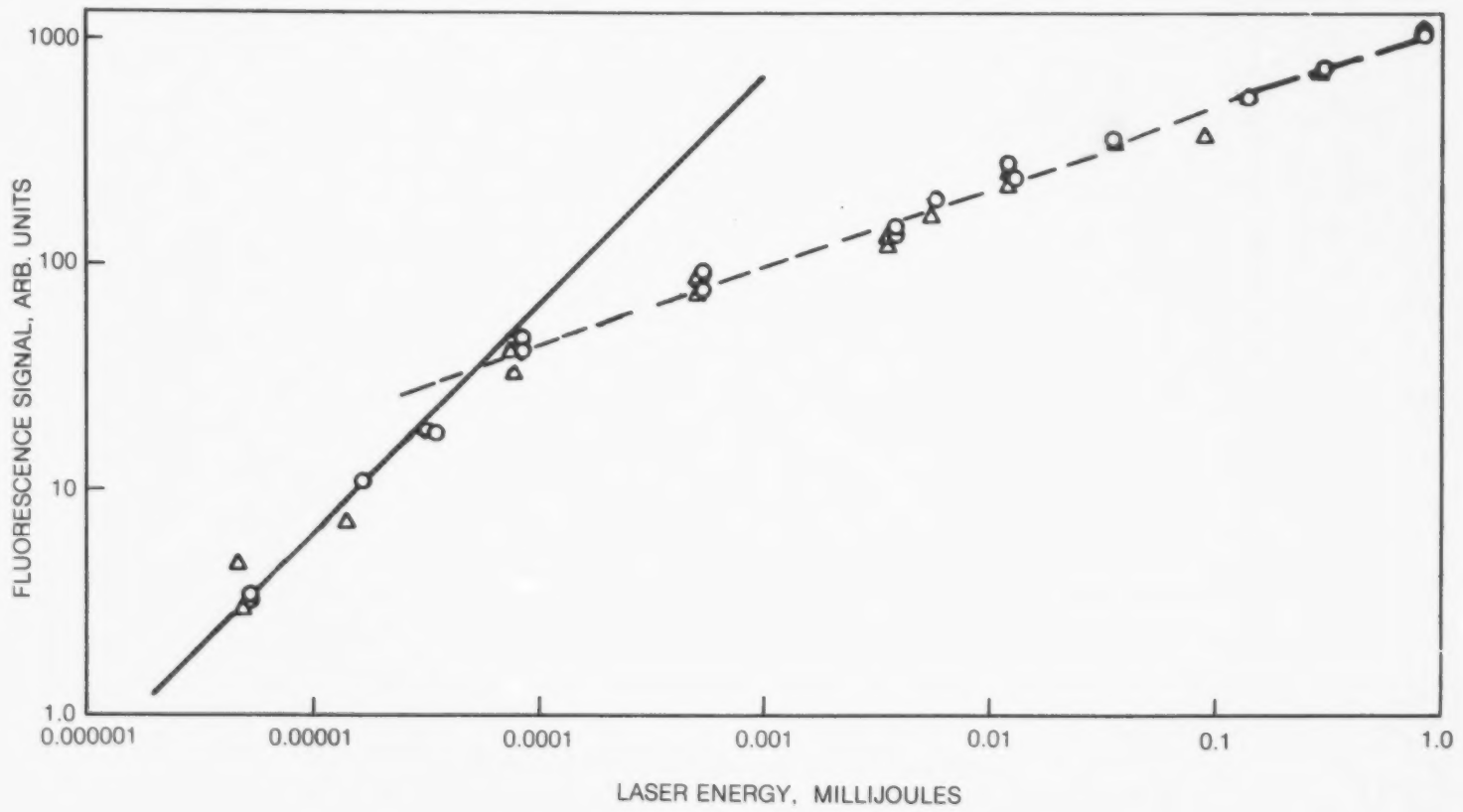

79-08-63-10

FIGURE 38. SATURATED FLUORESCENCE POWER FOR CN VERSUS INVERSE LASER SPECTRAL IRRADIANCE

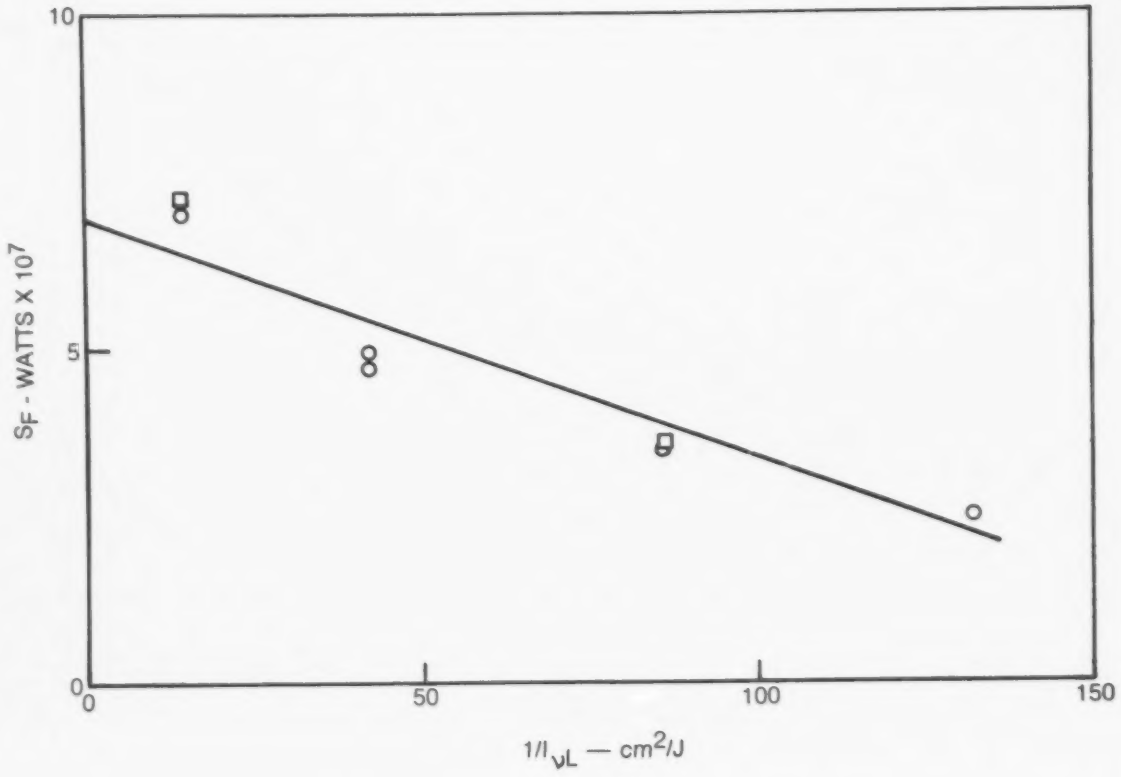

79-09-63-12

The Boltzmann factor for J = 20 of CN at 2800° C is 0.03. This gives a value of N_T from the saturated fluorescence data of 1.1×10^{15} cm^{-3}. The previously measured absorption value (Ref. 6) was $3.8 \pm 0.8 \times 10^{14}$ cm^{-3} for the same conditions and same position in the flame. These results are shown in Table 3. The fluorescence measurement is high by a factor of nearly three compared to the absorption measurement. This difference can be accounted for qualitatively by the two-level model if f is interpreted to be greater than $f_{Boltzmann}$. A quantitative value for f cannot be assigned because of lack of data about rotational relaxation rates. The direct comparison suggests a factor of 3 which must multiply the Boltzmann factor of 0.03. However, the accuracy of the absorption measurement is open to some question because of spatial averaging over the flame by the absorption beam. The distribution of CN in the flame in the horizontal direction, perpendicular to the slot direction, was mapped out by the fluorescence signal. The flame holder was translated relative to the laser beam and the relative fluorescence signal recorded as a function of travel. The double-humped distribution, shown in Fig. 39, was found. This distribution could make the absorption measurement low relative to the fluorescence determination, because the latter was performed on the maximum in the distribution toward the collecting lens. Hence the absorption results are considered a lower limit.

The quenching rate constant was found from the slope of Fig. 38, assuming that $Q_{21} >> A_{21}$. The value found is 1.9×10^{13} sec^{-1}, uncorrected for the f-factor discussed above. The effect of this factor on Q is small, a factor of two at most.

Estimate of Error

The experimental error in the determination of the number density N_1 could be found by means of the standard propagation of error technique; however, it is simpler to estimate the error in the intercept, S_F^o of the graph in Fig. 38. The extreme values are approximately 5.5 and 8.5×10^{-7}W. Hence the error about the chosen value 7×10^{-7} W is ± 20%. This may be a conservative estimate. Further error occurs in converting S_F^o to number density because of uncertainties in the laser beam area, A, and the transmission factor, ε. The error in A should not be much larger than ± 10% as two different methods gave good agreement. The error in ε is estimated to be ±30%, because several factors are involved. The most probable experimental error in N_T is then about ± 40%. Note that this is the experimental error and does not include uncertainties in A_{21} nor the f-factor of the modified two-level model introduced earlier.

NO Investigations

Apparatus

The apparatus used to measure laser-excited NO spectra is shown schematically in Fig. 40. It consists of a 2xNd:YAG laser-pumped tunable dye laser with

FIGURE 39. HORIZONTAL SCAN OF LASER-INDUCED FLUORESCENCE IN CN SLOT BURNER

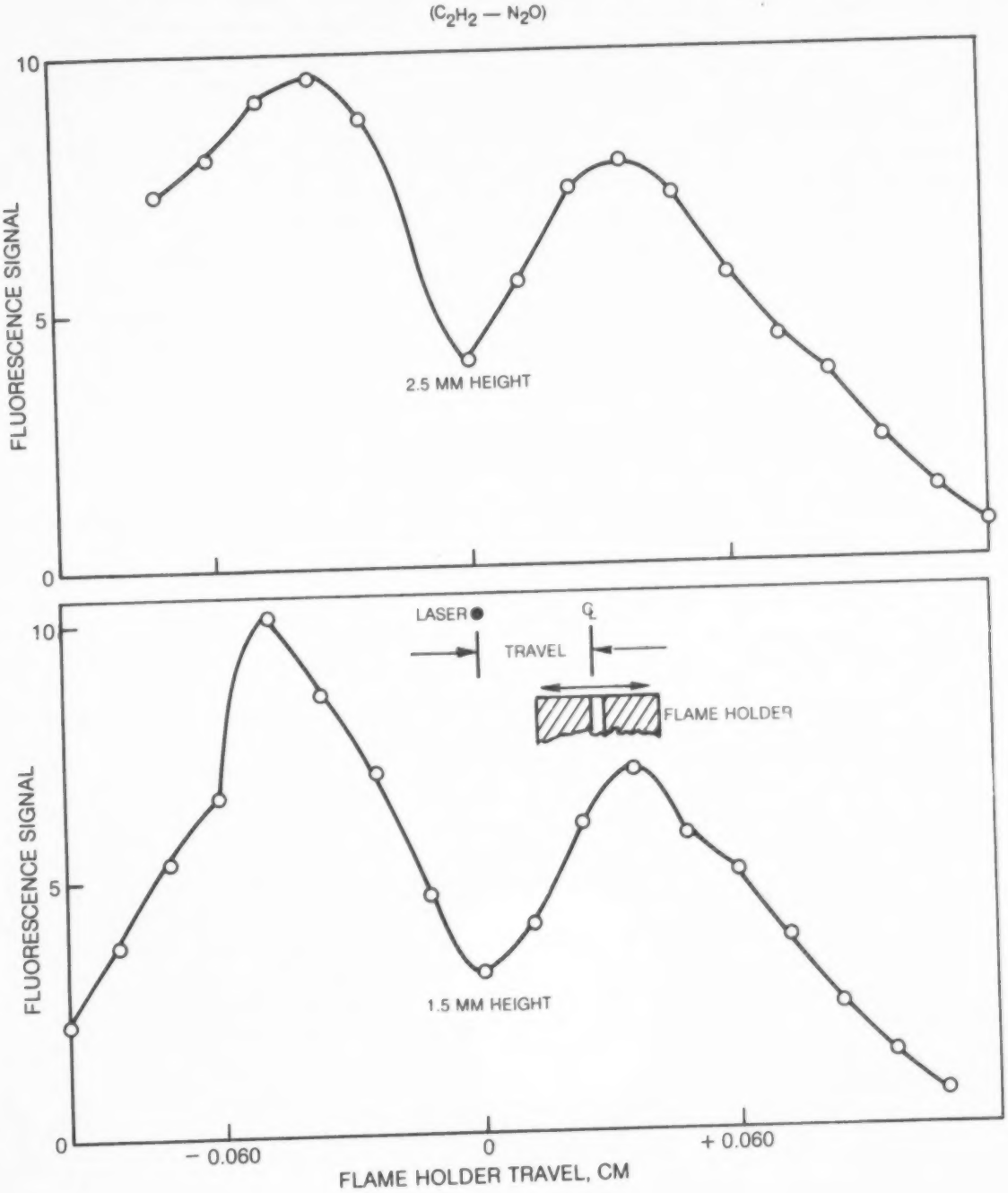

79-08-63-6

FIGURE 40. LASER INDUCED UV FLUORESCENCE APPARATUS

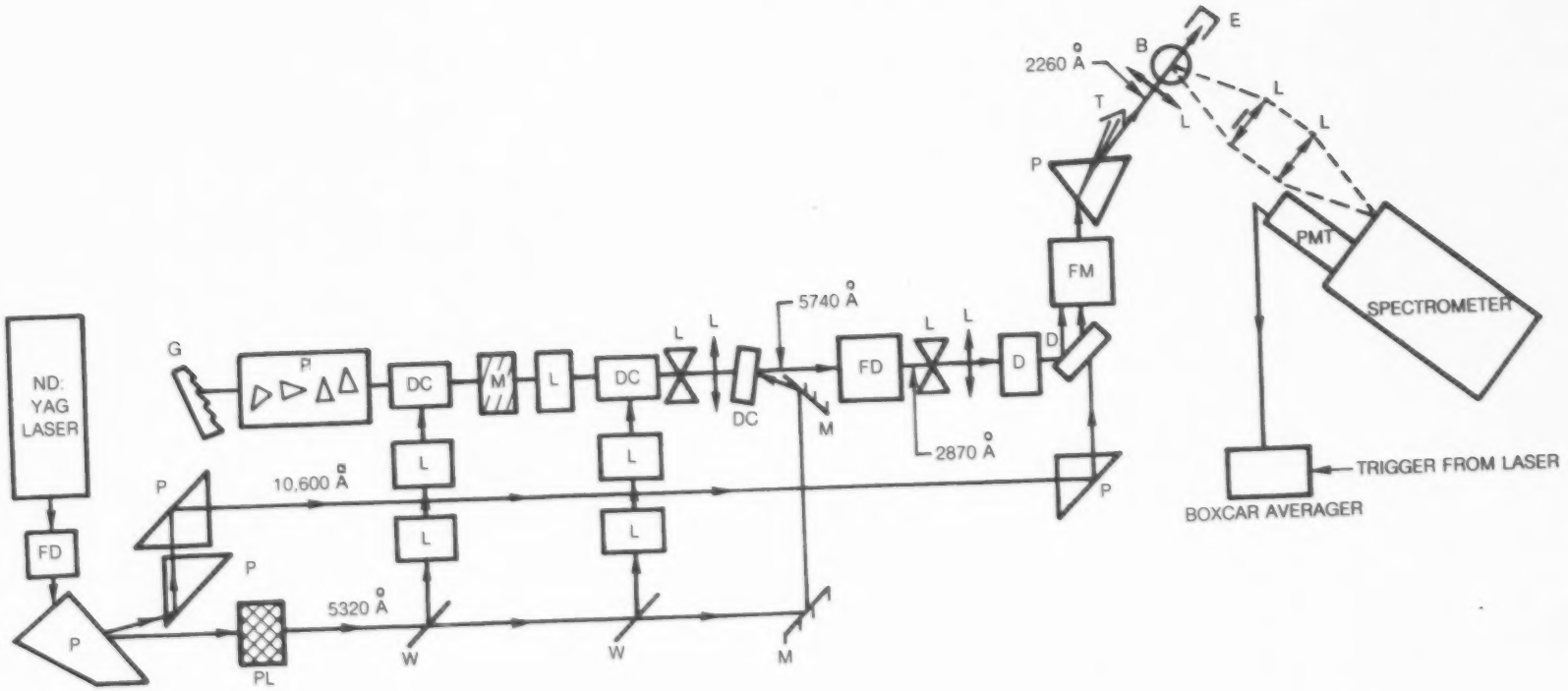

79-09-1-16

frequency doubling followed by subsequent mixing of the output with 1.06μ radiation to generate UV wavelengths. The UV output of the laser interacts with NO in a cell or burner. Light collection optics similar to that used for CH completes the system.

The laser consists of a laser-pumped tunable dye laser operating near 5740 Å, which is frequency-doubled to 2870 Å and mixed with 1.06μ radiation to yield frequency up-converted radiation near 2260 Å suitable for NO excitation. The 5740 Å dye laser in Fig. 40 is very similar to the stilbene dye laser in Fig. 21. The principal difference is that 2xNd:YAG pump radiation at 5320 Å is used to excite a rhodamine 590 dye as opposed to 3550 Å 3xNd:YAG excitation of stilbene. The laser output at 5740 Å is frequency-doubled in a KD*P Type I crystal to produce 2870 Å radiation. In order to better match the size of the 2870 Å beam to that at 1.06μ, it is beam-expanded by a factor of 1.7. A dichroic, oriented at 45-deg, reflects the 2870 Å beam in the direction of the frequency up-converting crystal, FM, also Type I KD*P, where it combines with the 1.06μ radiation passed unattenuated by the dichroic filter. There emerges from the crystal, FM, radiation at 2870, 10,600 and 2260 Å. In order to select 2260 Å, a dispersing quartz prism, P, and light trap, T, are used. The energy of the dye laser at 5740, 2870, and 2260 Å was (30-40) mJ, (2-3) mJ, and (~2-.3) mJ, respectively, for approximately 175 mJ of pump radiation at 5320 Å. The laser pulse widths were O(5-10) nsec and the laser bandwidth at 2260 Å was 0.1 Å. The estimated beam divergence of the UV dye laser was a factor of two larger than for CH or, in this case, equal to 4 mrad.

The UV beam is focussed into a burner, B, (or cell) with a lens having, typically, a 10 cm focal length. A meter, PM, measures the energy of the transmitted beam. The light collection optics are very similar to that for CH above. In this case, however, an image-rotating dove prism is not used in front of the spectrometer entrance slit. Instead, as the case for CN, the spectrometer is rotated 90-deg, that is, placed on its side so as to make the slit horizontal, duplicating the function of the dove prism. In order to enhance observation of 2260 Å emission, a UV-sensitive Hamamatsu R456 photomultiplier tube is used in conjunction with a Jobin-Yvon 0.6 meter Type HRP-1 spectrometer equipped with a 2400 groove/mm holographic grating, capable of 0.08 Å resolution and with peak efficiency near 3000 Å.

The burner and cell used for NO measurements are both simple in design. The cell consists of a standard pyrex cross with quartz entrance and exit windows; it can be evacuated to about 10^{-5} Torr pressure and filled with a known quantity of NO as measured accurately with a calibrated capacitance manometer. The optical absorbing path of the 2260 Å focussed laser radiation was 10 cm. The burner design is such that premixed fuel/air emerges from a 1-inch diameter, stacked honeycomb arrangement of stainless steel hypo tubing. This gave a flat, stable CH_4/air flame to which NO was added by injection into the premix chamber. The flame was operated at near stoichiometric

conditions, and the fraction of NO in the CH_4/air/NO mixture was 3.6%. Gas flows were measured with calibrated flow meters.

Data

Nitric oxide fluorescence observations were carried out successfully only in the case of the burner referred to above; difficulties were encountered with the cell measurements. Over a wide range of NO pressure, clean laser-excited fluorescence signals were not observed from the cell, because of excessive absorption of the focussed UV beam in the long path length (10 cm) cell. This was confirmed by a calculation of the absorption expected, which showed that the cell would be opaque to the UV radiation even for the lowest NO pressures attainable within limitations imposed by gas impurities and cell evacuation. Since any observation of NO saturation in the cell would not definitively determine the laser spectral intensities required to saturate NO in a flame, owing to radically different quenching conditions, the cell measurements were terminated in favor of laser-excited NO flame fluorescence measurements. Studies in specially-designed cells of NO fluorescence in various controlled gas mixtures could be quite valuable and should be seriously considered for future studies.

A laser-excited NO fluorescence spectrum observed in a premixed CH_4/air flame doped with NO is shown in Fig. 41. The wavelength region (2240-2280) Å is shown, scanned with and without NO doping of the flame. The laser wavelength was near 2258 Å, close to the $(R_{11} + Q_{21})$ = 13 1/2 (=J") line (Ref. 52). The signal at 2258 Å in both a) and b) is due to Rayleigh scattering with scattering from the burner face superimposed. The latter occurred since the strongest NO signals were observed very near the burner face. By removing the burner, the Rayleigh signal could be observed alone, and its intensity was about the same as the strongest NO signals. The amplitude of the NO fluorescence pulses was very erratic, much more so than for CH. This was due probably to laser amplitude variations induced by frequency instabilities at 2258 Å. This jitter was evident in oscilloscope traces of the fluorescence pulses at 2265 Å and, indirectly, from Fabry-Perot analysis of the laser mode structure at 5740 Å which demonstrated considerable instability. NO fluorescence pulses are shown in Fig. 42. About 100 pulses are superimposed since the photographic exposure time was 10 sec and the laser repetition rate was 10 Hz. Considerable amplitude variation is evident; in isolated cases, the location of the pulse in time shifted a full 10 nsec pulse length. The pulse duration may not be taken as true since the rise time of the photomultiplier is 3 nsec. The spectrum in Fig. 41 was taken with a 40 μ spectrometer slit width for which the measured spectrometer resolution is of order 0.25 Å. This precluded very high resolution of rotational spectra, but the 40 μ slit width was required in order to observe emission with good S/N. In spite of the foregoing, it was possible to observe distinctly the band heads identified in Fig. 41, and thereby confirm observation of NO emission.

FIGURE 41. NO SPECTRA

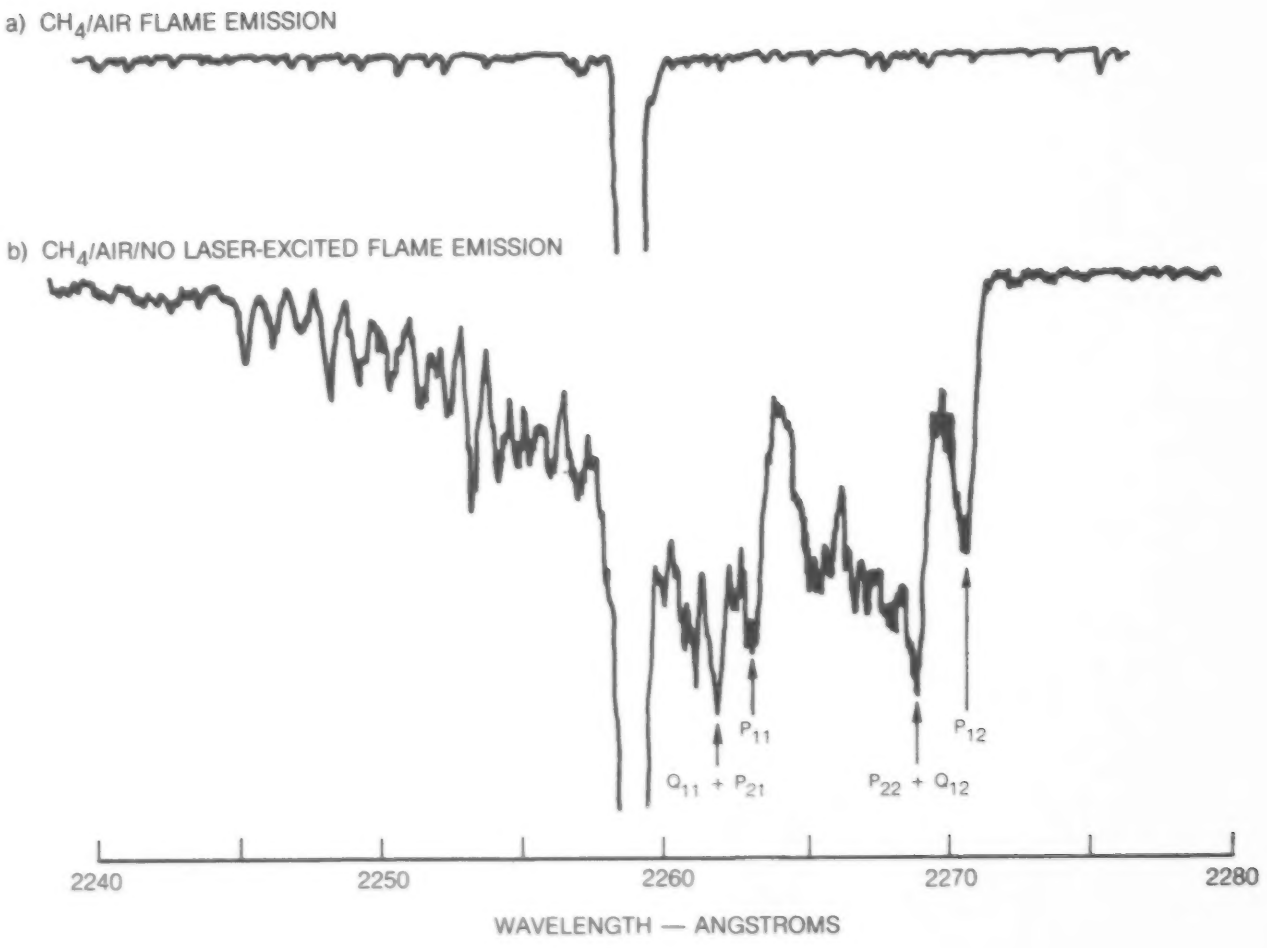

FIGURE 42. NO FLUORESCENCE PULSES

$\lambda_{EXC} \simeq 2258$ Å

$\lambda_{OBS} \simeq 2265$ Å

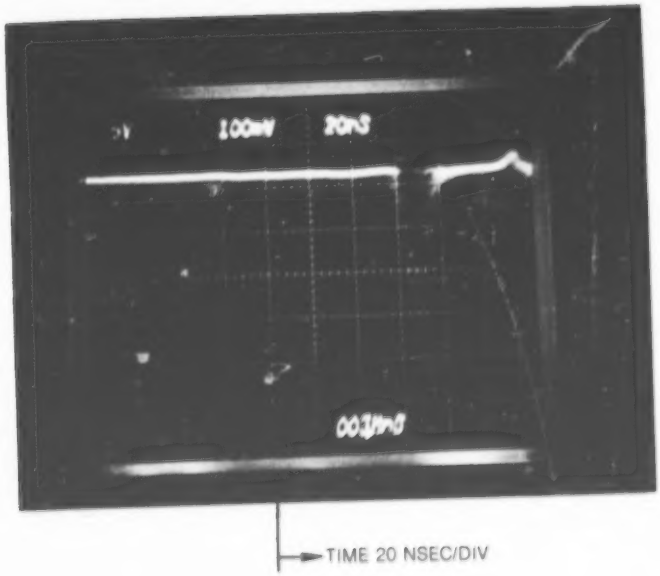

79-09-1-13

NO emission at 2265 Å was monitored as a function of laser energy to look for NO saturation. Saturation of the fluorescence was not observed as may be seen from Fig. 43. As in previous experiments, fluorescence was observed at a wavelength shifted from that of the laser in order to avoid Rayleigh scattering. The dependence of fluorescence intensity on laser energy was strictly linear, and this was confirmed by repetition of the measurement. The highest laser energy in Fig. 43 corresponds to a 6.4×10^6 W/cm^2 cm^{-1} laser spectral intensity incident on the CH_4/air/NO flame. In Table XXIII of Ref. 1, it was estimated that the laser spectral intensity required to saturate NO in a flame is 4×10^8 W/cm^2 cm^{-1}. This estimate is consistent with present observations.

Discussion

Since saturation of the NO fluorescence was not observed, it is not possible to determine the flame NO concentration employing the saturated fluorescence data reduction approach described earlier. On the other hand, the data given in Fig. 43 does permit evaluation of the fluorescence efficiency or Stern-Volmer factor, $A_{21}/(Q_{21}+A_{21})$, provided that the NO concentration is known and, secondly, Rayleigh data are used to evaluate the apparatus factor, ϵ. Since a calibrated flowmeter is used for doping the CH_4/air flame, the NO concentration corresponding to the Fig. 43 data can be estimated. In experiments at UTRC, Seery has found that 25-50% of NO doped into low pressure, premixed flames can be lost at equivalence ratios of 0.9 and above. Only if the flame is very lean is the NO likely to be conserved. Since the NO fluorescence was strongest at the burner surface, it is clear that some NO loss occurred in the flame used for the fluorescence experiments. If it is assumed that no NO loss occurred, then the estimates of required saturation spectral intensity will err on the conservative side.. The Stern-Volmer factor measures the degree to which fluorescence intensity is diminished by collisional quenching of the excited electronic state. Evaluation of this factor is important because the ratio, $I_{L\nu}(B_{12}+B_{21})/(Q_{21}+A_{21})$, a measure of saturation, can then be computed. For the NO study, this factor is apparently small since saturation was not observed. Evaluation of the preceding ratio makes it possible to predict the increase in $I_{L\nu}$ required for saturation to occur. The Stern-Volmer factor was calculated to be $A_{21}/(Q_{21}+A_{21}) = 4.4 \times 10^{-6}$, and the saturation parameter $I_{L\nu}(B_{12}+B_{21})/(Q_{21}+A_{21}) = 2.5 \times 10^{-2}$. By contrast, the saturation parameter for CH corresponding to the highest laser energy was 2.5. The foregoing indicates that $I_{L\nu}$ for the NO measurements must be increased by about a factor of 100 for application of the saturated fluorescence technique to species measurement, consistent with the earlier estimates (Ref. 1). Similarly, it is instructive to note that the highest value of $I_{L\nu}$ achieved at 2258 A would correspond in the case of CH (see Fig. 27) to measurements at laser energies of less than 0.04 mJ, in the linear region. Such a comparison is reasonable in that Q_{21} for NO and CH are both, approximately, 10^{12} sec^{-1}.

FIGURE 43. LASER EXCITED NO FLAME FLUORESCENCE

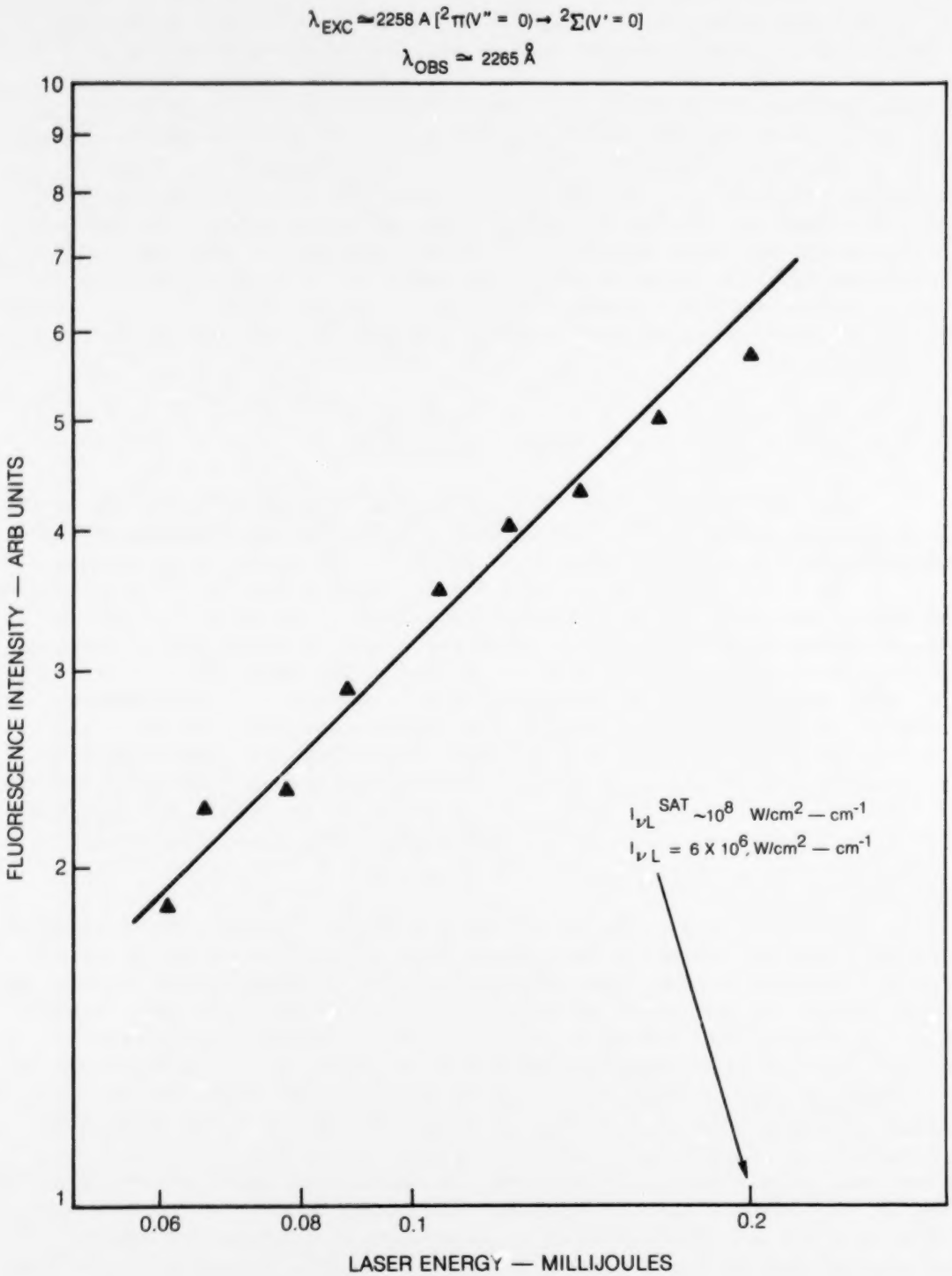

79-09-1-14

As indicated above, an increase in $I_{L\nu}$ by a factor of 100 is required to saturate NO. It appears that such an increase is feasible if the present breadboard laser is replaced by a commercial dye laser system. The laser spectral intensity is given by $I_{L\nu} = (E/\tau)\,(\pi D^2/4)^{-1}(\Delta\nu)^{-1}$, where E and τ are the pulse energy and length, respectively; D is the focussed beam diameter; and $\Delta\nu$ is the laser bandwidth. The time, τ, is not expected to differ for the two systems since the pump lasers are identical. Of the remaining factors, numerical values for the commercial dye laser system at 2260 Å, for 200 mJ of 5320 Å pump energy, are: E = 2mJ; D = 100 microns; $\Delta\nu$ = 1 cm^{-1} (Ref. 53). This represents a 10x increase in E, a 4x reduction in D, and a 2x reduction in $\Delta\nu$ when compared with our system, which implies a 320x increase in $I_{L\nu}$. Consequently, saturated NO measurements appear feasible with an improved laser pumped dye laser system.

General Discussion

The most significant result of the saturated fluorescence research is the relatively good agreement of the saturated fluorescence measurements with the absorption measurements as tabulated in Table 3. The agreement is roughly a factor of two for the CH radical and a factor of three for CN. These measurements were made on extremely reactive radical species in an atmospheric pressure flame at temperatures of O(2500 °C) by means of a still-developing technique; for these reasons, the agreement should be considered quite satisfactory. In the only other molecular case known to the authors where a comparison between absorption measurements and saturated fluorescence was made (Ref. 33), the agreement was good only to a factor of ten. There is, of course, uncertainty in the f-factor which accounts for the extent of rotational redistribution. As mentioned above, this factor cannot be determined until rotational relaxation effects are modeled and compared with experiment. The importance of solving this particular problem is discussed below.

The three radical species chosen for this study form an interesting series with respect to ease of saturating the fluorescence transitions. Both CH and CN could be saturated with attainable laser energies, CN being easier to saturate than CH because of the larger spontaneous emission coefficient, A_{21}, (hence, larger B_{12} coefficient) for CN. The NO radical represents a particularly difficult species to saturate for two reasons: the A to X gamma bands are not strong transitions, and they lie nearly in the vacuum UV region of the spectrum. Although presently available commercial dye laser systems attain reasonable power levels in this region by wave-mixing processes, these techniques were untried when this program was initiated. Saturation of the NO radical fluorescence was not achieved in this investigation mainly because of low laser energy at 2260 Å, $\sim$ 0.1 millijoule. However, laser-induced fluorescence spectra were obtained from NO doped flames, and it appears that saturation of NO fluorescence could be achieved with commercial dye laser systems.

From a purely experimental viewpoint, the choice of the short-pulse Nd:YAG laser pumped dye laser systems was a good one. Dye lasers operating in the orange, yellow, and blue were constructed which performed well with good beam quality and narrow spectral width, both essential properties for obtaining high laser spectral irradiance. Doubling and mixing of these dye-laser beams to generate UV radiation was achieved. The less than 10 nanosecond pulse duration of these lasers, in addition to generating high peak powers, ensures that very little laser-induced chemistry (characteristic time scale of microseconds) will take place. If chemistry occurs during the fluorescence observation period, molecules are lost from the system leading to erroneous measurements. During a 10 nanosecond pulse, this effect is negligible.

Through the use of the boxcar averager, high-resolution scans of the entire fluorescence spectrum were made for all species. It should be stressed that these spectra represent 10 nanosecond "snapshots" of the fluorescence. Contained in these spectra is a wealth of information regarding the relationship of rotational relaxation rates to quenching rates, spontaneous emission rates, and the length of the laser pulse. It is precisely this relationship which must be understood in order to properly interpret the saturated fluorescence data in terms of a model which incorporates rotational energy transfer.

The modified two-level model introduced in this report exhibits the proper limiting behavior for both fast and slow extremes of rotational energy transfer. For intermediate rotational rates the f-factor cannot be determined without detailed knowledge of all of the rate processes involved. Computer modeling of the time-dependent solutions of the rate equations, along with experimental measurements, will be required to obtain this knowledge.

The detectivity limits for the CH and CN radicals can be found by calculating the number of photons corresponding to the fluorescence power induced by the maximum laser spectral irradiance employed. Based upon a shot-noise limit analysis and choosing a signal-to-noise ratio of 5, these limits are:

for CH, 14 ppm

CN, 2 ppm

It must be stressed that these limits apply to the conditions used in this investigation, that is, for the specified values of laser power, fluorescence fraction collected, rotational level excited, etc. These limits could be improved upon with increased laser power and more efficient fluorescence collection and other modifications. For example, changing the collection optics from f/8 to f/3 would improve the signal by a factor of seven. The spectrometer could be replaced with a bandpass filter, once the proper spectral region for collection was determined. This could improve signal strength by a factor of 2-3 or more.

REFERENCES

1. Eckbreth, A. C., P. A. Bonczyk, and J. F. Verdieck: Review of Laser Raman and Fluorescence Techniques for Practical Combustion Diagnostics, Report EPA-600/7-77-066, June 1977.

2. Eckbreth, A. C., P. A. Bonczyk, and J. F. Verdieck: Laser Raman and Fluorescence Techniques for Practical Combustion Diagnostics, Appl. Spect. Rev., Vol. 13, pp. 15-164, 1978.

3. Under corporate sponsorship, an updated and revised version of Reference 2 was prepared and appeared in Progress in Energy and Combustion Science under the title "Combustion Diagnostics by Laser Raman and Fluorescence Techniques", Vol. 5, pp. 253-322, 1979.

4. Lapp, M., and C. M. Penney: Laser Raman Gas Diagnostics, Plenum Press, New York, 1974.

5. Lederman, S.: The Use of Laser Raman Diagnostics in Flow Fields and Combustion, Prog. Energy Comb. Sci., Vol. 3, pp. 1-34, 1977.

6. Eckbreth, A. C., P. A. Bonczyk, and J. A. Shirley: Investigation of Saturated Laser Fluorescence and CARS Spectroscopic Techniques for Combustion Diagnostics, Report EPA-600/7-78-104, June 1978.

7. Bonczyk, P. A., and J. A. Shirley: Measurement of CH and CN Concentration in Flames by Laser-Induced Saturated Fluorescence, Combust. Flame, Vol. 34, pp. 253-264, 1979.

8. Nibler, J. W., W. M. Shaub, J. R. McDonald and A. B. Harvey: Coherent Anti-Stokes Raman Spectroscopy, in Vol. 6 Vibrational Spectra and Structure, J. R. Durig Ed., Elsevier, Amsterdam, 1977.

9. Druet, S., and J. P. Taran: Coherent Anti-Stokes Raman Spectroscopy, in Chemical and Biological Applications of Lasers, C. B. Moore, Ed., Academic Press, New York, 1979.

10. Nibler, J. W., and G. V. Knighten: Coherent Anti-Stokes Raman Spectroscopy, in Raman Spectroscopy of Gases and Liquids, A. Weber, Ed., Springer-Verlag, Berlin, 1979.

11. Zinn, B. T., Ed.: Experimental Diagnostics in Gas Phase Combustion Systems, AIAA, New York, 1977.

12. Eckbreth, A. C.: Effects of Laser Modulated Particulate Incandescence on Raman Scattering Diagnostics, J. Appl. Phys., Vol. 48, pp. 4473-4479, 1977.

13. Leonard, D. A.: Field Tests of a Laser Raman Measurement System for Aircraft Engine Exhaust Emissions, AFAPL-TR-74-100, 1974.

14. Hall, R. J.: CARS Spectra of Combustion Gases. Comb. Flame, Vol. 35, pp. 47-60, 1979.

15. Roh, W. B., and P. W. Schreiber: Pressure Dependence of Integrated CARS Power, Appl. Opt., Vol. 17, pp. 1418-1424, 1978.

16. Eckbreth, A. C. and R. J. Hall: CARS Thermometry in a Sooting Flame, Comb. Flame, Vol. 36, pp. 87-98, 1979.

17. Eckbreth, A. C.: CARS Investigations in Sooting and Turbulent Flames, Project SQUID Report UTRC-5-PU, 1979.

18. Hong, N. S., A. R. Jones and F. J. Weinberg: Doppler Velocimetry Within Turbulent Phase Boundaries, Proc. Roy. Soc. Lond. A, Vol 53, pp. 77-85, 1977.

19. Stenhouse, I. A., D. R. Williams, J. B. Cole and M. D. Swords: CARS in an Internal Combustion Engine, Appl. Opt., Vol. 18, pp. 3819-3825, 1979.

20. Switzer, G. L., W. M. Roquemore, R. P. Bradley, P. W. Schreiber and W. B. Roh: CARS Measurements in a Bluff-Body Stabilized Diffusion Flame, Appl. Opt., Vol. 18, pp. 2343-2345, 1979.

21. Attal, B., M. Pealat and J. P. Taran: CARS Diagnostics of Combustion, AIAA Paper No. 80-0282, 1980.

22. Switzer, G. L., L. P. Goss, W. M. Roquemore, R. P. Bradley, P. W. Schreiber and W. B. Roh: The Application of CARS to Simulated Practical Combustion Systems, AIAA Paper No. 80-0353, 1980.

23. Eckbreth, A. C.: BOXCARS: Crossed-beam Phase-matched CARS Generation in Gases, Appl. Phys. Lett., Vol. 32, pp. 421-423, 1978.

24. Eckbreth, A. C.: Remote Detection of CARS Employing Fiber Optic Guides, Appl. Opt., Vol. 18, pp. 3215-3216, 1979.

25. Beer, J. M.,and N. A. Chigier: Combustion Aerodynamics, John Wiley, New York, 1972.

REFERENCES (Cont'd)

26. Eckbreth, A. C.,: R. J. Hall and J. A. Shirley: Investigations of Coherent Anti-Stokes Raman Spectroscopy (CARS) for Combustion Diagnostics, AIAA Paper 79-0083, New Orleans, La., 1979.

27. Eckbreth, A. C.,: and R. J. Hall: CARS Diagnostic Investigations of Flames, Proceedings of the NBS 10th Materials Research Symposium on Characterization of High Temperature Vapors and Gases, Gaithersburg, Md., 1978.

28. Hall, R. J.: Pressure-broadened Linewidths for N_2 CARS Thermometry. Submitted to Applied Spectroscopy, January 1980.

29. Colket, M. B., et. al.: NO Measurement Study; Probe Measurements, Task II Report under Contract DOT-FA77WA-4081, United Technologies Research Center Report R79-994150-2, 1979.

30. Baronavski, A. P. and J. R. McDonald: Measurement of C_2 Concentrations in an Oxygen-Acetylene Flame: An Application of Saturation Spectroscopy. J. Chem. Phys., Vol. 66, pp. 3300-3301, 1977.

31 Baronavski, A. P. and J. R. McDonald: Application of Saturation Spectroscopy to the Measurement of C_2, $^3\pi_u$ Concentrations in Oxygen-Acetylene Flames. Appl. Opt., Vol. 16, pp. 1897-1901, 1977.

32. Lucht, R. P., Private Communication.

33. Pasternack, L., A. P. Baronavski, and J. R. McDonald: Application of Saturation Spectroscopy for Measurement of Atomic Na and MgO in Acetylene Flames. J. Chem. Phys., Vol. 69, pp. 4830-4387, 1978.

34. Becker, K. H. and D. Haaks: Lifetime Measurements on Excited SH ($A^2\Sigma^+$) Radicals. Journal of Photochemistry, Vol. 1, pp. 177-179, 1972/73.

35. Müller, C. H. III, K. Schofield, M. Steinberg, and H. P. Broida: Sulfur Chemistry in Flames (Preprint).

36. Daily, J. W. and C. Chan: Laser-Induced Fluorescence Measurement of Sodium in Flames. Comb. and Flame, Vol. 33, pp. 47-53, 1978.

37. Smith, B., J. D. Winefordner, and N. Omenetto: Atomic Fluorescence of Sodium under Continuous-Wave Laser Excitation. J. Appl. Phys., Vol. 48, pp. 2676-2680, 1977.

38. Kuhl, J. and H. Spitschan: Flame-Fluorescence Detection of Mg, Ni, and Pb with a Frequency-Doubled Dye Laser as Excitation Source. Opt. Comm., Vol. 7, pp. 256-259, 1973.

39. Omenetto, N., P. Benetti, L. P. Hart, J. D. Winefordner, and C. Th. J. Alkemade: Non-Linear Optical Behavior in Atomic Fluorescence Flame Spectrometry. Spectrochimica Acta, Vol. 28B, p. 289-300, 1973.

40. Olivares, D. R. and G. M. Hieftje: Saturation of Energy Levels in Analytical Atomic Fluorescence Spectrometry-I. Theory. Spectrochimica Acta, Vol. 33B, pp. 79-99, 1977.

41. Daily, J. W.: Saturation Effects in Laser Induced Fluorescence Spectroscopy. Appl. Opt., Vol. 16, pp. 568-571, 1977.

42. Lucht, R. P. and N. M. Laurendeau: Two-Level Model for Near Saturated Fluorescence in Diatomic Molecules. Appl. Opt., Vol. 18, pp. 856-861, 1979.

43. Berg, J. O. and W. L. Shackleford: Rotational Redistribution Effect on Saturated Laser-Induced Fluorescence. Appl. Opt., Vol. 18, pp. 2093-2094, 1979.

44. Daily, J. W.: Saturation of Fluorescence in Flames with a Gaussian Laser Beam. Appl. Opt., Vol. 17, pp. 225-229, 1978.

45. Dewey, H. J.: Second Harmonic Generation in $KB_5O_8 \cdot 4H_2O$ from 217.1 to 315.0 nm. IEEE J. Q. E., Vol. QE-12, pp. 303-306, 1976.

46. Wolfhard, H. G. and W. G. Parker: A New Technique for the Spectroscopic Examination of Flames at Normal Pressures. Proc. Phys. Soc., Vol. 62, pp. 722-730, (1949).

47. Smith, G. P., D. R. Crosley, and L. W. Davis: Rotational Populations Distributions in Laser-Excited OH in an Atmospheric Pressure Flame. Paper presented at Eastern State Division of the Combustion Institute, Atlanta, GA, November 1979.

48. Littman, M. G.: Single-Mode Operation of Grazing Incidence Pulsed Dye Laser, Optics Lett., Vol. 3, pp. 138-140, 1978.

49. Littman, M. G., and H. F. Metcalf: Spectrally Narrow Pulsed Dye Laser Without Beam Expander, Appl. Optics, Vol. 17, pp. 2224-2227, 1978.

50. Shoshan, I., N. N. Danon, and U. P. Oppenheim: Narrowband Operation of a Pulsed Dye Laser Without Intracavity Beam Expansion. J. Appl. Phys., Vol. 48, pp. 4495-4497, 1977.

REFERENCES (Cont'd)

51. Van Calcar, R. A., M. J. M. Van de Ven, B. K. Van Vitert, K. J. Biewenga, T. Hollander and C. Th. J. Alkemade: Saturation of Sodium Fluorescnce in a Flame with a Pulsed Tunable Dye Laser, J. Quant. Spectros. Rad. Trans., Vol. 21, pp. 11-18, 1979.

52. Zacharias, H., A. Anders, J. B. Halpern, and K. H. Welge: Frequency Doubling and Tuning with $KB_5O_8 \cdot 4H_2O$ and Application to NO A $^2\Sigma^+$ Excitation. Opt. Comm., Vol. 19, pp. 116-119, 1976.

53. Private communication with S. Brosnar of Quanta-Ray, Inc.